LATERAL-LOAD RESPONSE OF TWO REINFORCED CONCRETE PIERS

WA-RD 305.3

Final Technical Report
March 1994

Washington State Department of Transportation

Washington State Transportation Commission
Transit, Research, and Intermodal Planning (TRIP) Division
in cooperation with the U.S. Department of Transportation
Federal Highway Administration

25/90

12067

TECHNIC **AGE**

1. REPORT NO.	NTS CATALOG NO.
WA-RD 305.3	

4. TITLE AND SUBTITLE	DATE
LATERAL-LOAD RESPONSE OF TWO REINFORCED CONCRETE PIERS	March 1994
	6. PERFORMING ORGANIZATION CODE
7. AUTHOR(S) Tom O'Donovan, Marc O. Eberhard, Jeffrey A. MacLardy, M. Lee Marsh	8. PERFORMING ORGANIZATION REPORT NO.
9. PERFORMING ORGANIZATION NAME AND ADDRESS Washington State Transportation Center (TRAC) University of Washington, JD-10 University District Building; 1107 NE 45th Street, Suite 535 Seattle, Washington 98105-4631	10. WORK UNIT NO. 11. CONTRACT OR GRANT NO. GC8719, Task 37
12. SPONSORING AGENCY NAME AND ADDRESS Washington State Department of Transportation Transportation Building, MS 7370 Olympia, Washington 98504-7370	13. TYPE OF REPORT AND PERIOD COVERED Final Technical Report 14. SPONSORING AGENCY CODE

15. SUPPLEMENTARY NOTES

This study was conducted in cooperation with the U.S. Department of Transportation, Federal Highway Administration.

16. ABSTRACT

This study was part of a Washington State Department of Transportation (WSDOT) program to assess the vulnerability of multiple-span highway bridges built before 1984. During the first series of static tests (Phase I), discussed in a previous report, a three-span, reinforced concrete bridge was subjected to large lateral loads. In Phase II, described in this report, the researchers greatly reduced the resistance that the abutments provided so that they could evaluate the lateral-load resistance of the piers. The researchers then subjected the piers to large, transverse cyclic displacements with drift ratios of 0.5, 1.0, 2.0, and 3.0 percent.

The piers resisted repeated loadings to a force equal to one third of the bridge's weight. The envelope to the pier's hysteretic response indicated that the system yielded at a drift ratio of 0.7 percent. Whereas the top of the columns spalled at large drift ratios, the damage to the bottom of the columns was limited to flexural cracks. The pier's measured response was compared to that calculated by the researchers, the California Department of Transportation, and the WSDOT. The calculated responses were found to be strongly sensitive to the assumed steel and soil properties.

On the basis of the experience gained in performing the tests, the researchers made recommendations for those planning to perform future tests of large structures. In addition, while acknowledging the limitations of a single series of static tests, the researchers concluded that (1) the tests should serve as a benchmark against which to evaluate proposed analytical models, (2) at an effective acceleration of 0.2g, the seismic damage to the isolated bridge would probably be minor, (3) at an effective acceleration of 0.4g, the piers would likely sustain heavy damage, and (4) the WSDOT should investigate the influence of soil properties on column damage to determine when geotechnical tests are warranted.

17. KEY WORDS	18. DISTRIBUTION STATEMENT
bridge, earthquakes, piers, reinforced concrete, tests, modeling, lateral loads	No restrictions. This document is available to the public through the National Technical Information Service, Springfield, VA 22616

19. SECURITY CLASSIF. (of this report)	20. SECURITY CLASSIF. (of this page)	21. NO. OF PAGES	22. PRICE
None	None	160	

Final Technical Report
Research Project GC8719, Task 37
Bridge Full Scale Test

LATERAL-LOAD RESPONSE OF TWO REINFORCED CONCRETE PIERS

by

Tom O'Donovan
Research Assistant
University of Washington

Marc O. Eberhard
Assistant Professor of Civil Engineering
University of Washington

Jeffrey A. MacLardy
Research Assistant
University of Washington

M. Lee Marsh
Assistant Professor of Civil Engineering
Washington State University

Washington State Transportation Center (TRAC)
University of Washington, JD-10
University District Building
1107 NE 45th Street, Suite 535
Seattle, Washington 98105-4631

Washington State Department of Transportation
Technical Monitor
Harvey Coffman
Bridge Engineer

Prepared for

Washington State Transportation Commission
Department of Transportation
and in cooperation with
U.S. Department of Transportation
Federal Highway Administration

March 1994

DISCLAIMER

The contents of this report reflect the views of the authors, who are responsible for the facts and the accuracy of the data presented herein. The contents do not necessarily reflect the official views or policies of the Washington State Transportation Commission, Department of Transportation, or the Federal Highway Administration. This report does not constitute a standard, specification, or regulation.

TABLE OF CONTENTS

TABLE OF CONTENTS (CONTINUED)

TABLE OF CONTENTS (CONTINUED)

LIST OF FIGURES

LIST OF FIGURES (CONTINUED)

LIST OF TABLES

SUMMARY

This study was part of a Washington State Department of Transportation (WSDOT) program to assess the vulnerability of multiple-span highway bridges built before 1984. During the first series of static tests (Phase I), discussed in a previous report, a three-span, reinforced concrete bridge was subjected to large lateral loads. Resistance to these loads was provided by both the intermediate piers (bents) and the abutments. With the exception of minor column cracking, the Phase I tests did not damage the piers. In Phase II, described in this report, the researchers greatly reduced the resistance provided by the abutments. They then subjected the piers to large, cyclic, transverse displacements. The purposes of the Phase II study were (1) to determine the lateral stiffness, strength, and toughness of the piers; (2) to identify the most vulnerable components; (3) to calibrate an analytical model that was consistent with the observed response; and (4) to compare the calibrated model with models commonly used by bridge engineers.

The piers that were tested were typical of bridges that were constructed in the 1960s. At the intermediate piers, the deck and prestressed girders were integral with a crossbeam. This crossbeam was supported by two 3-foot diameter columns; the columns were in turn supported by 9.5-foot by 9.5-foot spread footings. The columns had little confinement reinforcement, the lap splices were short (35 bar diameters), and the footings had no top reinforcement. Atypically, compacted fill surrounded the 25-foot high columns to midheight.

After the researchers had greatly reduced the resistance that the abutments provided, the piers were subjected to pairs of transverse-displacement cycles at drift ratios of 0.5, 1.0, 2.0, and 3.0 percent. To impose these displacements, the researchers constructed a loading system which consisted of the following: four deadmen, to provide reactions to the applied loads; 128 prestressing cables, to transmit forces among the

load-train components; eight hydraulic rams enclosed in jacking frames, to apply the loads to the cables; and four harnesses, to transfer the cable forces to the piers.

The researchers measured the applied loads, the transverse pier displacements, and the relative rotations of several crossbeam and column cross-sections near the tops of the columns. To observe damage to the bottom of the column, the researchers excavated trenches to access the west pier footings. In addition to monitoring the bottom-of-column curvatures, the researchers installed instrumentation to measure footing translation and rotation for the west pier. The instruments were supplemented by extensive sketches, photographs, and logs.

The piers resisted repeated loadings to a force equal to 400 kips, which corresponded, approximately, to one third of the bridge's weight. The envelope to the pier's hysteretic response indicated that the system yielded at approximately 2 inches of displacement, which corresponded to a drift ratio of 0.7 percent. The pier's resistance deteriorated very little with repeated loading. The measured column curvatures at the top of the column were consistent with each other, whereas the measured curvatures at the bottom of the columns were severely affected by soil that fell into the trenches.

Most of the column damage was restricted to the column tops. At a drift ratio of 0.5 percent, the damage was largely confined to flexural cracks that were less than 0.05 inches wide. At a drift ratio of 1.0 percent, the crack widths increased, and the researchers observed minor flaking of the concrete in compression. The extent of spalling increased markedly at a drift ratio of 2.0 percent, and by the time the piers reached a displacement ratio of 3.0 percent, many of the column longitudinal bars had buckled. In contrast, the bottom of the columns had only a few flexural cracks; the largest cracks were in the range of 3 to 6 feet above the footing.

The pier's measured response was compared with values calculated by the researchers (UW model), the California Department of Transportation (CALTRANS models), and the Washington State Department of Transportation (WSDOT model).

Though the researchers did not distort their model to fit the measured response, they had the advantage of knowing the measured material properties and the observed response. In contrast, the CALTRANS and WSDOT models were more representative of standard practice. The UW model, which used measured steel and soil properties to model the pier's nonlinear response, provided a good fit of the measured response. The accuracies of the CALTRANS and WSDOT models were greatly reduced by inaccurate estimates of the soil and steel properties.

On the basis of the experience gained in performing this study, the researchers determined that many of the load-train and instrumentation concepts should be considered again for future tests. The tests could have been improved by applying the loads with center-hole rams, using larger isolation devices, installing more sensitive instrumentation in the footings, and better protecting the footing instrumentation from falling soil.

The researchers acknowledge the test's limitations. The loads were applied statically, whereas an earthquake would induce dynamic response. Furthermore, the researchers applied only transverse loads to the bridge; an earthquake would subject the bridge to longitudinal and vertical accelerations in addition to transverse accelerations. Perhaps most importantly, the fill that surrounded the columns greatly affected the pier's response; many columns are surrounded by less fill.

Nevertheless, the researchers concluded that the tests should serve as a benchmark against which to evaluate proposed analytical models of bridge response. On the basis of crude estimates of dynamic response, the researchers also estimated the damage that might occur to a similar bridge in which the abutments provided little resistance. At an effective acceleration of 0.2g, the damage would probably be minor. At an effective acceleration of 0.4g, the piers would likely be severely damaged, but would probably not collapse. On the basis of the analyses, the researchers concluded that good estimates of steel and soil properties are essential because the calculated response is sensitive to these

parameters. Given the expense of performing soil tests, the researchers recommended that the WSDOT investigate the influence of soil properties on column damage to determine when geotechnical tests are warranted.

CHAPTER 1

INTRODUCTION

1.1 CONTEXT

Extensive testing has been directed at predicting the resistance of reinforced concrete components to cyclic displacements. On the basis of these tests, many investigators have identified deficiencies in existing reinforced concrete components and have developed retrofit schemes that increase the ability of older bridges to withstand earthquakes. In contrast, researchers have performed few destructive, lateral-load tests of large, structural systems.

In the late 1980s, the Washington State Department of Transportation (WSDOT) decided that it would be better to remove a pair of obsolete reinforced concrete bridges than to renovate them. The bridges, located on I-90 in eastern Washington, spanned an abandoned railroad right-of-way (Figure 1.1). Although eastern Washington is not a seismically active area (1, Figure 1.2), the bridge piers (bents) had deficiencies that were typical of bridges built in the 1960s throughout the state. These deficiencies included insufficient confinement of the column concrete, inadequate reinforcing splices, and a lack of top reinforcement in the footings (Figure 1.3).

Prior to demolition, the researchers applied large lateral loads to the south bridge, while traffic was diverted onto the north bridge. An overview of the tests is provided in Figure 1.4. Phase I, described by Eberhard (2), studied the response of the full bridge system, including the piers, abutments, and superstructure. As shown in Figure 1.5, the bridge was extremely strong and stiff. The bridge resisted 770 kips of applied load, corresponding to 65 percent of the bridge's weight. Because the maximum pier displacement, 0.5 inches, was less than 0.2 percent of the clear column height, the bridge sustained only minimal damage. The tops of the pier columns cracked and, in later

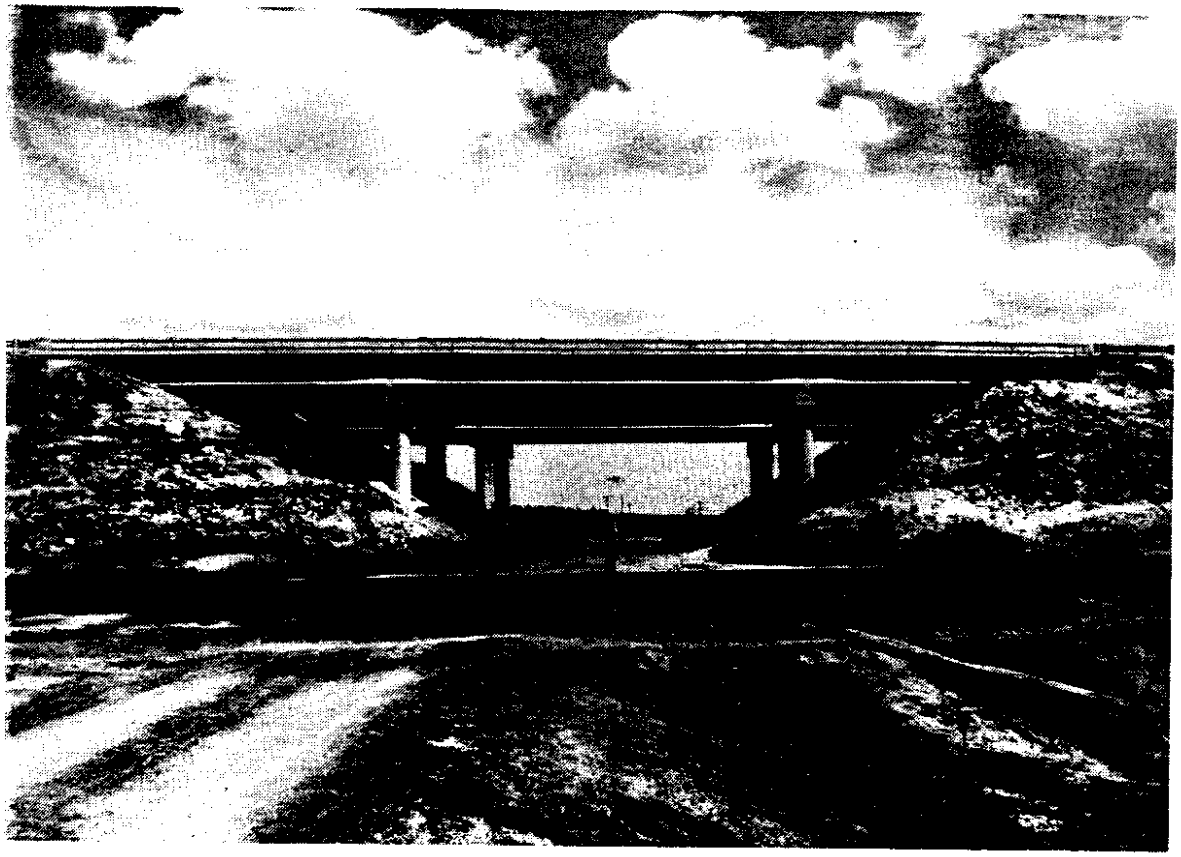

Figure 1.1. Photograph of Bridge

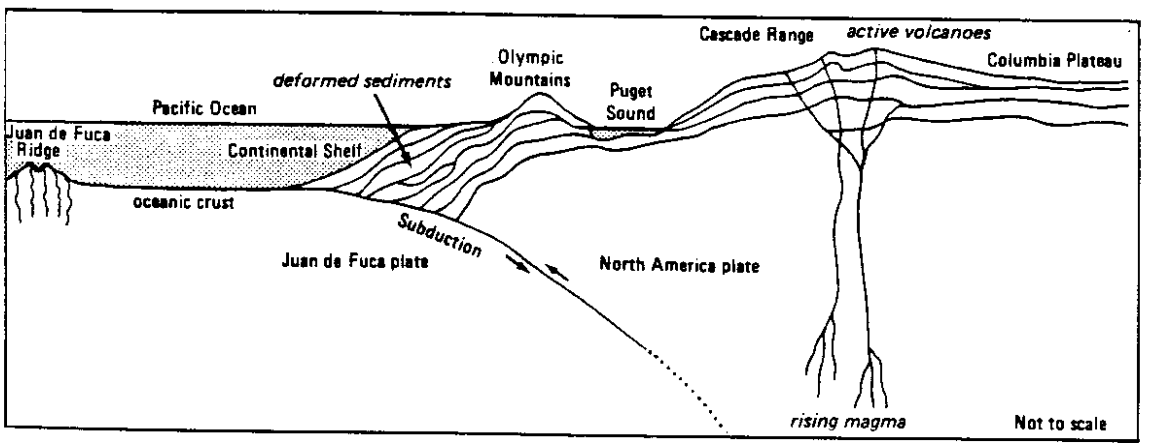

Figure 1.2. Washington State Tectonic Activity (1)

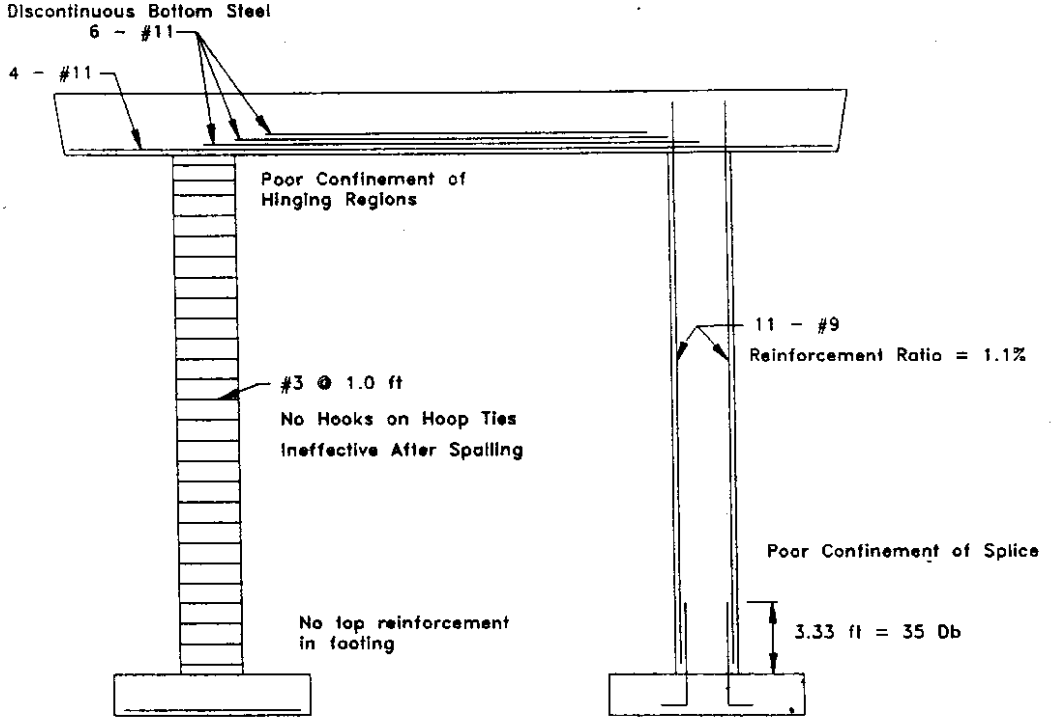

Figure 1.3. Pier Deficiencies

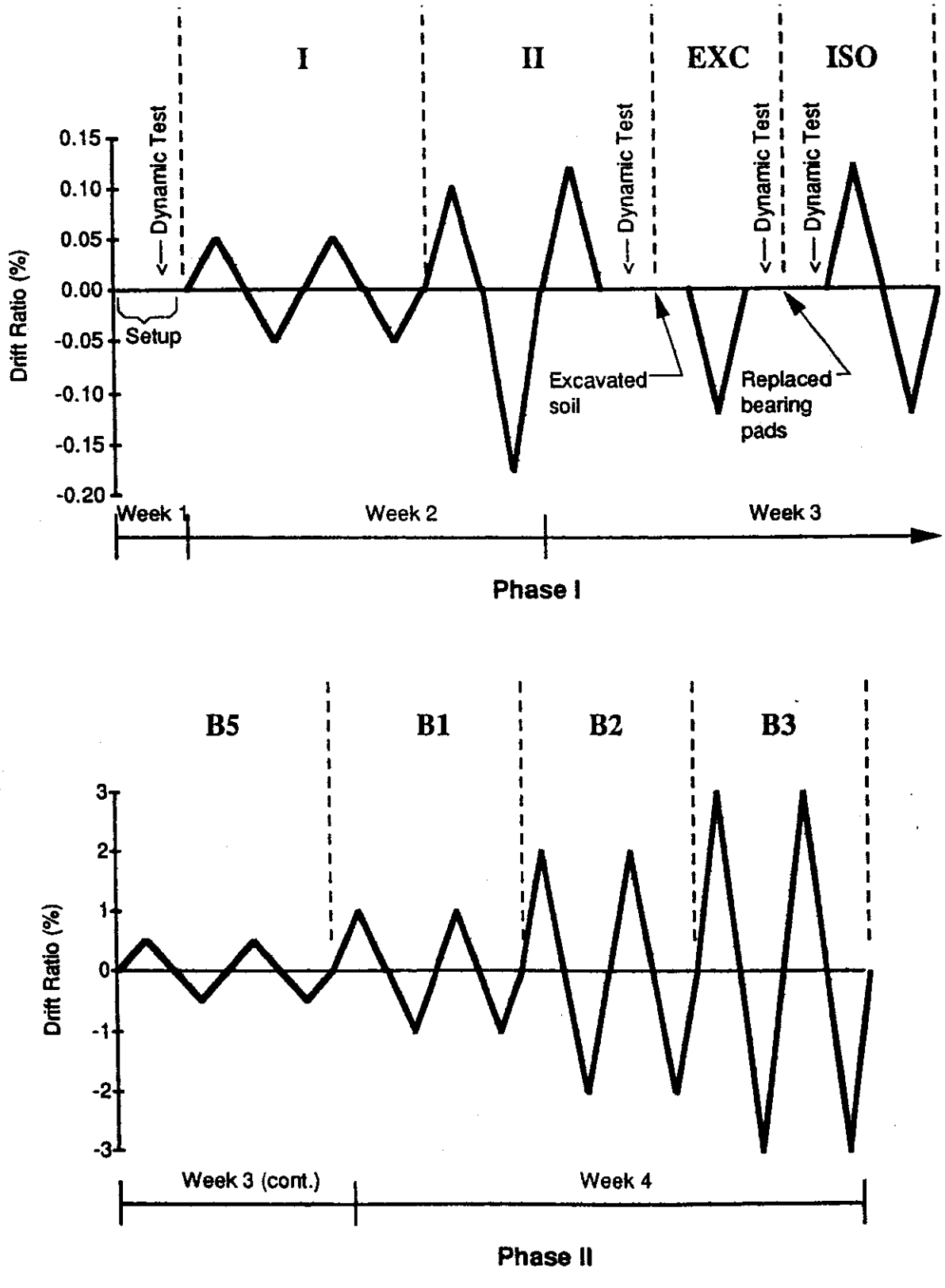

Figure 1.4. Loading History

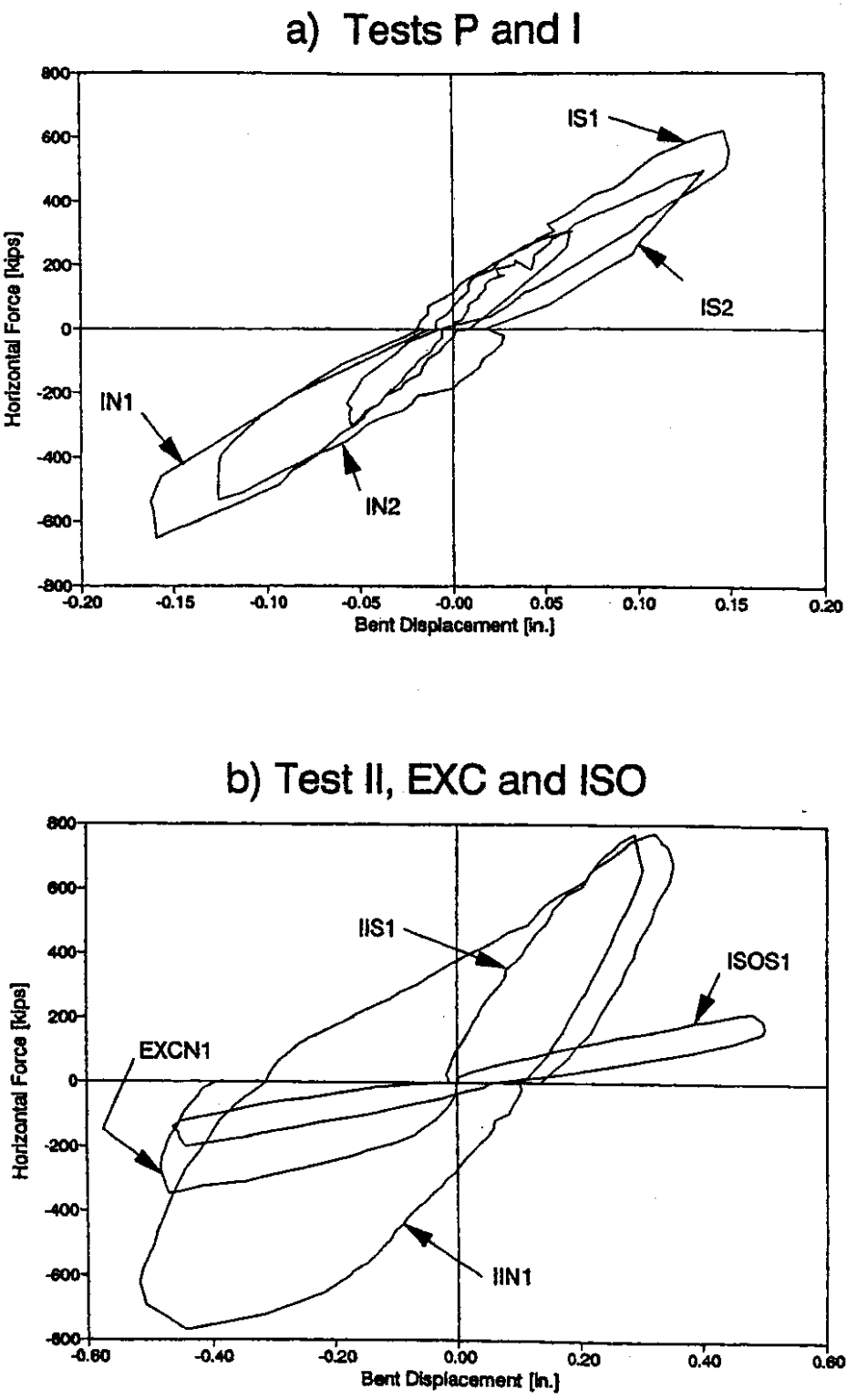

Figure 1.5. Phase I Pier (Bent) Response

cycles, the wingwalls yielded. The researchers attributed the bridge's large strength and stiffness during Phase I to the resistance that the abutments provided. (2)

At the end of Phase I, the superstructure was isolated from the abutments so that the researchers could directly observe the resistance that the piers provided. During Phase II, described in this report, much larger pier displacements were imposed than had been imposed in Phase I (Figure 1.4).

1.2 OBJECTIVES

The Phase II tests and analyses focused on the lateral-load response of the piers (bents). The objectives for the Phase II tests and analyses were the following:

1. to determine the lateral-load stiffness, strength, and toughness of the piers;
2. to identify the most vulnerable structural components of the piers;
3. to develop and calibrate an analytical model that was consistent with the observed response of the piers; and
4. to compare the calibrated model with models commonly used by bridge engineers.

1.3 SCOPE OF REPORT

This report addresses Phase II only. Extensive inspection and laboratory tests were performed to document the bridge's properties. Chapter 2 describes the bridge, as well as laboratory tests of steel coupons, concrete cores, and bearing pads that were recovered from the bridge. The researchers installed a loading system to displace the 1.2-million-pound bridge. The design, construction, and operation of this load train are discussed in Chapter 3. To eliminate the lateral-load resistance that the abutments provided, the superstructure was isolated from the abutments. The isolation procedure is described in Chapter 4. Chapter 5 describes the instrumentation and data acquisition system, and Chapter 6 discusses the data reduction procedures. The measured response histories and the observed damage to the structure are reported in Chapter 7. A series of nonlinear, finite element models was formulated and analyses were performed by the

University of Washington, California Department of Transportation (CALTRANS), and WSDOT to study the behavior of the structure. These analyses are detailed in Chapter 8. The implications of these tests and analyses are reported in Chapter 9.

CHAPTER 2

DESCRIPTION OF BRIDGE

This chapter reports the bridge's geometry and reinforcing details, as well as the measured properties of the concrete, reinforcing steel, and soil. The structural plans and excerpts of the designers' calculations are given in Appendices A and B. Other sources that document the design and construction of this bridge are the 1964 Washington State Department of Transportation Standard Specifications (3) and the 1961 American Association of State Highway Officials Standards (4).

The bridge was located in eastern Washington state, 188 miles east of Seattle and 13 miles east of the city of Moses Lake. It was designed in late 1964 and early 1965; construction began in 1965 and was completed in 1966.

2.1 GEOMETRY AND REINFORCING DETAILS

The 142-foot long bridge had three spans, two intermediate piers (bents), and two abutments (Figures 1.1 and 2.1). The central span was the longest at 60 feet, and the end spans were 41 feet each. The crossing was on a 12.8 degree skew. The primary structural components of the bridge were the deck, girders, diaphragms, crossbeams, columns, footings, and abutments. Each component is addressed in the following paragraphs.

The deck was 6.5 inches thick and was reinforced transversely with #5 bars, spaced at 5.5 inches. The longitudinal deck reinforcement, consisting of #4, #5, and #7 bars at various spacings, was continuous over the bents. The construction specifications mandated monolithic placement of the deck concrete. The deck was overlain by 3 to 3.5 inches of asphalt. The deck was crowned so that the roadway centerline would be 4 inches higher in elevation than the edge of the bridge.

The girders were precast, prestressed, 3.5 feet deep, spaced 6 feet 10 inches on center and had 8-inch deep intermediate diaphragms at midspan. At each pier, the girders

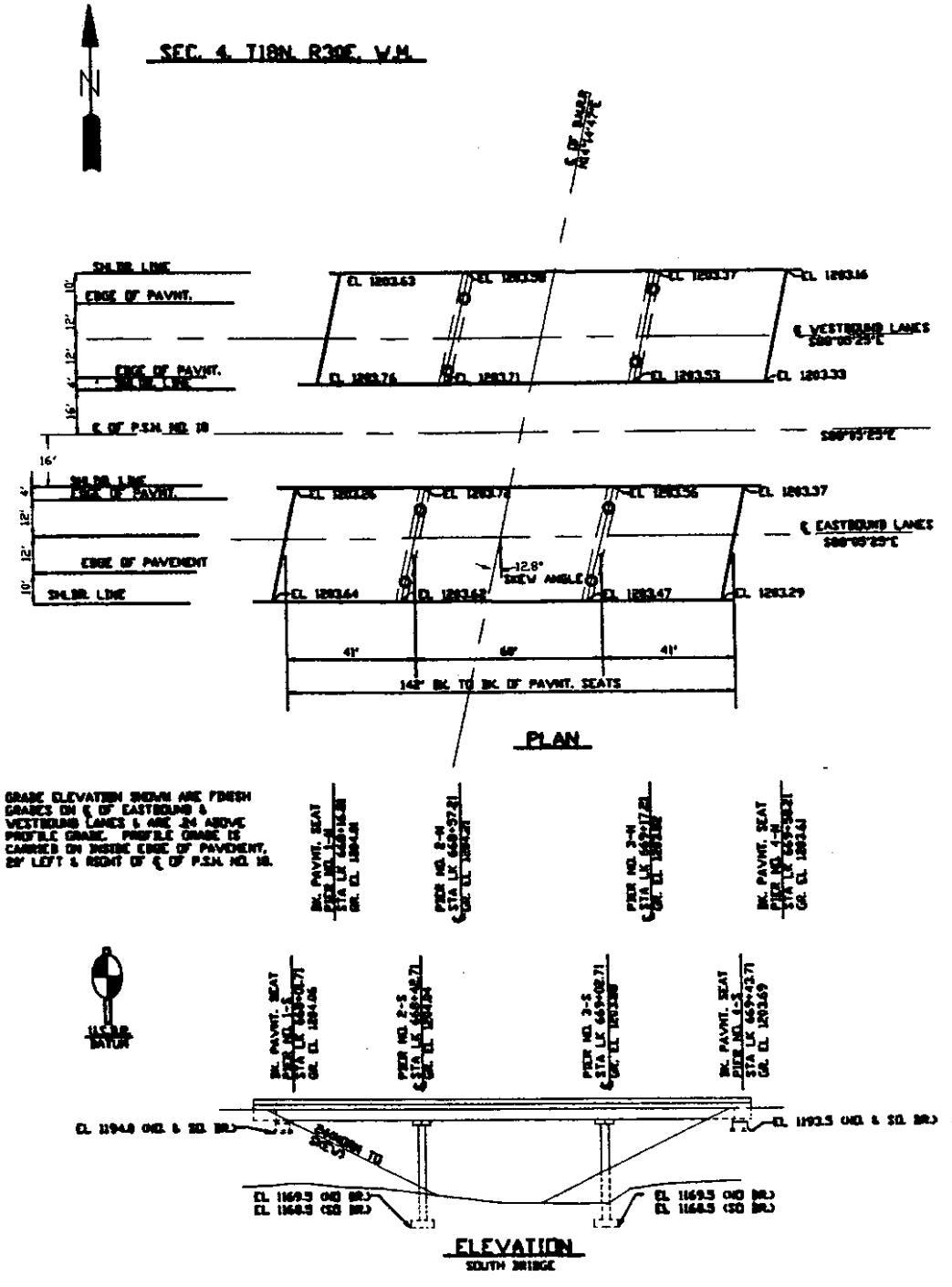

Figure 2.1. Plan and Elevation of Bridge

were embedded 2 inches into a cast-in-place diaphragm. Four prestressing strands in the bottom of each girder extended into the diaphragm and were bent 90 degrees. The total extension, including the hook, was 14 inches (28 strand diameters). The heavily reinforced diaphragm was 1-foot thick and extended from the bottom face of the deck slab to the top of the crossbeam.

The crossbeam was located 4 inches below the bottom flange of the prestressed girders. The crossbeam was 3-foot deep and 3.5-foot wide (Figures 1.3 and 2.2). The crossbeam's heavy reinforcement consisted primarily of #10 and #11 bars at the top and bottom. The crossbeam was crowned at the roadway centerline and contained #5 stirrups at various spacings (Figure 2.2).

The pier crossbeams were supported by two 3-foot diameter columns, which were reinforced longitudinally with eleven #9 bars. This longitudinal steel extended 30 inches into the crossbeam. The column's transverse reinforcement consisted of #3 hoops at 1-foot spacings (Figures 1.3 and 2.2). The ends of the hoops overlapped by 14 inches, but the hoops had no hooks. The equivalent spiral reinforcement ratio for this arrangement of hoops, 0.14 percent, was extremely low in comparison to current requirements. The specified cover over the reinforcing bars was 2 inches.

Reinforcing bar locations within the columns were confirmed with a pacometer prior to testing. Further confirmation of the bridge's conformance to the plans was provided when the concrete cover spalled during the tests. At the end of the tests, the longitudinal bars and some of the hoops were visible.

When the researchers excavated trenches to observe the bases of the columns, they found that the bottom 12 inches of the columns had an octagonal cross section. It is likely that an octagonal collar had been used to form the bases of the columns. The column footings were 2-foot thick and 9.5-foot square (Figure 2.2). Eleven #9 dowels extended a minimum of 3 feet 4 inches (35 bar diameters) upward from the footing to lap with the column steel. In the footings, these dowels were bent to 90 degrees and

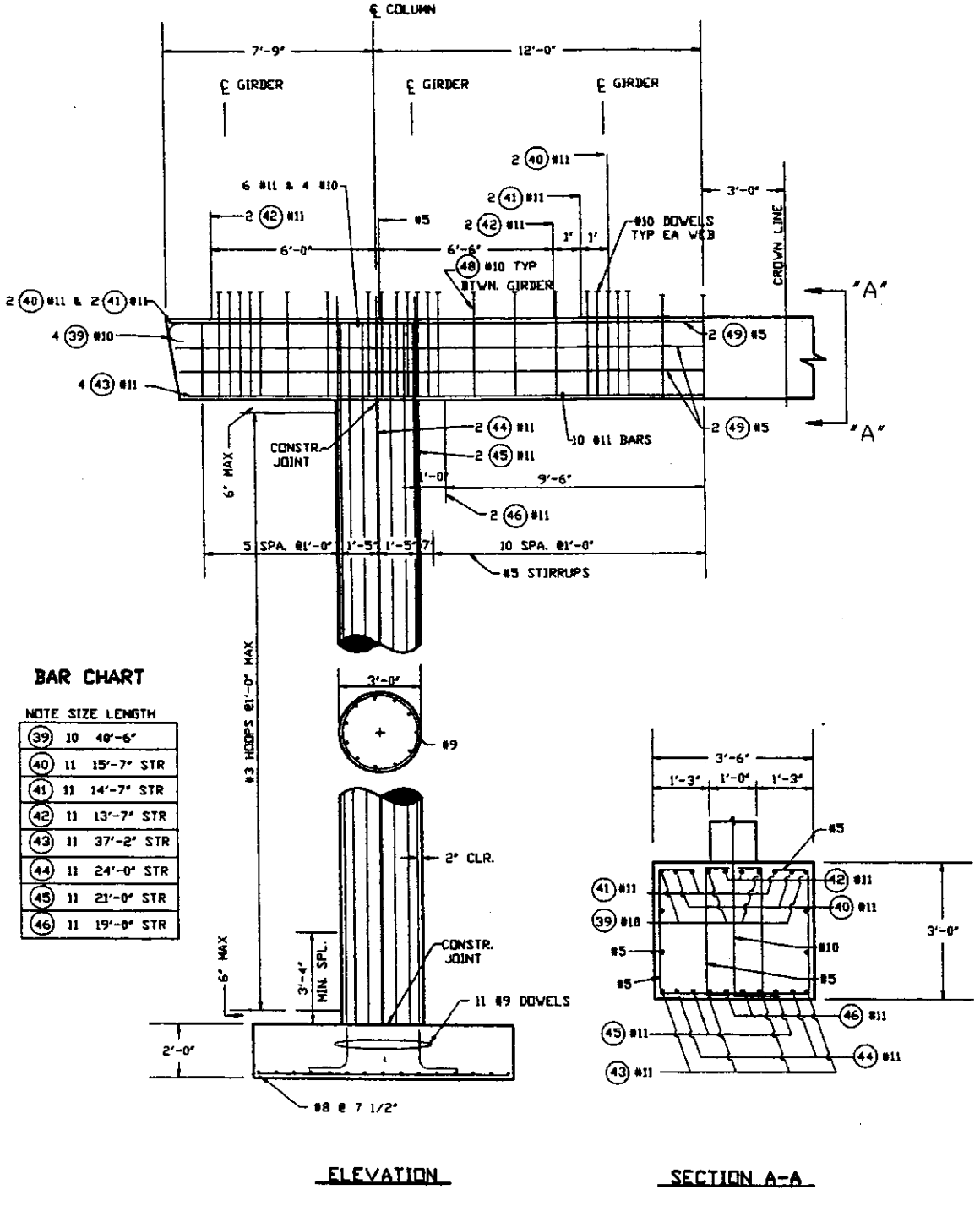

Figure 2.2. Pier

extended 23 inches (20 bar diameters) horizontally. The footings were reinforced with #8 bars at 7 1/2 inches running both ways on the bottom. The footings had no shear or top reinforcement.

At the abutments (Figure 2.3), the girders terminated in a 1.5-foot thick endwall. The endwall rested on six elastomeric bearing pads, which measured 10 5/8 x 10 5/8 x 7/8 inches. Each pad was aligned with one of the prestressed girders and was placed directly below steel plates that were embedded in the bottom face of the endwall. The pads were surrounded by expanded polystyrene. The pads rested on a 2.5-foot wide pedestal. At the ends of the endwalls, 1-foot thick, 4-foot high wingwalls extended 5.5 feet along the edge of the pavement. There was no approach slab.

2.2 CONCRETE

The cast-in-place concrete for the superstructure was WSDOT class AX mix, which had a specified 28-day compressive strength of 4,000 psi. After the structural tests had been completed, 12 concrete cores were taken from the columns. Two to four cores were obtained from the mid-height of each column to avoid cracks developed during testing. The cores were 3.75 inches in diameter and were cut to 8-inch lengths for laboratory testing.

The cores were tested in accordance with American Society for Standards and Material Standard ASTM C39 (5); the measured compressive stress-strain relationships are shown in Figure 2.4. The measured compressive strength greatly exceeded the 4,000 psi specified strength. The mean compressive cylinder strength, f'_c, was 6,400 psi, and the mean modulus of elasticity was 4.7×10^3 ksi. The measured elastic modulus was consistent with the measured compressive strength. Combining the measured compressive strength with the American Concrete Institute 318-89 expression for the elastic modulus produced an elastic modulus equal to 4.6×10^3 ksi. (6) The flexibility of the testing machine made it impossible to measure the descending portion of the stress-strain curve.

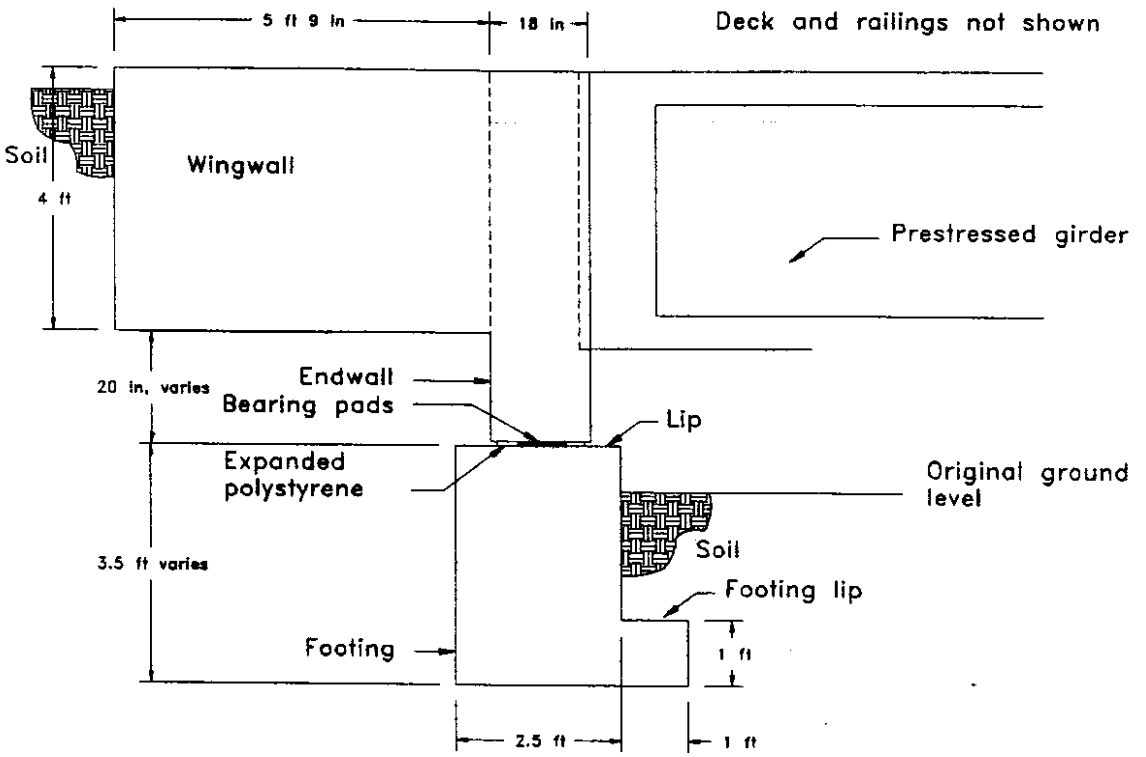

Figure 2.3. Abutment

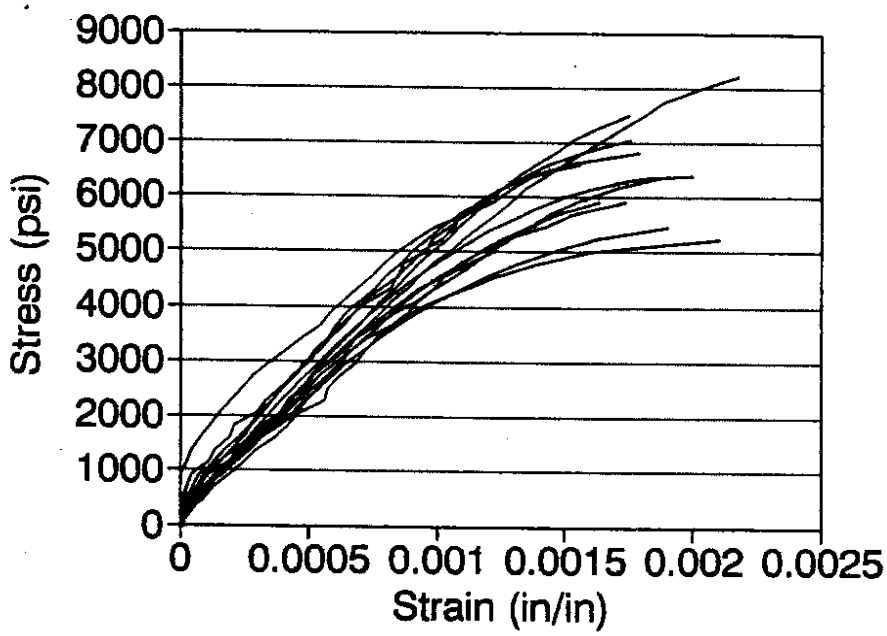

Figure 2.4. Compressive Stress-Strain Relationship for Concrete

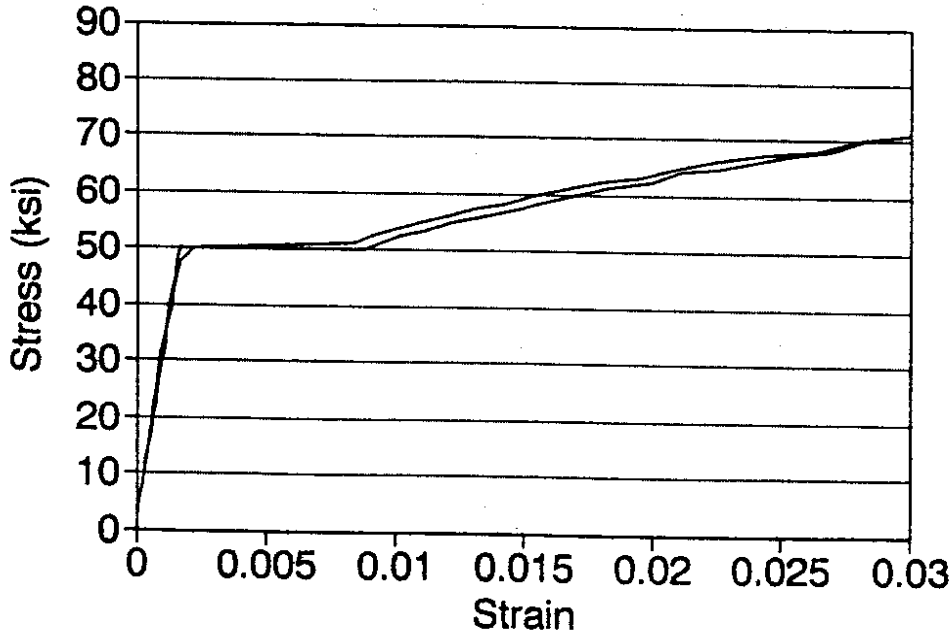

Figure 2.5. Tensile Stress-Strain Relationship for Reinforcement

Forstie and Schnormeir found that small cylinders of high strength concrete with strengths of over 5,000 psi overestimate standard cylinder results by about 10 percent. (7) However, cores generally underestimate cylinder tests by about 15 percent. (6) Therefore, the measured strengths were assumed to be similar to those that would have been obtained from standard cylinders.

2.3 REINFORCING STEEL

The reinforcing steel was specified to be Grade 40. After testing had been completed, two 24-inch long specimens of longitudinal reinforcing steel were recovered from mid-height of the northeast and southeast columns. In these regions, little cracking and no signs of yielding were observed. The specimens were cut free of the concrete with diamond and carborundum blades on a gas-driven, hand-held rescue saw. The specimens were not damaged during the removal process.

The reinforcing steel was tested in accordance with ASTM A370 (5); the resulting stress-strain curves for both specimens are shown in Figure 2.5. The mean yield strength was 51 ksi, the mean ultimate strength was 86.3 ksi, and the mean modulus of elasticity was 29.5 x 10^3 ksi. These properties are consistent with those reported by Mirza and MacGregor. (8)

2.4 SOIL

Compacted backfill surrounded the columns to a height of about 12 feet above the footings (about mid-height). The backfill was a dry, silty sand, with a high percentage of hard cobbles from 1 to 6 inches in diameter. A measure of the soil's cohesion was that vertical faces cut into the soil (over 15-foot high and 20-foot wide) did not slump in over 2 months. This slope stability was expected because the bottom of the footings was located above the water table, and the soil was protected from rainwater by the deck above it. Though the soil beneath the footings was not exposed during the test, the

original borings indicated that the soil also was a sandy silt, with an average blow count of 30. The boring logs are given in Appendix A.

One year after the tests, the researchers collected undisturbed soil samples from the bridge site. On the basis of its low liquid limit (24.2 percent) and low plasticity index (3.5 percent), the soil was classified as a low plasticity silt. The measured soil properties are summarized in Table 2.1. Undrained triaxial test results (Figure 2.6) indicated that the angle of internal friction was approximately 38 degrees.

Table 2.1. Soil Properties

Item	Result
General Description	Medium-Dense, Silty Sand; low dry strength
USCS classification	ML, low plasticity silt
Sieve Analysis	Approximately 70% fines and 30% coarse grained
Color	Tan; uniform
Dilatancy	Medium to medium fast
Plastic Limit, PL	20.7
Liquid Limit, LL	24.2
Plasticity Index, PI	3.5
Undisturbed Samples:	
Unit Weight, In-Situ	110.1 pcf
Unit Weight, Dry	99.2 pcf
Void Ratio, e	0.67
Porosity, n	0.40
Water Content, In-Situ	11%
Degree of Saturation, S	43.8%
Standard Proctor Test:	
Unit Weight, Max. Dry	105.0 pcf
Unit Weight, at 95% Compact.	99.8 pcf
Unit Weight, at 95% Compact. &	111.0 pcf
Optimal Water Content	
Water Content, Optimal	17%
Undrained Triaxial Tests:	
Initial Tangent Compressive	
Elastic Modulus	1600 psi at 7 psi confining stress (average)
Strength	40 psi at 7 psi confining stress (average)
Strength	70 psi at 14 psi confining stress (average)

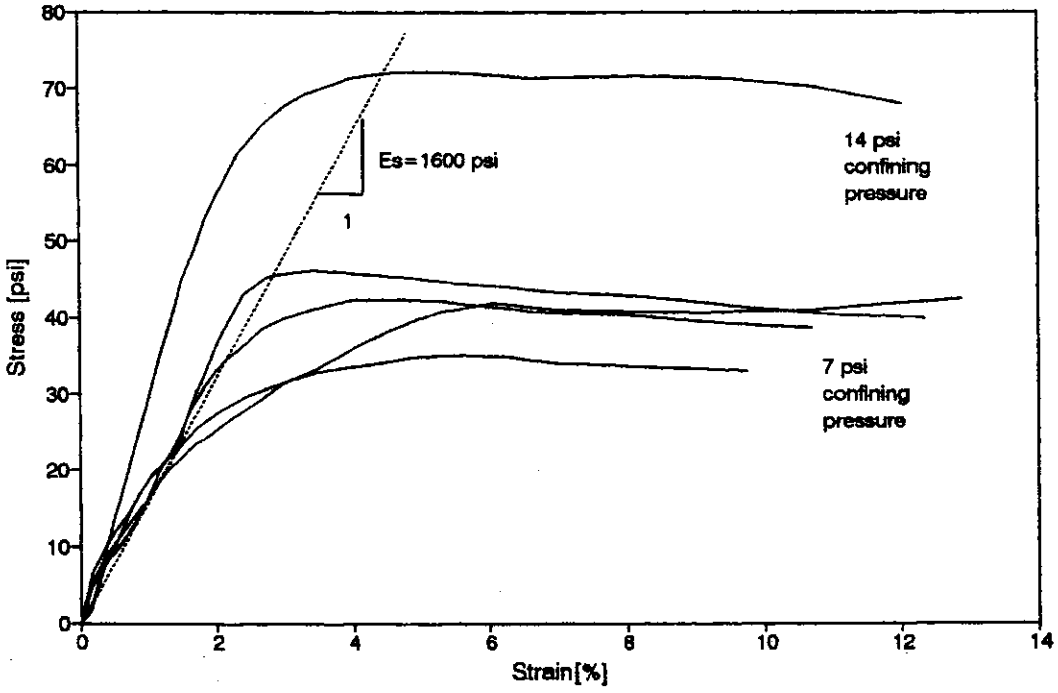

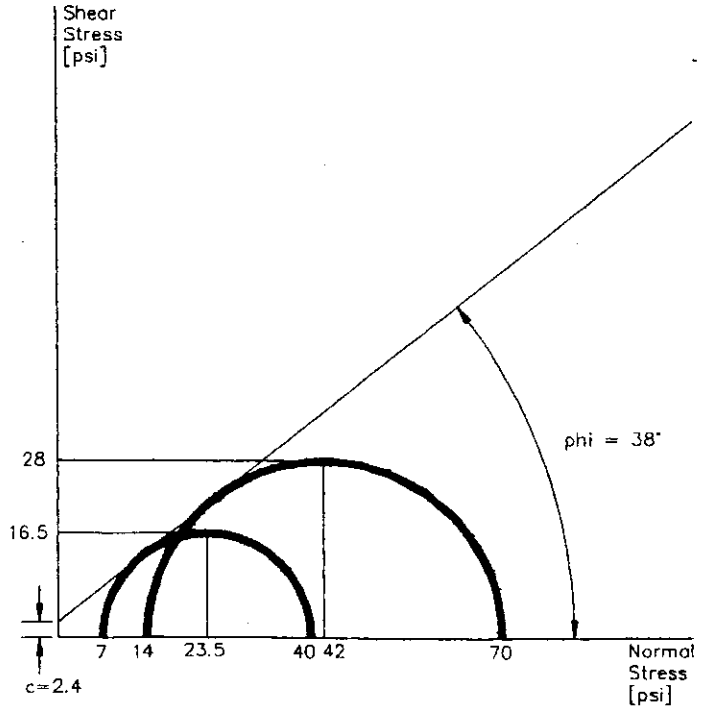

Figure 2.6. Triaxial Test Results

CHAPTER 3

LOADING SYSTEM

A loading system was constructed to impart large, cyclic, transverse loads to the piers. This chapter describes the design, installation, and operation of the system; the final section suggests improvements to the loading system's design.

3.1 DESIGN

The design of the load train was constrained by time restrictions, funding limits, and site limitations. To minimize inconvenience to contractors and to the public, WSDOT limited the time during which the tests could be performed. The researchers were required to complete their tests within 30 days of the day traffic on the south bridge was rerouted to the north bridge (Figure 2.1). To satisfy this constraint, the researchers designed a loading system that could be installed before traffic was rerouted.

Before selecting a loading system, the researchers considered several systems. Loading systems in which a load train alternately carried compression and tension were found to be expensive because of the need to prevent compressive instability in the load train. The disadvantage of tension-only systems was that reactions had to be provided on both the north and south sides of the structure. Initial cost estimates indicated that construction of large reaction towers would be expensive. In addition, steel-pile and sheet-pile reaction systems were found to be expensive because of the mobilization costs. On the basis of discussions with contractors, a deadman system was found to be the most economical way of providing large, horizontal, reaction forces.

Site limitations were particularly difficult to overcome. These limitations included obstruction by a county road, the bureaucratic impediments of installing the system on private land, the need to avoid disturbing the north bridge, and a high water table. Figure 3.1 shows some of these site limitations.

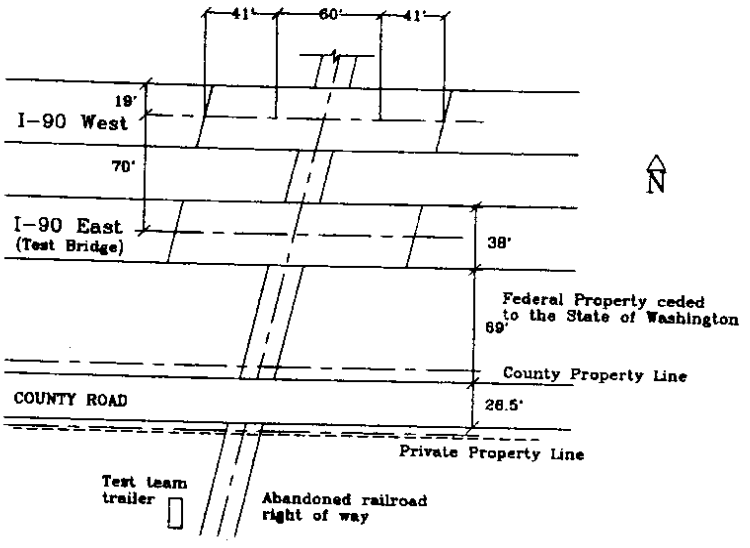

Figure 3.1. Site Plan

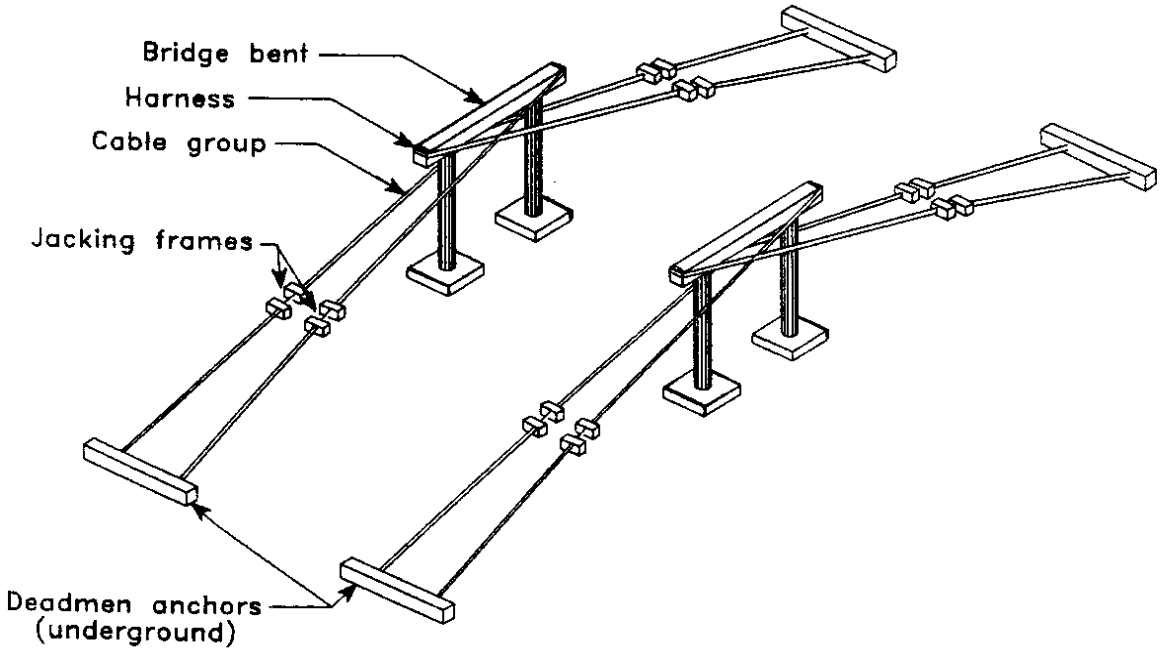

Figure 3.2. Loading System Schematic

Figure 3.2 shows the four basic components of the loading system. The deadmen provided reactions to the applied loads. The jacking frames contained the hydraulic jacks that provided the loading force. The cable groups transferred the load among the components, and the harnesses transferred the cable forces to the pier crossbeams. Details of the deadmen, cable groups, jacking frames, and harnesses are discussed in the following subsections.

Deadmen

The purpose of the deadmen was to provide reactions to the applied loads. The deadmen's design was based on a design load of 300 kips per anchor, estimated soil properties, and the observed water-table depth. The 600-kip working load for the system had been determined on the basis of preliminary estimates of the structure's strength. The soil properties were estimated from borings shown on the bridge plans. The borings indicated that the soil was a sandy silt with an average blow count of 30 (Appendix A). The soil classification was confirmed when researchers excavated the soil in critical locations to depths of 3 to 4 feet. These excavations also indicated that, near the south-side deadmen, the water table was only 2 feet below the ground surface.

With design equations proposed by N.K. Ovesen and H. Stromann (9), the researchers determined that a 25-foot long deadman at a depth of 10 feet and with a vertical bearing surface of 3 feet would provide adequate resistance to the applied loads (Figure 3.3). In proportioning the steel beams, the concrete strength was neglected, and the researchers assumed that the soil resistance was uniform. Holes were cut in the steel beam web to ensure that voids would not form beneath the beam during concrete placement. To support the beam at the correct angle and elevation in the trench, steel reinforcing bars were welded to the beam. Steel tubes, through which the prestressing strands were to be inserted, were welded to the steel beam to prevent the concrete from bonding to the prestressing cables. Such bonding might have cracked the concrete

because of differences in strain between the cables and concrete. Stiffeners were added to the beam to prevent local buckling and to confine the concrete.

Cable Groups

Steel prestressing cables transmitted the load among the components of the loading system (Figure 3.2). One set of cables ran from the deadmen to the jacking frames, and another set connected the jacking frames to the pier crossbeam harnesses. The prestressing strands were new, one-half-inch in diameter, and had a nominal strength of 270 ksi. It was necessary to use 32 strands, working in parallel, to provide sufficient stiffness and strength. At the load train's design capacity of 800 kips, the nominal stress in each cable was 163 ksi, which corresponded to 60 percent of the steel's nominal strength. Standard three-wedge, barrel, prestressing chucks anchored the strands at each end.

The 14-degree slope of the cables was selected as a compromise among competing goals. The researchers wanted to maximize the horizontal transverse force, minimize the compressive axial downward force, and conform to the site's limitations. The vertical component of the applied load (200 kips) increased the column compressive stress by only 50 psi. Figure 3.4 shows the dead load on each column, the column vertical load, and the column horizontal load as functions of the applied force. The excavation permit for the county road stipulated that the cables be buried at least 36 inches below the county road. In addition, the cables had to clear the north bridge's footings (Figure 3.5).

Jacking Frames

Solid rams were used to place the cables in tension because it was difficult to obtain center-hole, post-tensioning jacks. Consequently, the researchers had to surround the jacks with a frame to transfer the ram forces to the cables and to prevent load-train instability (Figure 3.6). The 6-inch stroke of the rams posed another difficulty. The sum of the slack in the cable, the elongation of the cable under load, the deadmen's

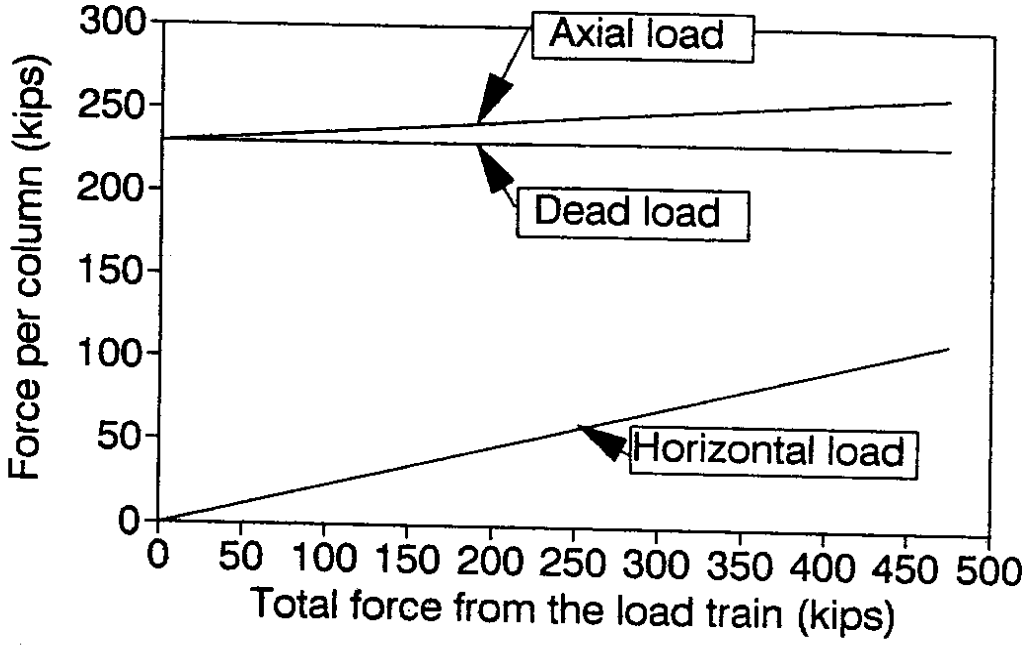

Figure 3.4. Effect of Applied Load on Column Axial Load

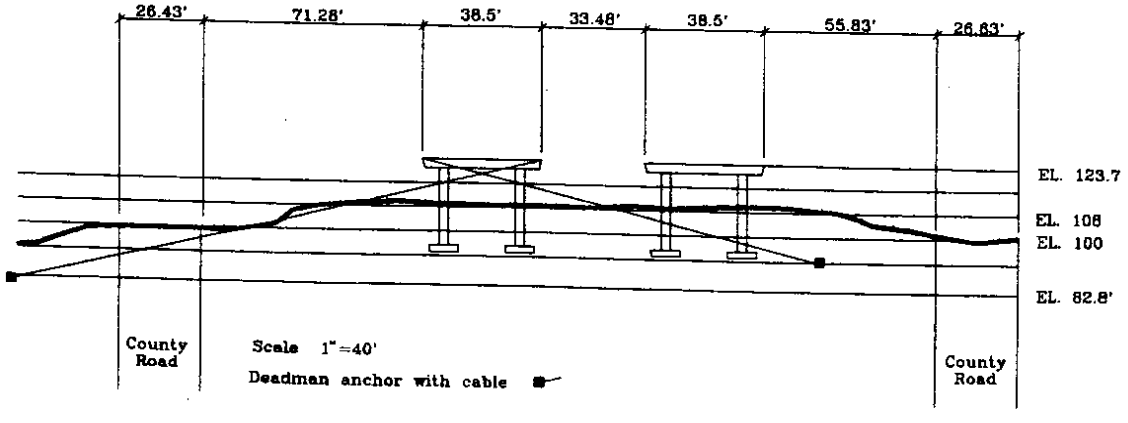

Figure 3.5. Site Profile

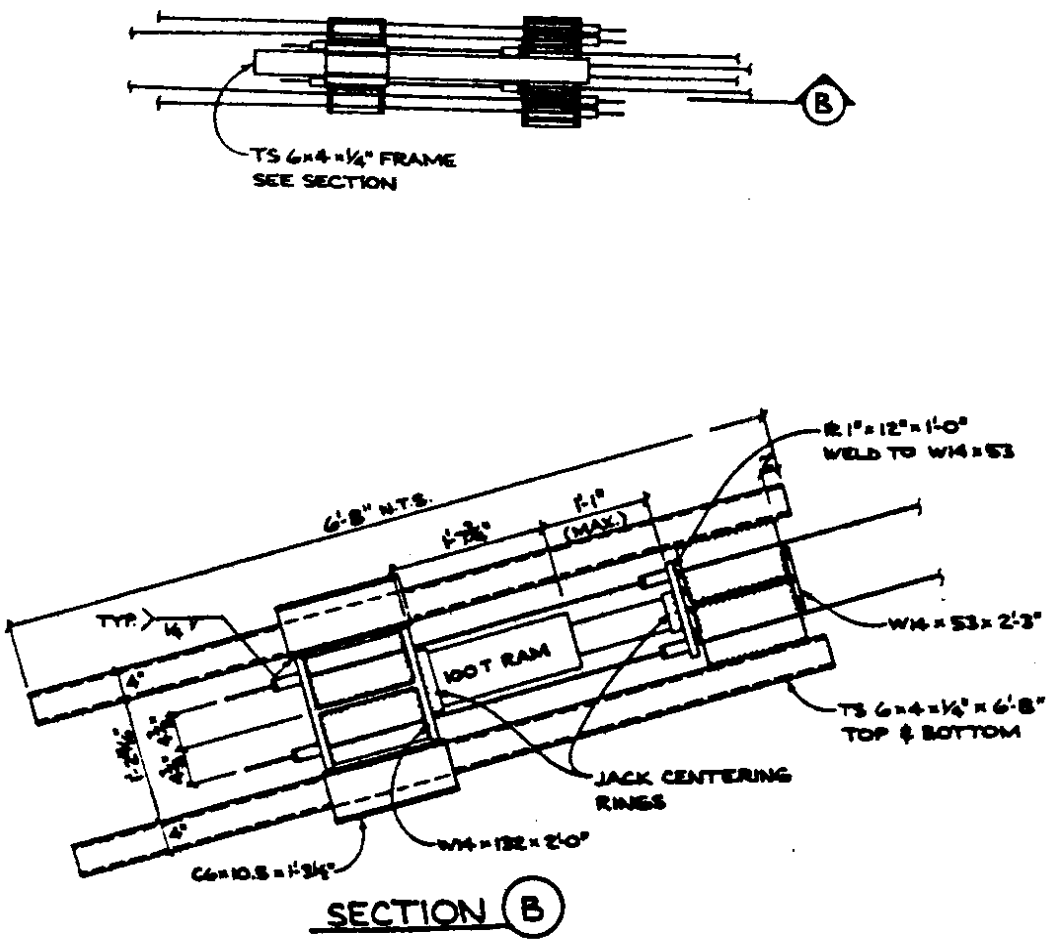

Figure 3.6. Jacking Frame Detail

displacement under load, and the bridge's deformation greatly exceeded the 6-inch ram stroke. To apply large displacements to the structure, the frames were designed to maintain tension in the cables while the rams were readjusted.

Harnesses

Harnesses transferred the cable forces to the pier crossbeams, as shown in Figure 3.7. To prevent crushing of the pier crossbeams by the cable forces, back-to-back channel sections distributed the forces across the crossbeam face. To prevent buckling within the harnesses, bearing stiffeners were used extensively, and concrete was placed between the stiffeners.

3.2 INSTALLATION

Preparation

Installation of the loading system involved considerable construction effort, and, as with any construction activity, safety was a primary concern. To address this safety concern, a site hazard analysis was prepared and a safety plan was designed before construction began. The plan addressed protective measures such as work rules, traffic control, eye/ear protection, and safety harnesses for high-level work. Despite the fact that the workforce was relatively inexperienced, no accidents occurred.

Because the site was remote, extensive site support was required. It was necessary to provide the site with electrical power, a trailer, phone lines, toilet facilities, tools, and support vehicles. In addition, before the load train was installed, a team surveyed the site with an electronic distance meter. The survey provided accurate information about the site's characteristics and the extent to which these characteristics differed from those shown on the plans. The survey also established the vertical and horizontal control needed to install the load train.

Deadmen

The researchers had planned to excavate a 3-foot wide, 10-foot deep, 25-foot long trench for each deadman (Figure 3.8). Sloping trenches were to be excavated to provide

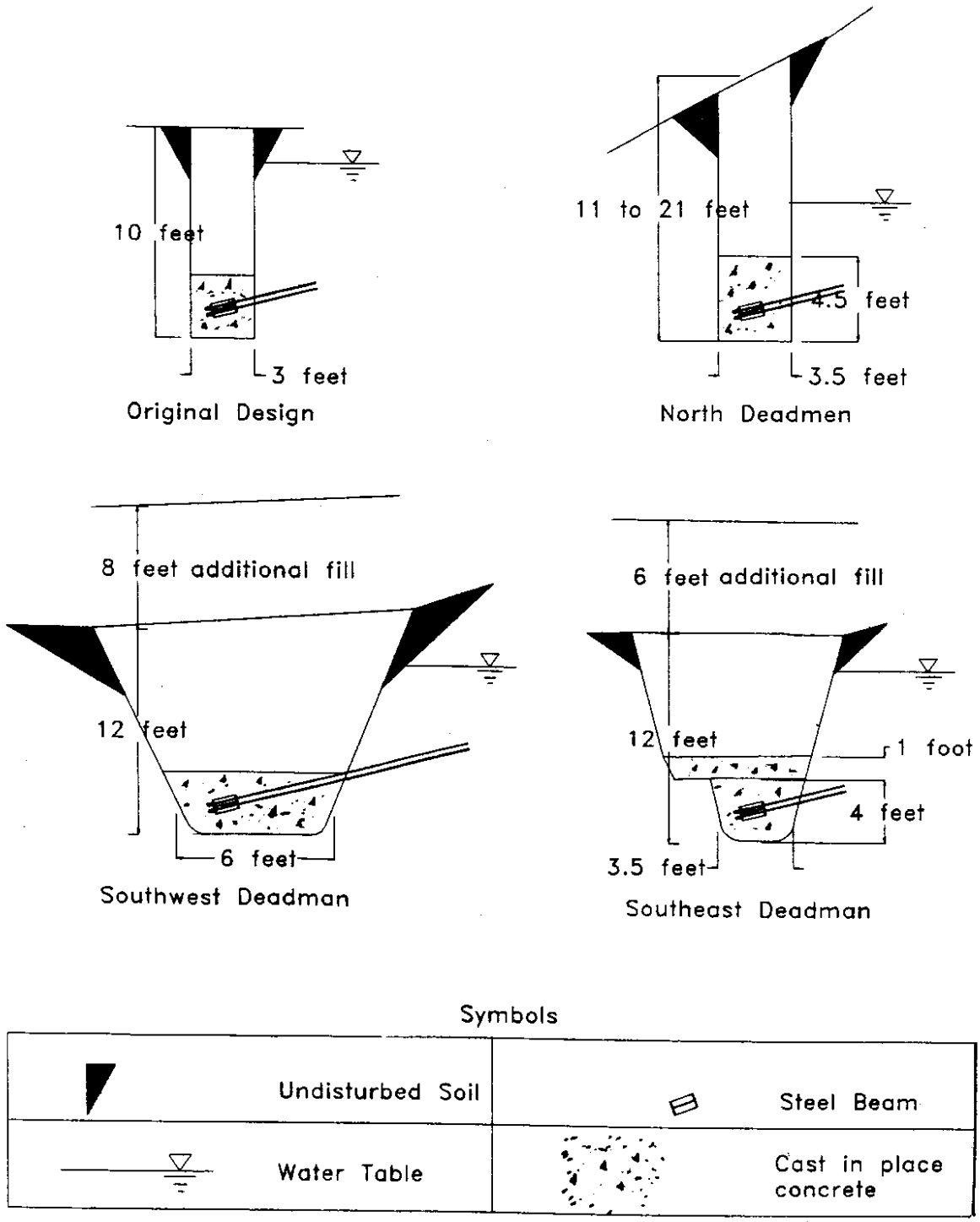

Figure 3.8. Excavations to Install Deadmen

clearance for the prestressing cables. Then, the steel beam would be lowered into the trench, with the cables already attached, until the rebar legs supported the beam at the bottom of the trench. After alignment, concrete would be placed into the trench and vibrated. Finally, the excavation would be backfilled. To reduce the cost and time required to install the deadmen, the trenches were not to be shored and, consequently, personnel were not to be allowed to enter the trenches. To reduce slaking into the trenches, the trenches were not pumped.

The trenches were excavated with a JD510 wheeled backhoe with a 3-foot wide excavation bucket. Though some cave-in had been expected, the researchers had felt that the trenches would hold up long enough to install the deadmen. This expectation was overly optimistic for locations in which the water table was high. As shown in Figure 3.8, a large excavation was required to install the southwest deadman. On the southeast deadman, benching reduced the cave-in problem, and on the north side, a lower water table eliminated the problem. To help ensure the south deadmen's capacity, extra concrete was placed in the trenches, and after backfilling, additional fill was placed on top of the deadmen.

Alignment of the cables was difficult. The cables became twisted while the beams were lowered into the trenches, and it was impossible to safely and completely untangle them. The problem became more manageable with each successive installation; however, the twisted cable problem was never completely eliminated. Nonetheless, aside from soil heaving, the vertical cable misalignment did not affect the test. Once the beams and cables had been prepared, four days were required to install the four deadmen.

Cable Groups

Before the deadmen trenches were excavated, the cables that connected the deadmen to the jacking frames were cut to length, threaded into the deadmen beams, and secured with prestressing chucks. To prevent the cables from being pushed through the chucks during installation, cable clamps were put on the strands at the location where

they threaded into the beam. To install the upper cable groups, the researchers lifted individual cables to the elevation of the crossbeam and threaded them through the harnesses, which had already been positioned.

Jacking Frames

Sloped, compacted soil platforms were constructed to support each jacking frame at the appropriate angle and elevation. The platform elevations were selected such that the jacking frames would lift off the platforms when the cables were put into tension. Therefore, the ground surrounding the jacking frames did not inhibit the jacking frame's movement.

The jacking frames arrived on-site with the jacks already installed. Following installation of the deadmen and the lower cable groups, the jacking frames were placed on the platforms, the lower cables were threaded through the jacking frames, and the cables were secured with prestressing chucks. Then, hydraulic hoses were installed so that each bent's pair of jacks could operate from a single pump. The jacks were calibrated in the same pairs that they operated in during the test.

Harnesses

The harnesses arrived on-site with the internal concrete already in place (Figure 3.7). They then were lifted onto the pier crossbeams with a hydraulic crane. To prevent the harnesses from falling off the crossbeams, the researchers secured them to the crossbeams with steel all-thread. The large amount of welding that occurred during fabrication had deformed the harnesses, and as a result, the harnesses did not fit flush against the crossbeam. The original plan to account for this expected misfit was to seat the harnesses in hydrostone; however, this operation proved to be too difficult. Instead the harnesses were allowed to deform under load until they fit snugly onto the crossbeam. Despite the misfit, the crossbeam concrete did not spall during the test.

3.3 OPERATION

In each half cycle, a target displacement was imposed on the piers in one direction, and then the load was slowly removed. At the end of each half cycle, the pumps were disconnected, moved to the other side of the bridge, reconnected, and the next half cycle of loading was applied. The duration of one half cycle ranged from two to six hours; one or two cycles were completed each day.

Increments in applied force were selected by monitoring the bent displacement. Directions to increase or reduce the pump pressure were transmitted from the data acquisition trailer to the pump operators with a wire intercom system. The pump operators monitored pressures and reported pressure values to the trailer for recording. When the rams approached maximum extension, the jacking frames held the applied load while the rams were retracted. Such "recycling" occurred two to four times during a typical loading sequence. For unloading, more cycles were required than had been required for loading. During unloading, the rams were recycled from three to six times until the strands had sufficient slack to remove the chucks.

Jacking Frames

Operation of the jacking frames during loading and unloading was tedious because of the ram's limited stroke. Several steps were involved in loading the structure, as illustrated in Figure 3.9. First, the cables were pulled as tight as possible by hand, and the rear chucks were pushed forward and locked (forward was toward the bridge). Second, the rams were extended to tighten the cables. When the ram had reached the end of its stroke, the front chucks were pushed forward and locked. This allowed all the cable force to be transferred through the W14 x 53. Third, while pressure was released in the rams, the W14x132 was pulled forward with a chain hoist until the ram was completely retracted. Finally, the rear chucks were locked, and the cycle was repeated until the structure reached the target displacement.

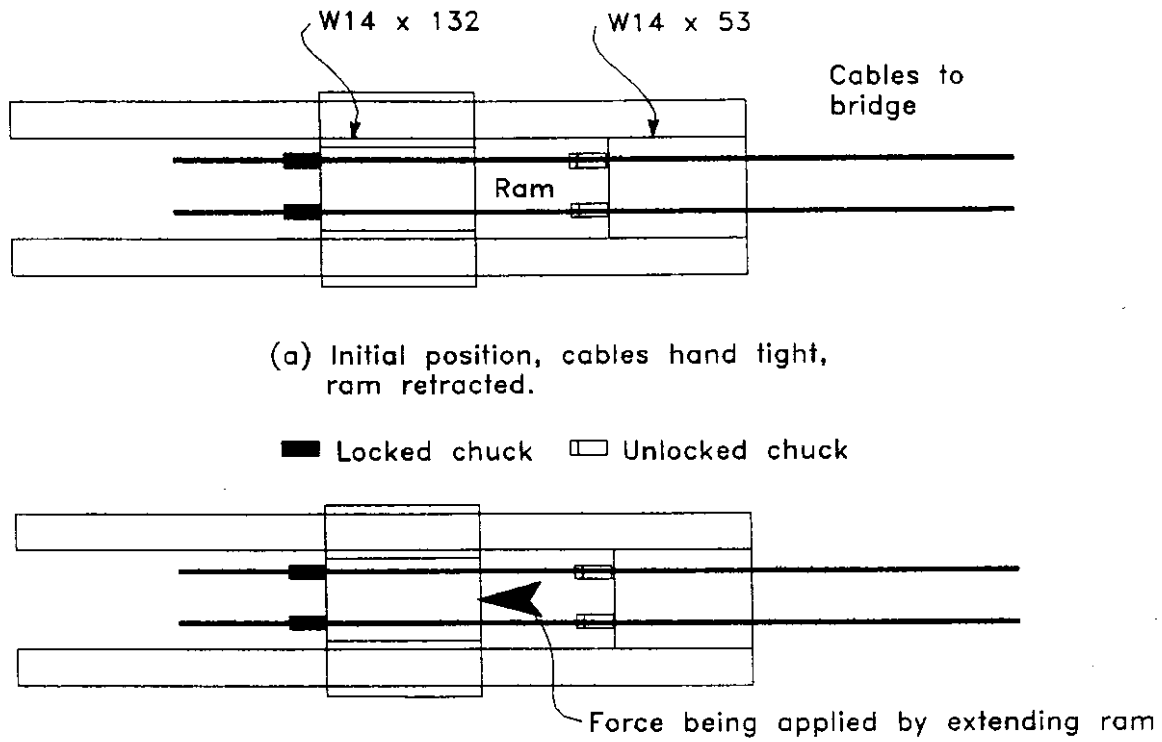

Figure 3.9. Jacking Frame Operation

Unloading was particularly tedious. To recycle the rams during unloading, the following procedure was followed. Pressure in the rams was bled off until approximately half an inch of stroke remained. The front chucks were locked, and the rest of the pressure was released in the jacks. The researchers used chain hoists to pull the W14x132 forward until the rear chucks could be released. Then, the rear chucks were set at about 3.5 inches from the W14x132, and the jack was extended until the ram had taken up sufficient tension to release the front chucks. Finally, the front chucks were moved backwards. Unloading continued until the procedure had to be repeated. Each repetition took from 15 to 30 minutes and four to eight workers.

The chucks that secured the deadmen cables to the jacking frames were rarely adjusted. Before the tests started, the deadmen cables had been stressed by jacking each frame against its counterpart on the other side of the bridge. On the few occasions when a jacking frame was out of alignment, its alignment was adjusted by tightening some of the deadmen cables with a Freyssinet, post-tensioning jack.

3.4 SUGGESTIONS FOR IMPROVEMENT

The load train did what it was designed to do; it safely applied large, cyclic loads to the structure. Nonetheless, improvements could be made. The problems encountered in implementing the design concept provided valuable lessons that should guide future load-train designs.

Deadmen

The deadmen were sufficiently strong and stiff to provide reactions to the applied loads. At 800 kips, corresponding to 133 percent of the design load, no movement was observed. The only problems experienced during testing were caused by sag in the deadmen cables and cable misalignment. The straightening of these cables under load caused the soil to heave near the upper part of the cable trenches.

Installation of the deadmen would have been simplified by omitting the cable tubes from the front of the steel beams. The tubes hung up on the side of the trenches

during lowering and made alignment of the deadmen difficult. If the design had been less conservative, this misalignment could have caused significant problems.

The rebar system that supported the beam during installation was inadequate. The legs bent too easily during handling, and the beams settled too deeply in the soft soil at the bottom of the trench. To reduce the settlement at the bottom of the trench, steel angles were placed between the rebar legs. This solution reduced but did not eliminate the settlement. Future designs should provide a greater bearing surface for the beam support system, particularly if the beam will be placed below the water table.

Cable Groups

The cable groups performed well, and even at the maximum design load, none of the cables were seriously damaged. Nonetheless, with time, the chuck teeth began to serrate the cables at the jacking frames. This progressive damage might have eventually caused a strand or cable to fail if many more cycles of testing had been imposed on the bridge.

To verify that the force in the cables was the same as the force applied by the jacks, an LVDT was attached to one of the cables. Displacements over a 24-inch length were converted to strains and applied forces. In Figure 3.10, the applied forces that were calculated on the basis of the cable strain are compared with the forces that were calculated on the basis of the pump pressure. As shown in the figure, the force calculated from the cable strains was consistently 100 kips above the force calculated from the pump pressure. This discrepancy was attributed to initial sag in the cable. Once the initial sag was overcome, the strain-based estimate for additional force was consistent with the pressure-based estimate. The pressure-based estimate was used in this report.

The lower cable groups could have been replaced with prestressing steel bars. This would have reduced the alignment difficulties and would have improved handling of the beams when they were lowered into the trench. The use of prestressing bars was explored during the design process; however, the idea was rejected as too expensive.

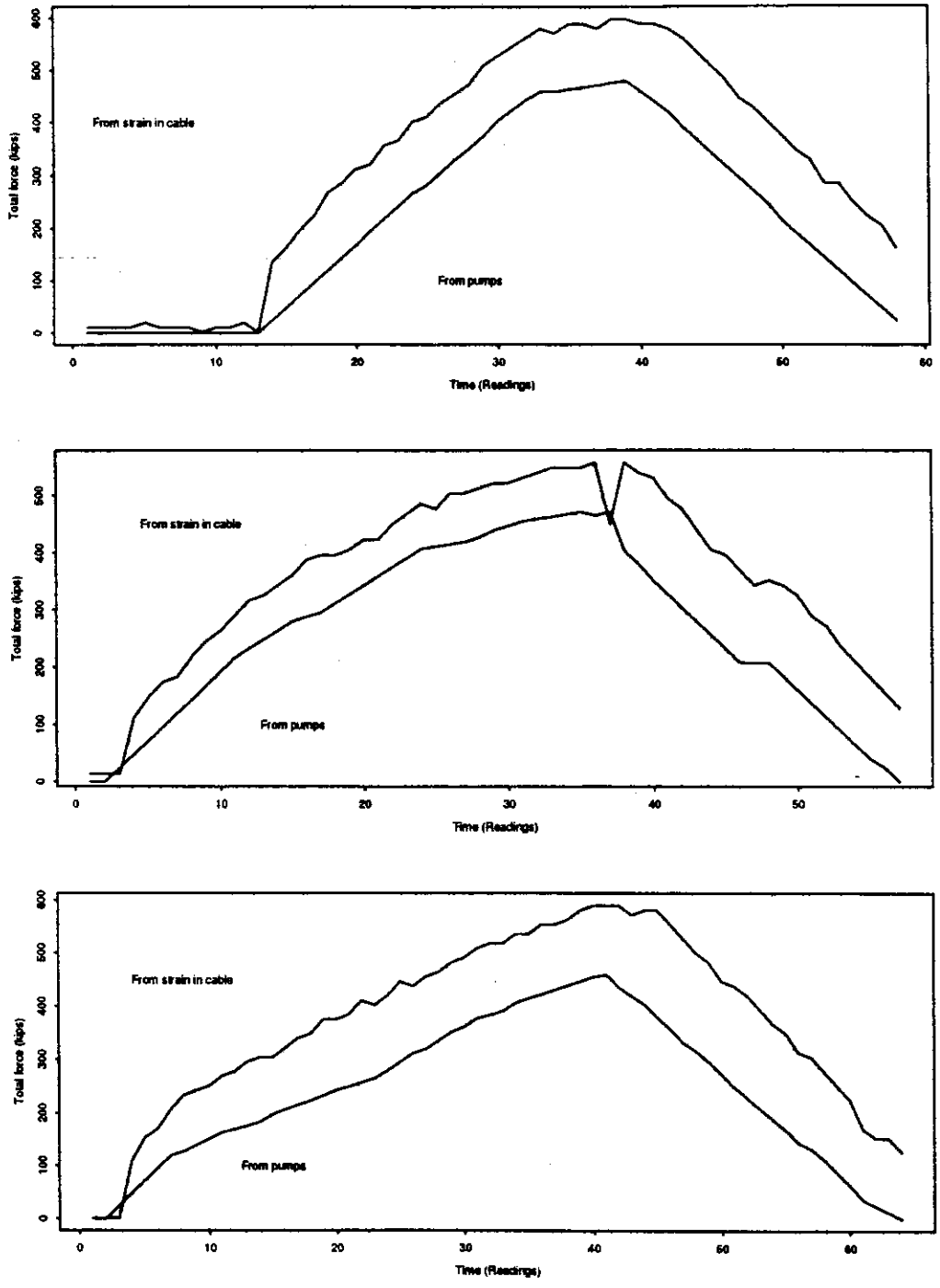

Figure 3.10. Comparison of Load Calculated From Pressure Measurements and From Strain Measurements

Jacking Frames

Though the jacking frames did not fail, they were tedious to operate. They occasionally had to be re-aligned and, more importantly, it took a long time to recycle the jacks. The operation would have been greatly simplified if the hydraulic rams had had longer strokes. Additionally, the jacking frames could have been greatly simplified if center-hole, post-tensioning jacks had been used instead of solid rams.

Harnesses

Though the heavy harnesses were unwieldy to place, they performed well. The researchers did not observe crushing of the crossbeam concrete. The harnesses were not affected by the slight (less than 1 degree) deviation from the design cable slope of 14 degrees.

CHAPTER 4

ISOLATION OF SUPERSTRUCTURE FROM ABUTMENTS

During Phase I, it had been impossible to measure the pier's contribution to the bridge's lateral-load resistance because the abutments were stiff and strong. In Phase II, the superstructure was isolated from the abutments to allow close scrutinization of the performance of the pier columns, footings, and crossbeams at large transverse displacements. The performance of the piers is particularly important for bridges in which the abutments do not greatly restrain pier displacements. Examples of bridges in which the abutments play only a limited role are those in which the bridge is long and those in which the abutments do not develop large reaction forces.

This chapter describes the design and installation of the system that isolated the superstructure from the abutments. An evaluation of the isolation system's performance and suggestions for its improvement are also provided.

4.1 DESIGN

Design of the isolation devices was influenced by considerations of effectiveness, cost, time requirements, ease of installation, and safety. The researchers considered a wide variety of schemes before deciding to remove the elastomeric pads and replace them with greased, stainless-steel/nylon sandwiches. This isolation system offered little resistance to transverse abutment displacements and allowed the researchers to recover the bearing pads for laboratory testing.

In order to replace the bearing pads, a system had to be installed to lift the abutment off the pedestal (Figure 4.1). The research team was uncertain about the amount of force that would be necessary to lift the abutments. This uncertainty arose because the exact deadweight of the bridge was unknown, and, more importantly, because the research team did not know the moment resistance of the girder/diaphragm

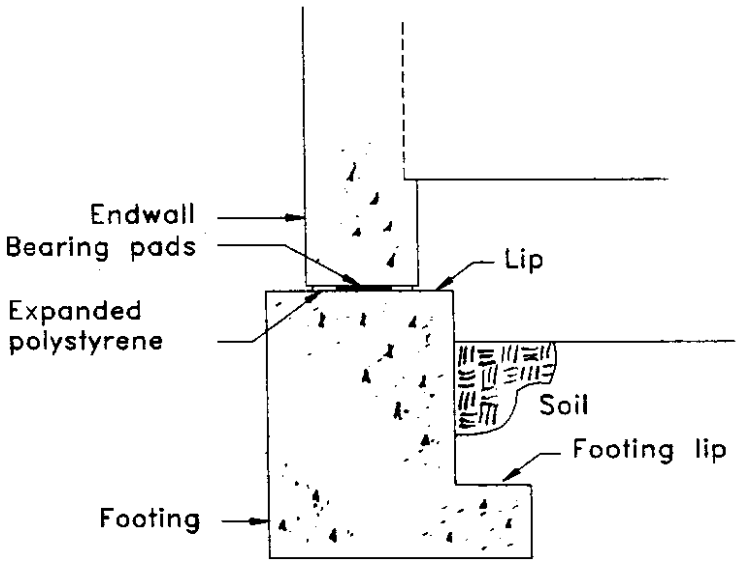

Figure 4.1. Abutment Detail

connection. These uncertainties led the researchers to design a lifting system with a much greater capacity than was necessary.

The lifting force was provided by six, 200-ton hydraulic jacks. These jacks were installed on top of steel columns, flush against the endwall, and centered under each girder. The jacks were connected to a single manifold and pump to ensure that each jack would carry the same load. The system is illustrated in Figure 4.2.

Six square (10 x 10 x 3/8 inch) structural steel tubes supported the hydraulic rams. To each end of the tubes, a 1/2-inch steel plate was welded (Figure 4.2). These plates distributed the jack forces to the lip of the pedestal and through the tubes and beams to the footing lip. Steel shims were placed under the columns and on the pedestal lip to ensure that the load would be distributed to both the pedestal lip and the footing lip.

Six wide-flange steel members supported the steel tubes and distributed the lifting force along the footing lip. Most of the steel beams were W8x28, although some were slightly larger. Stiffeners (3/8-inch thick) were placed on the beams at the locations of the steel tubes.

At each abutment, the isolation devices incorporated six 24 x 6-inch, T-304, 11-gauge, stainless-steel plates, which were hand polished to a mirror-like finish. Each plate supported a 5 x 5 x 1/2-inch plate of ultra-high molecular-weight (UHMW) polymer (TIVAR-100). The stainless-steel plates were greased with standard lithium axle grease to reduce friction. The UHMW plates and the steel were then placed in 3 x 5-foot polyethylene envelopes to prevent dust contamination. The size of the envelopes was selected to allow the nylon pads to move freely during testing. An isolation sandwich, with its polyethylene envelope, is shown in Figure 4.3. A sandwich was placed in each location where an elastomeric bearing pad had been located.

4.2 INSTALLATION

The structural steel components were cut and welded in the University of Washington machine shop to avoid on-site welding. Before closing the bridge to traffic,

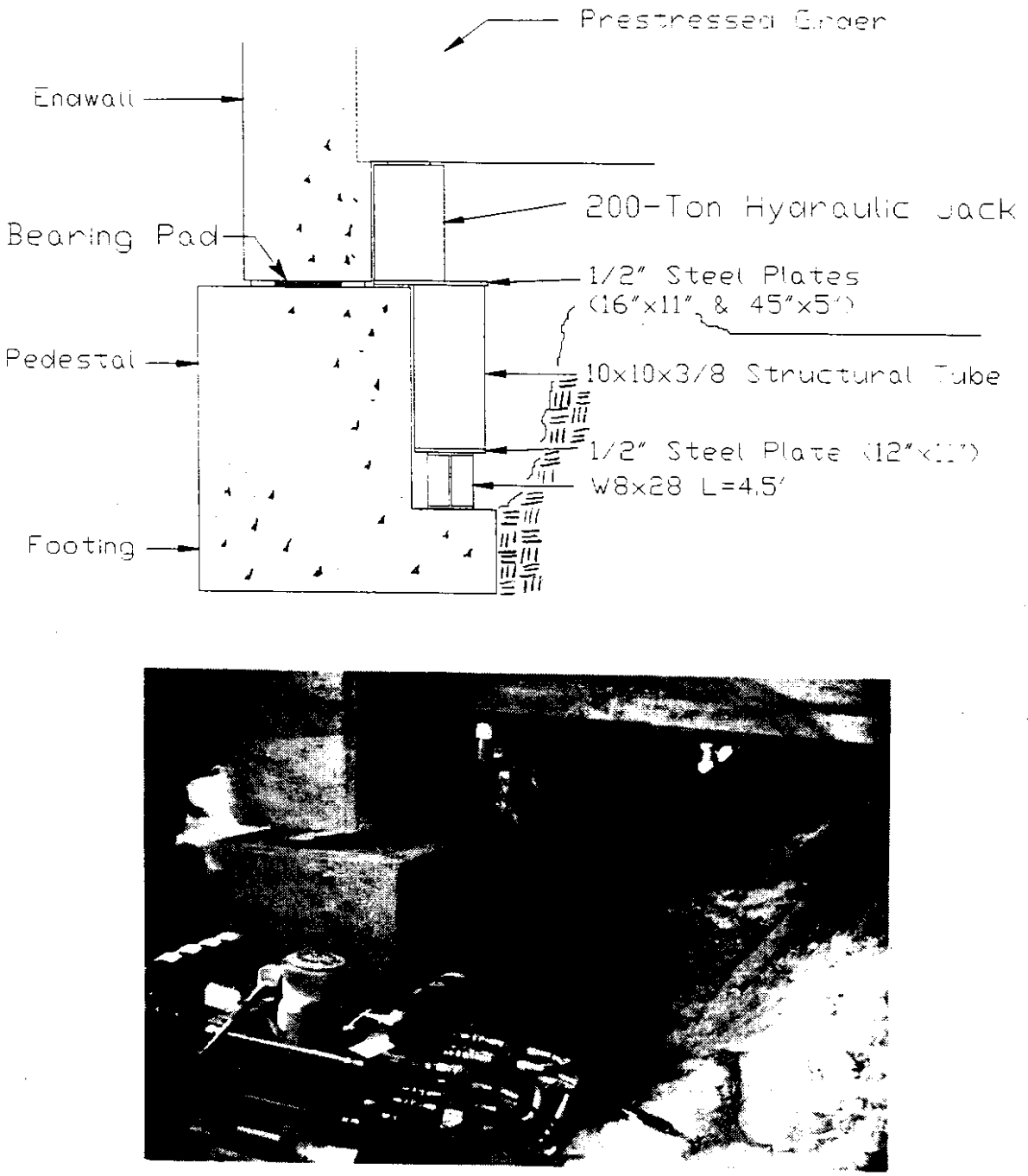

Figure 4.2. Lifting System

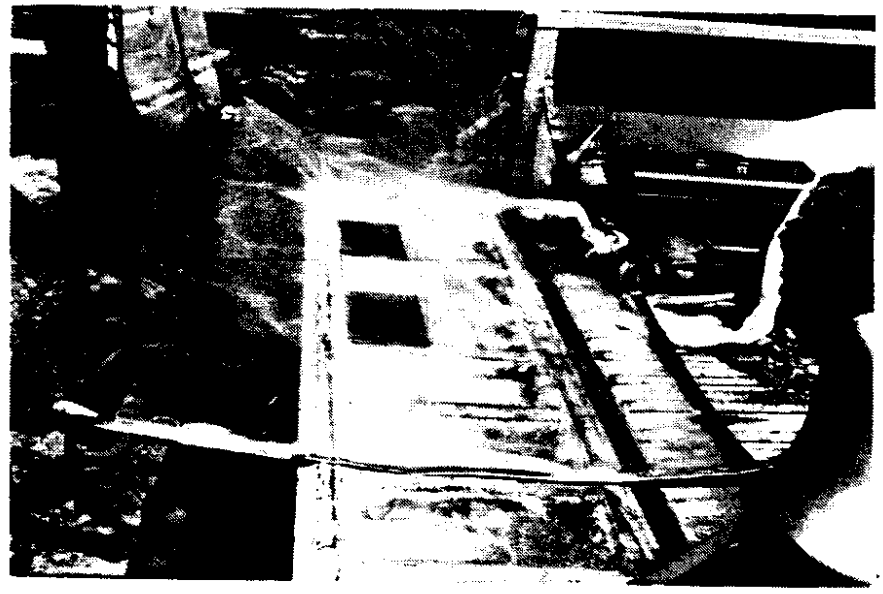

Figure 4.3. Isolation Device

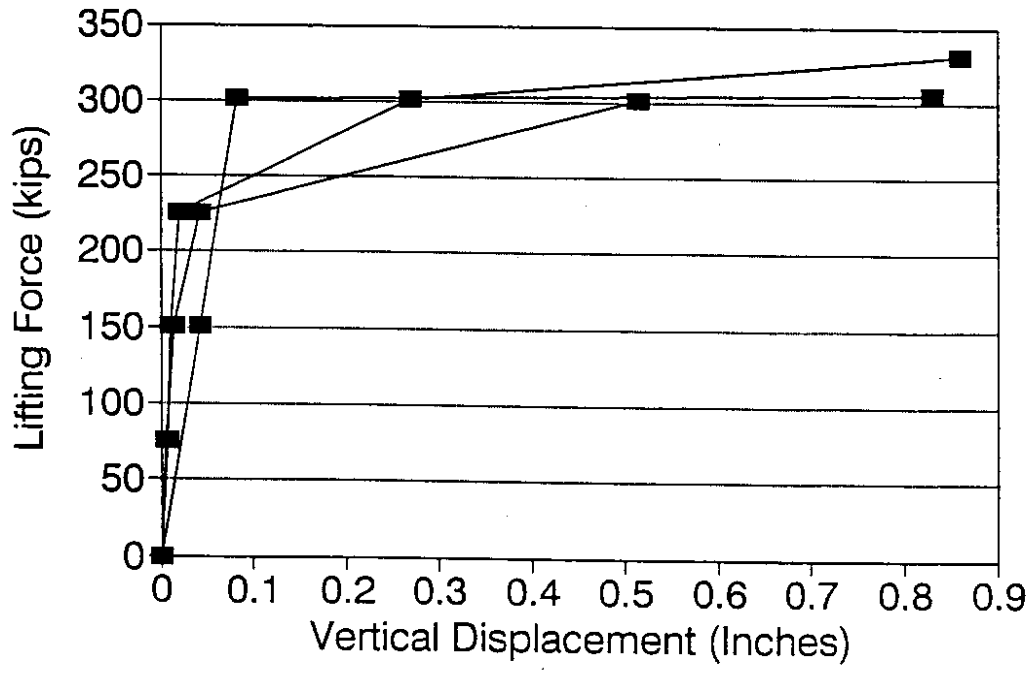

Figure 4.4. Lifting Force-Displacement Plot

the researchers manually excavated the soil above the footing lips on both the east west abutments. Then, the lifting system was installed on the bridge's west abutment. The jacks and steel components were lowered to the footing lip and then moved along the footing lip to their final locations on a small dolly. A gap was left between the lifting jacks and the girders to ensure that the lifting system would not affect the Phase I tests.

After the completion of Phase I, the bearing pads and polystyrene were replaced with the isolation system. At the west abutment, the lifting force, as determined by the pump pressure of 1,000 psi, was approximately 300 kips. A significant amount of uncertainty accompanied this measurement because the pump pressure of 1,000 psi corresponded to only 10 percent of the pump's capacity. Dial gauges were installed to measure the displacement between the pedestal and the endwall during lifting. These measurements are reported in Figure 4.4.

When the gap between the abutment endwall and the pedestal reached approximately 3 inches, the hydraulic valves were closed, and steel rails were placed in the gap to ensure that it would not close during installation. The expanded polystyrene was removed, and the original bearing pads were uncovered. When the pads were removed, the research team discovered that 10 x 10-inch steel plates were embedded into the bottom face of the endwall, directly above the bearing pads. The isolation devices were inserted and centered under these steel plates, and the structure was lowered onto the isolation devices.

During the lifting operation, the researchers did not observe buckling in the steel members of the lifting system. However, some cracking in the footing lip was noticed under one of the jacks. Also, large cracks formed at the girder/diaphragm connection at the intermediate pier crossbeams. Though some cracks were in the diaphragm, the crossbeams themselves were not damaged.

After the west end had been isolated, the lifting system was installed on the east end, and the installation and lifting processes were repeated. Again, the force required to

lift the structure was about 300 kips. When the east end of the bridge was lowered onto the isolation devices (at the point at which the jacks no longer supported the structure), the bridge moved 0.5 inches to the south. The jacks were then lowered further to ensure that they would not affect the Phase II tests. The jacks were left in place until the completion of all testing to allow recovery of the isolation devices.

4.3 EVALUATION OF PERFORMANCE

The force that was necessary to lift the endwall and endspan was twice the force that would have been necessary if the span had been simply supported. This discrepancy indicated that the girder prestressing strands and reinforcing steel that extended into the pier diaphragm provided some moment resistance. The magnitude of the lifting force was consistent with an estimate of the girder/diaphragm connection strength. In making this estimate, the research team assumed that (1) the neutral axis was near the deck/girder interface, and (2) the prestressing strands and reinforcing steel were fully developed. The large influence of the girder end moment made it difficult to reliably estimate the residual vertical load on the isolation devices during the bridge test. The difficulty of making this estimate was compounded by the crown of the pedestal. During transverse displacement of the bridge, this crown caused the endspans to lift; this lifting may have affected the normal force on the isolation system.

The isolation devices were routinely checked during testing. Upon completion of testing, the east end of the bridge was again lifted and the isolation devices were recovered. At this time, the researchers discovered that four of the UHMW pads on the east end were no longer supported on the stainless-steel plates. Instead, the UHMW pads were supported on the polyethylene envelopes, which remained intact. The same problem had occurred at the west abutment. The east end sandwiches were recovered and returned to the lab for testing.

The researchers used the setup shown in Figure 4.5 to measure the friction coefficient of the isolation devices. This setup simulated the field conditions and allowed

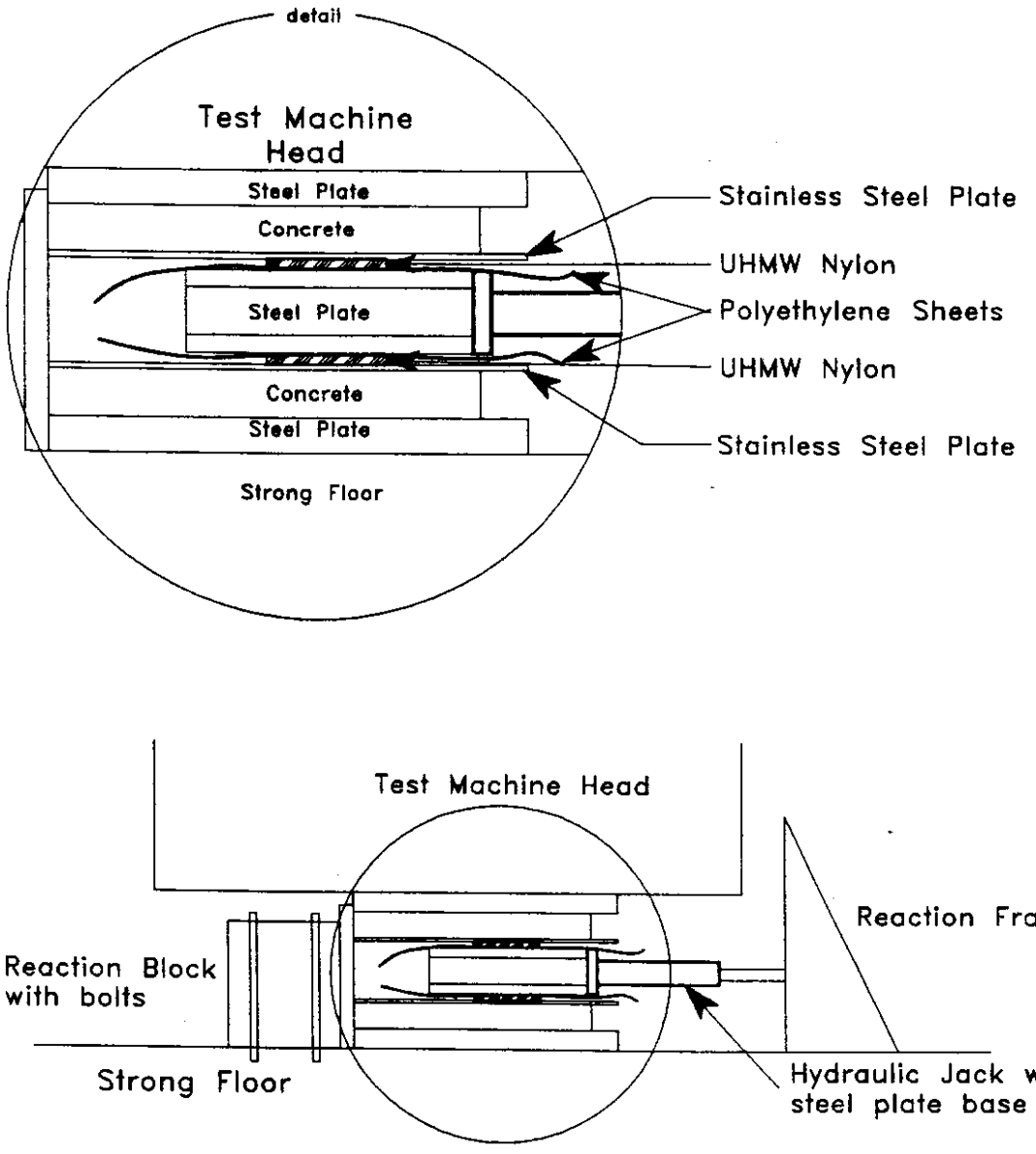

Figure 4.5. Coefficient of Friction Test Setup

testing of the devices both as originally designed and without the stainless-steel plates. Displacements were measured with dial gauges that were installed both on the central steel plate, on which the force was applied, and on the concrete plates. The measured coefficients of friction are summarized in Table 4.1 for the six isolation devices that were recovered from the east end of the bridge. Laboratory testing was performed at loading rates that were nearly as slow as those applied in the field.

Table 4.1. Friction-Test Results for TIVAR-100

Test Setup	Normal force (kips)	Lateral Force (mean)(kips)	Coefficient of Friction
UHMW on greased	26.66	1.83	.07±.01
stainless steel	33.33	2.05	.06±.01
	80	2.4	.03±.005
	120	2.35	.02±.003
UHMW on	26.66	2.23	.08±.01
polyethylene	30	2.2	.07
	80	4.35	.05±.005
	120	5.68	.05±.01
UHMW on concrete	26.66	8.5	.32

Note: Confidence interval represents 95 percent confidence.

Figure 4.6 reports the results of the isolation-system tests, as well as TFE bearing-pad tests reported by Campbell and Kong. (10) TFE has been reported to have a lower coefficient of friction than UHMW, but TFE is much more expensive. The coefficient of friction of the isolation devices was approximately 0.05 for a vertical load determined from the lifting operation. The coefficient was slightly lower on stainless steel and slightly higher on polyethylene. This friction coefficient compared favorably with the manufacturer's values of 0.15 to 0.20 for TIVAR-100 against mild steel without grease.

On the basis of the laboratory measurements, the effect of the isolation-devices' friction was estimated. It was assumed that the normal force on the isolation devices

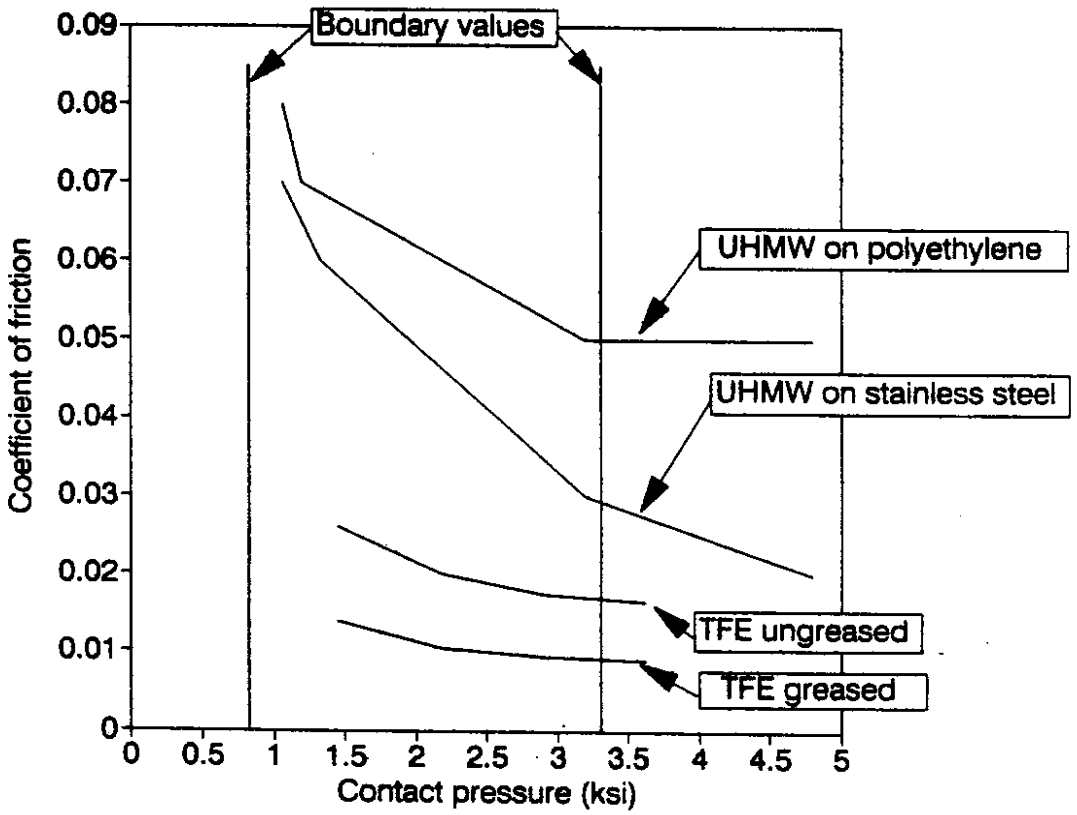

Figure 4.6. Measured Coefficients of Friction

was equal to the tributary dead load (180 kips) and that a coefficient of friction of 0.05 could be applied to field conditions. The calculated horizontal frictional force was 0.05 x 180 kips = 9 kips. Therefore, a force of 18 kips was necessary to overcome friction at both abutments. The researchers corrected the data for this frictional resistance (Chapter 6).

4.4 SUGGESTIONS FOR IMPROVEMENT

Because of the large number of small bridges throughout the United States and the greater ease with which lateral testing can be conducted on small bridges than on large ones, it is reasonable to assume that a superstructure may be isolated from the effects of the abutments again. For this reason, some comments on how the isolation procedure could be redesigned are appropriate.

Once the lifting system had been installed, the lifting procedure was fast and effective. Unfortunately, it was extremely tedious to excavate the interior face of the pedestal. Other bridges may not have this difficulty if they have sufficient clearance for mechanical excavation, or if their abutment configuration does not make excavation necessary .

The isolation devices should have incorporated a larger stainless-steel plate to ensure that the UHMW pads would not come off the plates at large displacements. Fortunately, this problem did not greatly affect these tests because the coefficient of friction for UHMW nylon on polyethylene was low. Round steel rods could also have been installed to isolate the superstructure from the abutments.

CHAPTER 5

INSTRUMENTATION AND DATA ACQUISITION

This chapter describes the instrumentation and data acquisition system used to record the bridge's response to lateral loads. The naming convention for the instruments is described in Appendix C. Except for the electronic distance meters (EDM), all the instruments were electro-mechanical transducers. These instruments included linear variable differential transformers (LVDTs), potentiometers, clinometers, and Temposonic linear displacement transducers. Strain gauges were not used.

The structure's instrumentation can be divided into the following categories:

- deck instruments (Figure 5.1),
- crossbeam instruments (Figure 5.2),
- top-of-column instruments (Figure 5.2), and
- bottom-of-column instruments (Figure 5.2).

Each category is addressed in the following sections.

5.1 DECK INSTRUMENTS

The deck instruments measured the horizontal translation of the bridge deck at the abutments and piers. The locations of these instruments are indicated in Figure 5.1. As shown in Figure 5.3, the transverse pier displacements were measured with a weight-and-pulley system. The displacement of the weights was measured by Temposonic linear displacement transducers with a 12-inch stroke. For cycles in which the displacements exceeded the instrument stroke, the setup was modified so that the instruments would not have to be reset during the test. Specifically, by adding a second pulley, the researchers increased the ratio of the pier displacement to the instrument displacement from 1:1 to 2:1.

Abutment displacements were measured with a system that was similar to the system used to measure pier displacements (Figure 5.4). However, at the abutments, the

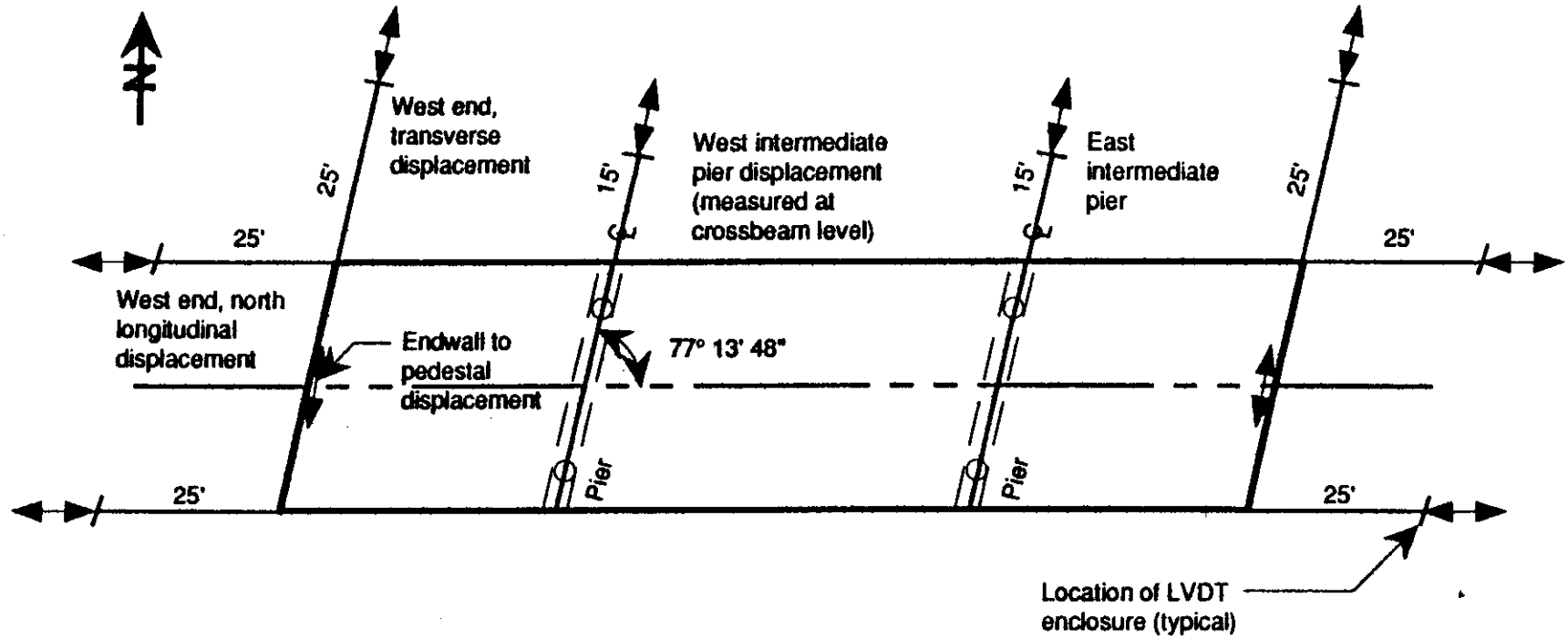

Figure 5.1. Deck Instrumentation Plan

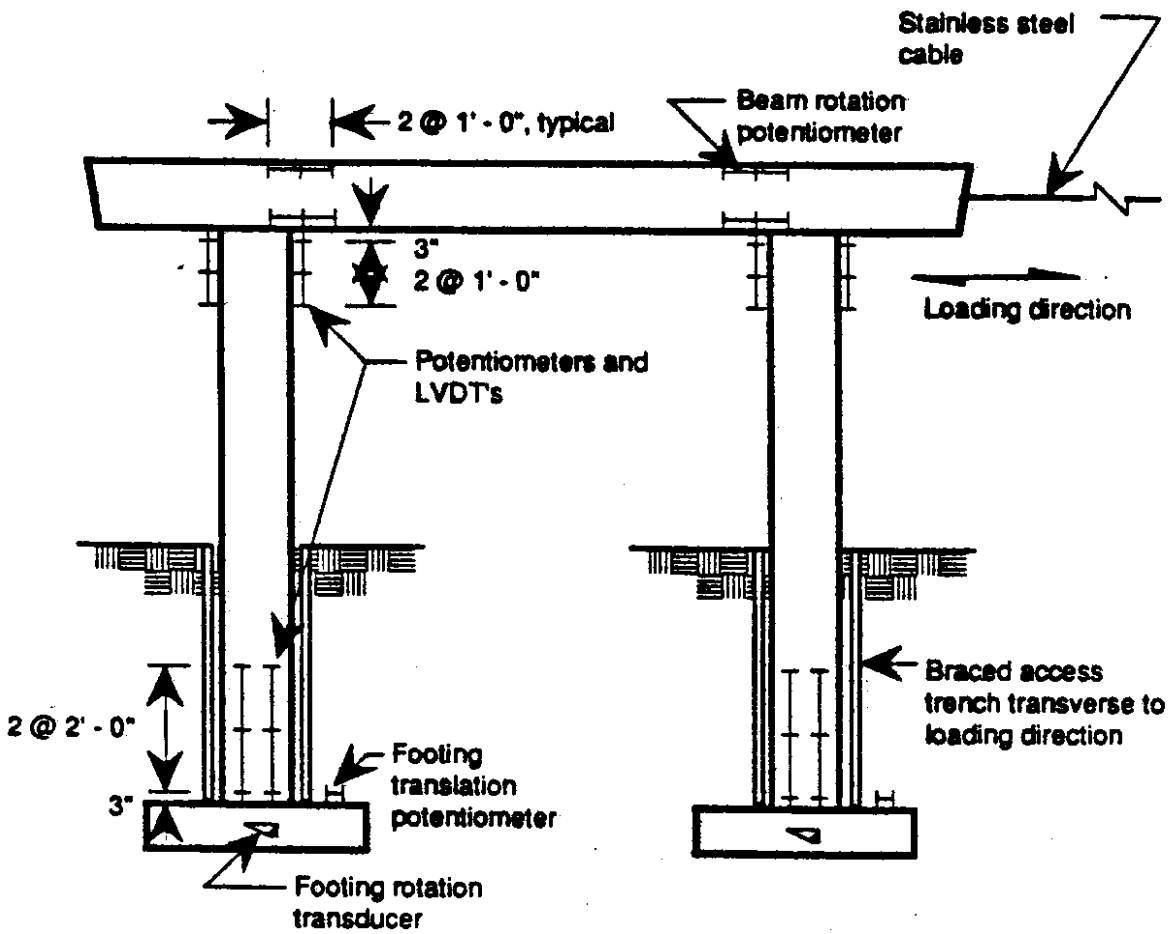

Figure 5.2. Pier Instrumentation Elevation

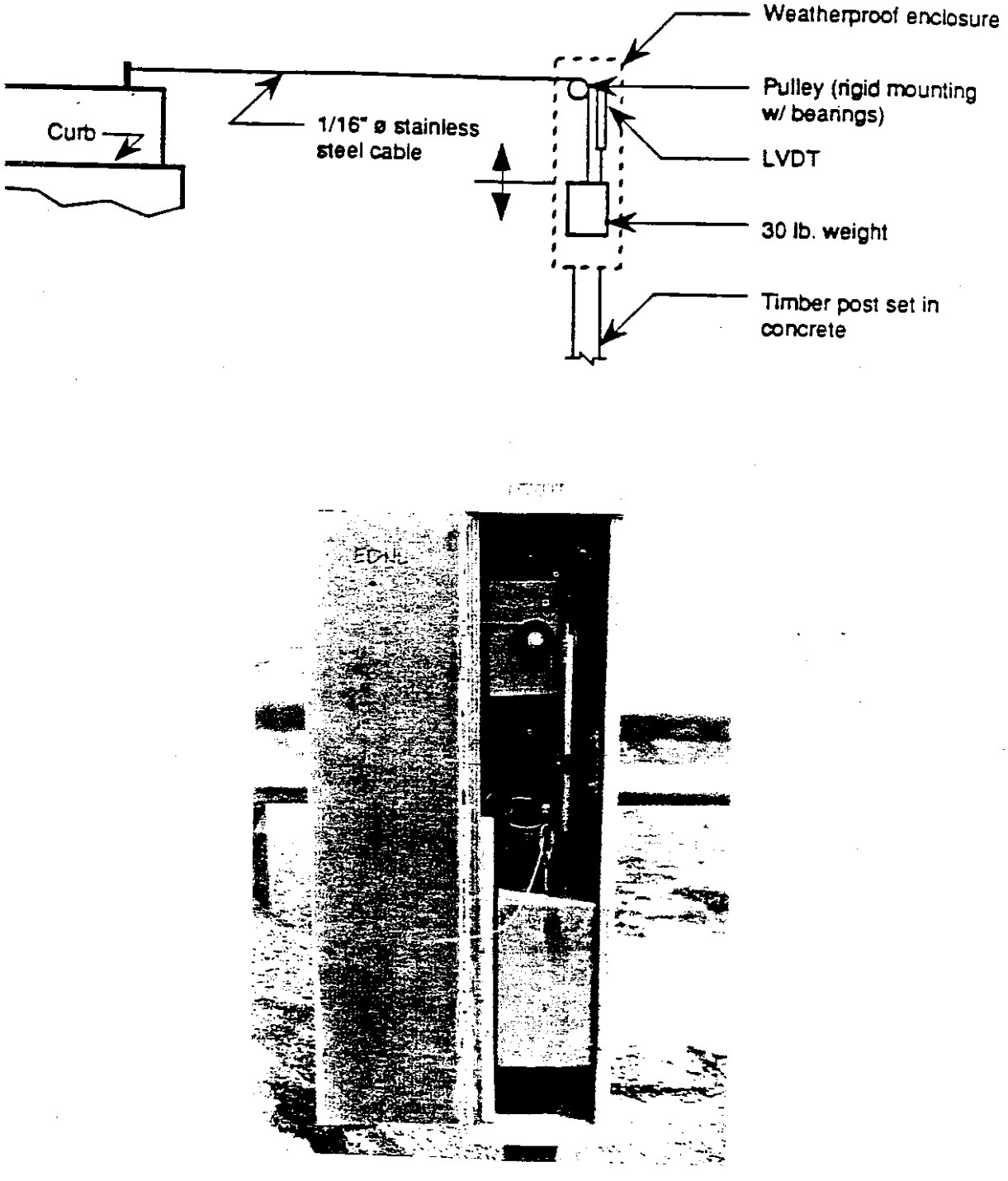

Figure 5.4. Endwall-Displacement Instrumentation

5.2 CROSSBEAM INSTRUMENTS

Crossbeam instruments monitored the flexural deformation of the crossbeam under transverse displacements. Their locations are shown in Figure 5.2, and a photograph of the installed setup is shown in Figure 5.5. On the west pier, two instrument pairs per column monitored crossbeam deformation; one pair monitored deformation over the first 12 inches from the column face; the second pair monitored the next 12 inches. On the east crossbeam, a single pair of instruments measured the beam's flexural deformation over the 24 inches nearest the column face.

5.3 TOP-OF-COLUMN INSTRUMENTS

The researchers installed instruments to measure relative rotations of column cross sections. These instruments worked in pairs on opposite sides of the columns, as depicted in Figure 5.5. On the basis of these measurements, the researchers calculated the average column curvature within each instrument gauge length. Because of financial and time constraints, instrumentation could not be deployed in every desired location. Therefore, the west bent was more heavily instrumented than the east bent. On each west-pier column, three pairs of instruments monitored rotations; the first instrument pair monitored the first 2 inches from the cross-beam soffit, the second pair monitored the next 12 inches, and the third pair monitored the next 12 inches (Figure 5.5). On the east-pier columns, one instrument pair measured rotations over the first 2 inches from the crossbeam soffit, and a second pair measured displacements over the next 24 inches.

To ensure that the LVDTs and potentiometers would measure displacements after the concrete cover had spalled, the researchers affixed the instruments to the column core by drilling through the cover and epoxying all-thread steel rods into the column (Figure 5.6). The mounting hardware (Figure 5.7) allowed the LVDTs to rotate freely about an axis that was perpendicular to the crossbeam.

Figure 5.5. Column and Crossbeam Curvature Instrumentation

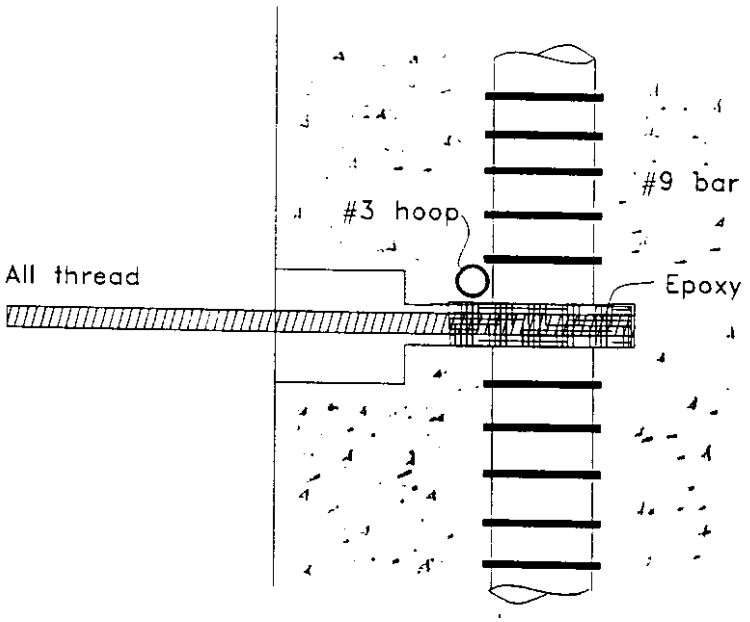

Figure 5.6. Curvature Instrumentation Attachment to Column Core

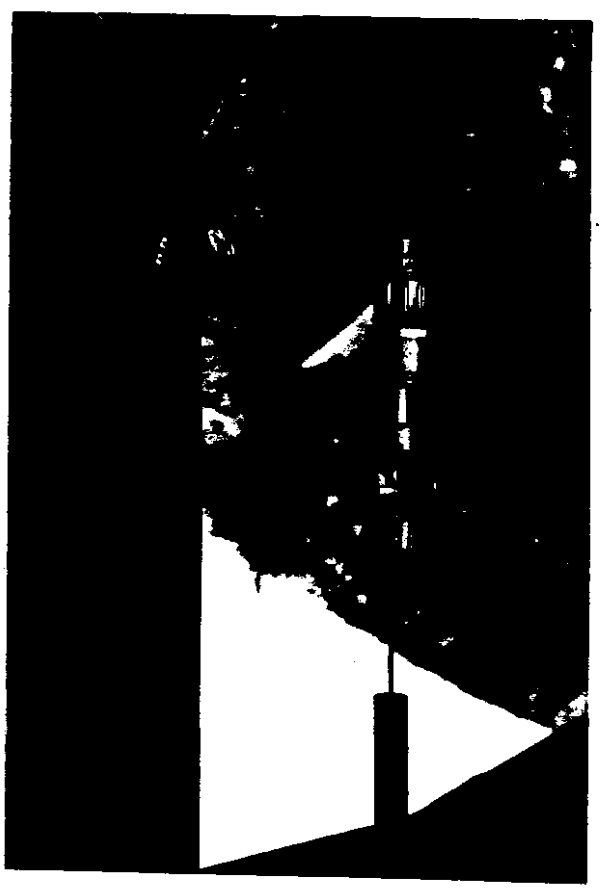

Figure 5.7. Curvature Instrumentation Photograph

5.4 BOTTOM-OF-COLUMN INSTRUMENTS

Excavation and instrumentation of the footings were unique aspects of this test. To minimize the extensive effort required to excavate and shore the trenches, and to minimize the impact on the bridge's resistance, only the west pier footings were excavated and instrumented (Figure 5.8). The instrumentation setup was similar to the top-of-column setup; however, to minimize soil disturbance, the pairs were not separated by 180 degrees, as shown in Figure 5.9. The resulting decrease in spacing between the bottom-of-column instruments, D, decreased their angular resolution in comparison to the top-of-column instruments. The lowest pair of instruments measured the column rotation over the 3 inches nearest the footing. The next two pairs of instruments had 24-inch gauge lengths.

Absolute footing rotation was measured with clinometers that were affixed to the top of the footing. To measure footing translation, the researchers constructed a boom from outside the expected zone of soil movement to the footing; a potentiometer then measured the relative displacement between the boom and the footing. A photograph of the bottom-of-column instrumentation is provided in Figure 5.10.

5.5 DATA ACQUISITION

Data were transmitted through 5 miles of shielded cable from the instrumentation to an on-site computer, which was located in the project trailer (Figure 5.11). To cross the road without interrupting traffic, the wires were run through underground, 6-inch PVC pipes. To minimize interference to the instrumentation wires, the power lines and the intercom system were routed in separate pipes.

The research team relied on four multiplexers to increase the number of channels that could be monitored by the analog-to-digital (A/D) converter. Researchers used the Labtech Notebook software package to store the incoming data. The first values recorded for each loading half-cycle were the INIT values, which consisted of a set of 10 to 15

Figure 5.8. Photograph of Footing Access Trench

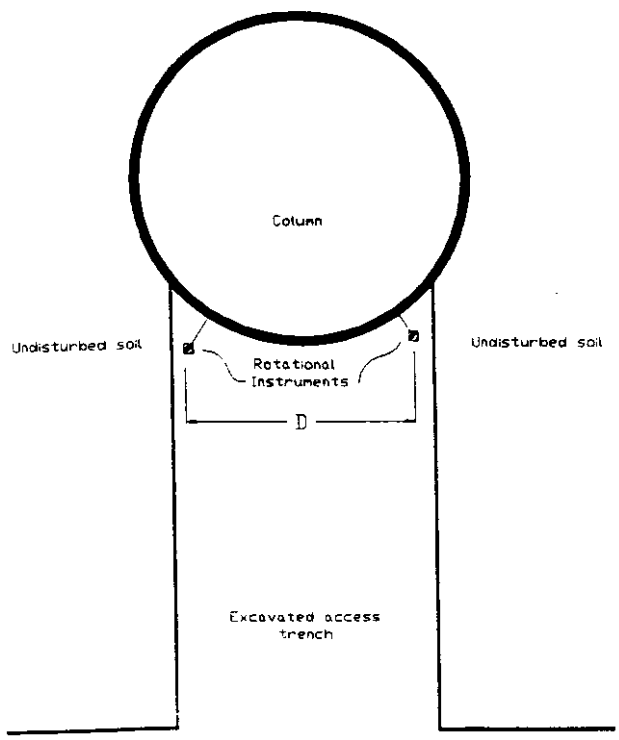

Figure 5.9. Plan of Bottom-of-Column Curvature Instrumentation

Figure 5.10. Bottom-of-Column Instrumentation

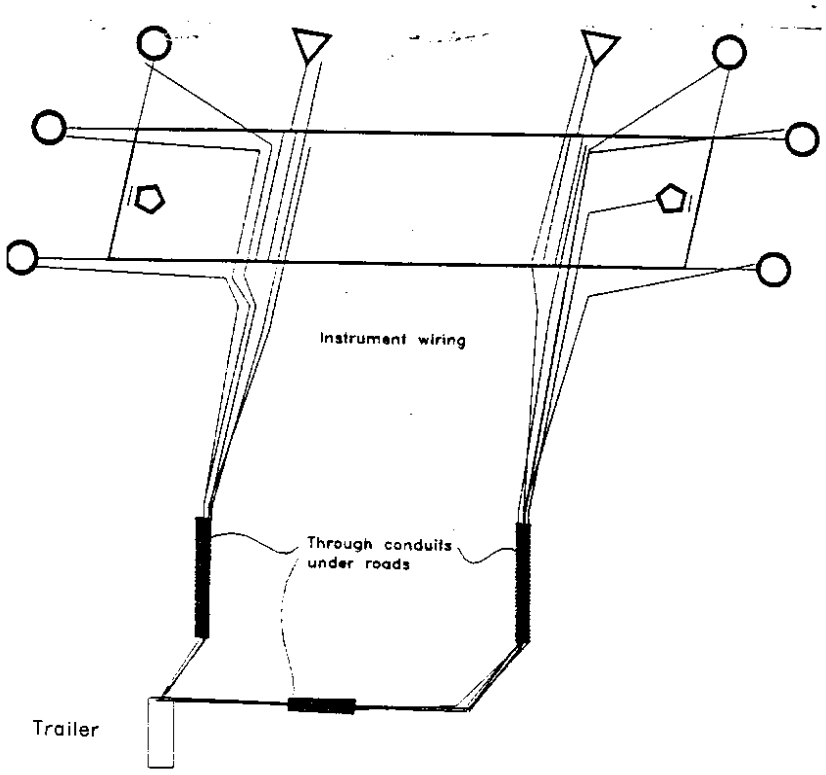

Figure 5.11. Site Plan

readings. These values were recorded over a 10- to 20-second period just before a test began. They were then reviewed to ensure that all instruments were working and that data were being recorded. These initial values also provided initial voltages from which the researchers could calculate relative displacements.

Calibration factors for the instruments were determined in the laboratory and were then confirmed in the field with calibration blocks. Once the load train and data recording systems were ready, a zero reading was taken with zero force applied to the structure. Following this reading, the researchers increased the pump pressure in increments of 200 to 300 psi.

5.6 EVALUATION

Overall, the instrumentation performed well. Initial problems involving the pulley systems were resolved prior to testing. Generally, instrument locations were satisfactory, in that instruments were located where large displacements and damage occurred. The significant exception was the location of the lower column rotation instruments; these instruments were positioned too low to record the cracking that was observed during the test.

The research team also experienced some problems with the footing instruments. Despite efforts to shelter the lower column instruments, falling rocks frequently struck the instruments, and they were often buried in soil. The translation measurements were particularly affected because the falling rocks often struck the reference booms. The clinometers were better protected from these hazards, but they lacked sufficient resolution to precisely measure the small footing rotations that occurred during the tests.

Occasionally, defective microchips caused the multiplexer output voltage to vary erratically. Fortunately, these voltage variations were sufficiently large that it was easy to detect the problem and halt testing until the variations stopped. Though the affected data points were easy to identify, some information was lost. The few data points that were affected by the multiplexer instability were corrected, as documented in Chapter 6.

CHAPTER 6

DATA REDUCTION

The procedure that the researchers followed to process the raw data is reported in this chapter. This chapter also details the corrections that were made to compensate for occasional multiplexer instability and operator blunders, as well as for the effects of the isolation system.

6.1 DATA REDUCTION PROCEDURE

The research team calculated the applied loads by multiplying the pressure readings for each pump by the pump's calibration factor. The displacement histories for the tests were calculated as follows.

- The 10 to 20 initial readings, which had been taken before the researchers applied the load, were averaged to calculate an initial voltage for each instrument.
- The initial voltage for each instrument was subtracted from each measured voltage to obtain changes in voltage.
- The changes in voltages were multiplied by the instrument calibration factors to determine relative displacements.
- The records were concatenated in chronological order.
- The initial displacement for each cycle was set equal to the previous half-cycle's final displacement.

The data reduction procedure did not take into account possible movement of the structure between the end of a half cycle and the beginning of the next half cycle. Though no data were recorded during these periods (2 to 24 hours), the researchers examined the dial-gauge readings to find evidence of movement. This examination determined that the displacements between half cycles were much smaller than those that had been imposed in Phase II by the load train. Most of the data analysis and plotting were performed with an object-oriented data analysis and statistics package, Splus. (11)

Most of the response histories are presented using the standard force-displacement presentation. For example, Figure 6.1 shows the force-displacement behavior of the structure. The ordinate is the total force applied by the load train to the piers, and the abscissa is the average of the two pier displacements. The individual instrument histories for the two piers are given in Appendix C. Occasionally, the response is presented by "unfolding" the data. In this presentation style, displacements are plotted as a function of reading number, as shown in Figure 6.2. Note that, though time increases with reading number, the elapsed time between sequential readings varied greatly.

6.2 CORRECTIONS OF OBVIOUS ERRORS

After all of the channel response histories had been plotted, the data were corrected for obvious errors. For example, the top plot in Figure 6.3 shows the measured record for a transducer that was located at the top of the west pier beam, near the north column (WNB1T). Though one cannot establish whether the large spike resulted from the multiplexer instability (Section 5.6) or an external disturbance, the data point is obviously in error. Consequently, the value for the reading at the spike was replaced with the average between the two adjacent readings; the corrected plot is shown in the lower portion of Figure 6.3. The corrected displacements for this instrument were so small (less than or equal to 0.002 inches) that the corresponding voltage magnitudes were on the order of the analog-to-digital converter's resolution. Out of 60,000 data points, only the seven points listed in Table 6.1 were modified.

Table 6.1. Corrections to Data Points

Instrument Name	Reading Number	Original Value	Corrected Value
ESB1T	533	0.03467	0.00079
ESB1T	868	0.01501	-0.00207
WSCB1S	533	-0.4646	-0.02314
WSCB1N	533	-0.4192	0.00049
WNB1T	144	0.01953	-0.00049
WNB1B	144	0.0247	0.00107
WSFCT	534	-0.7315	-0.16589

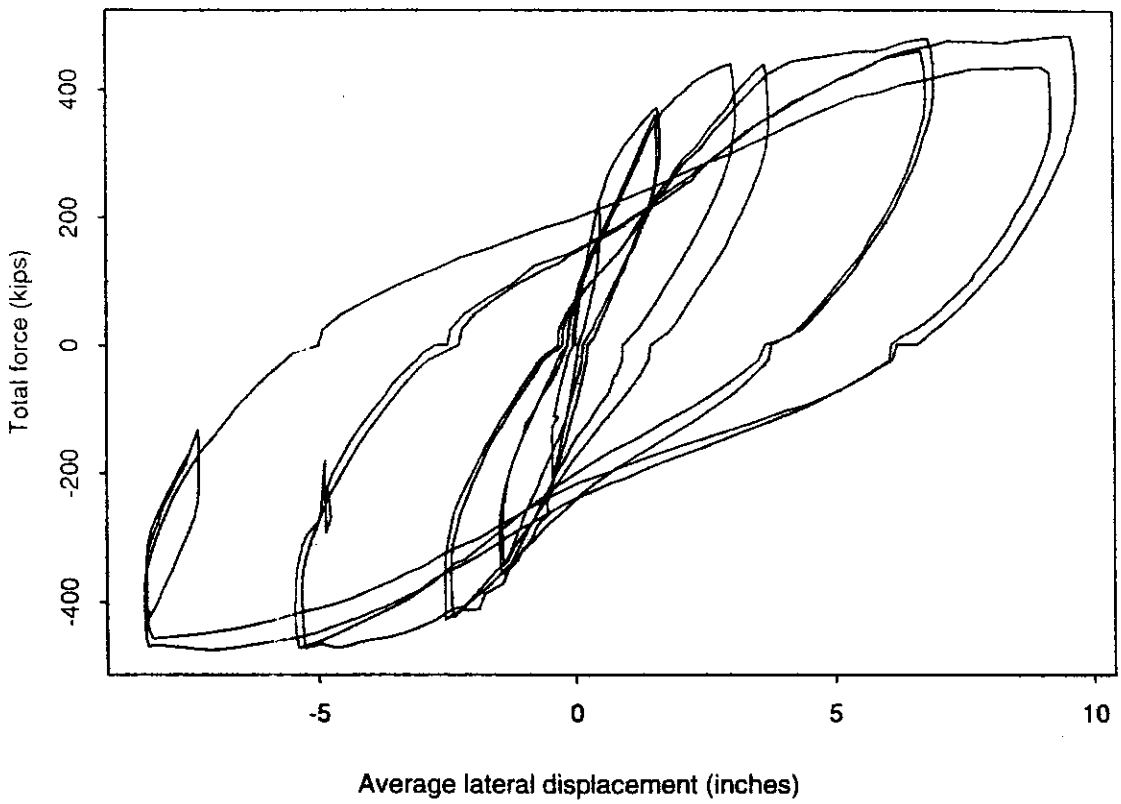

Figure 6.1. Isolated Structure Force-Displacement Response

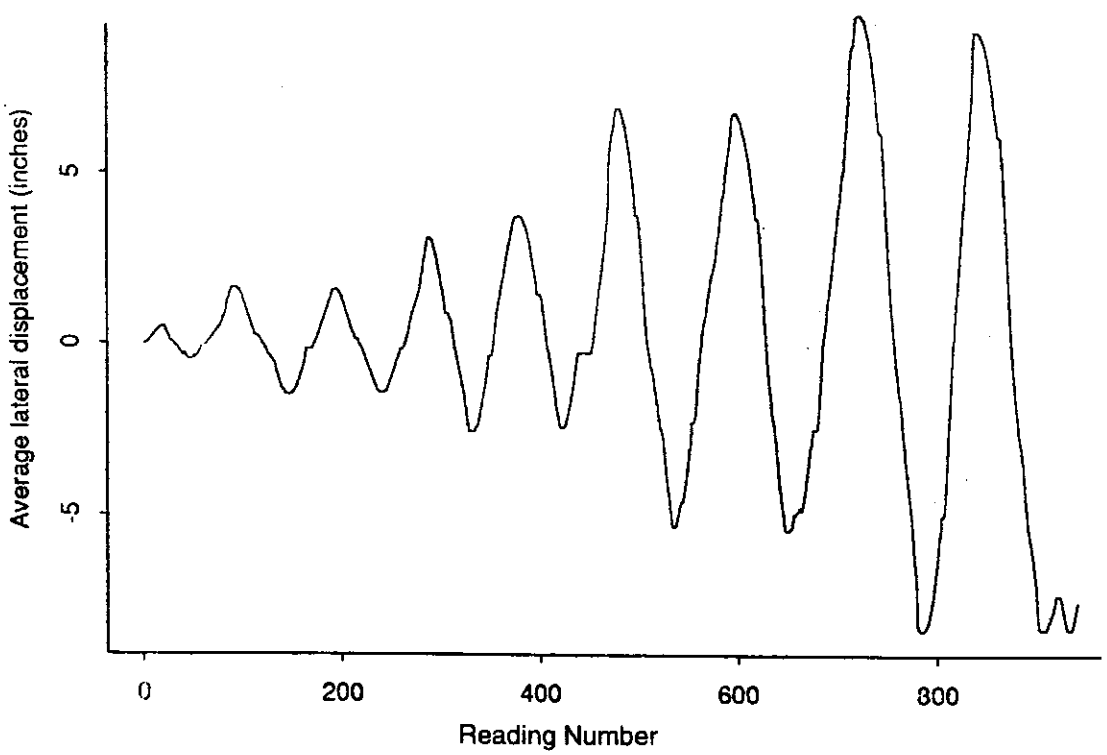

Figure 6.2. Isolated Structure Displacement History

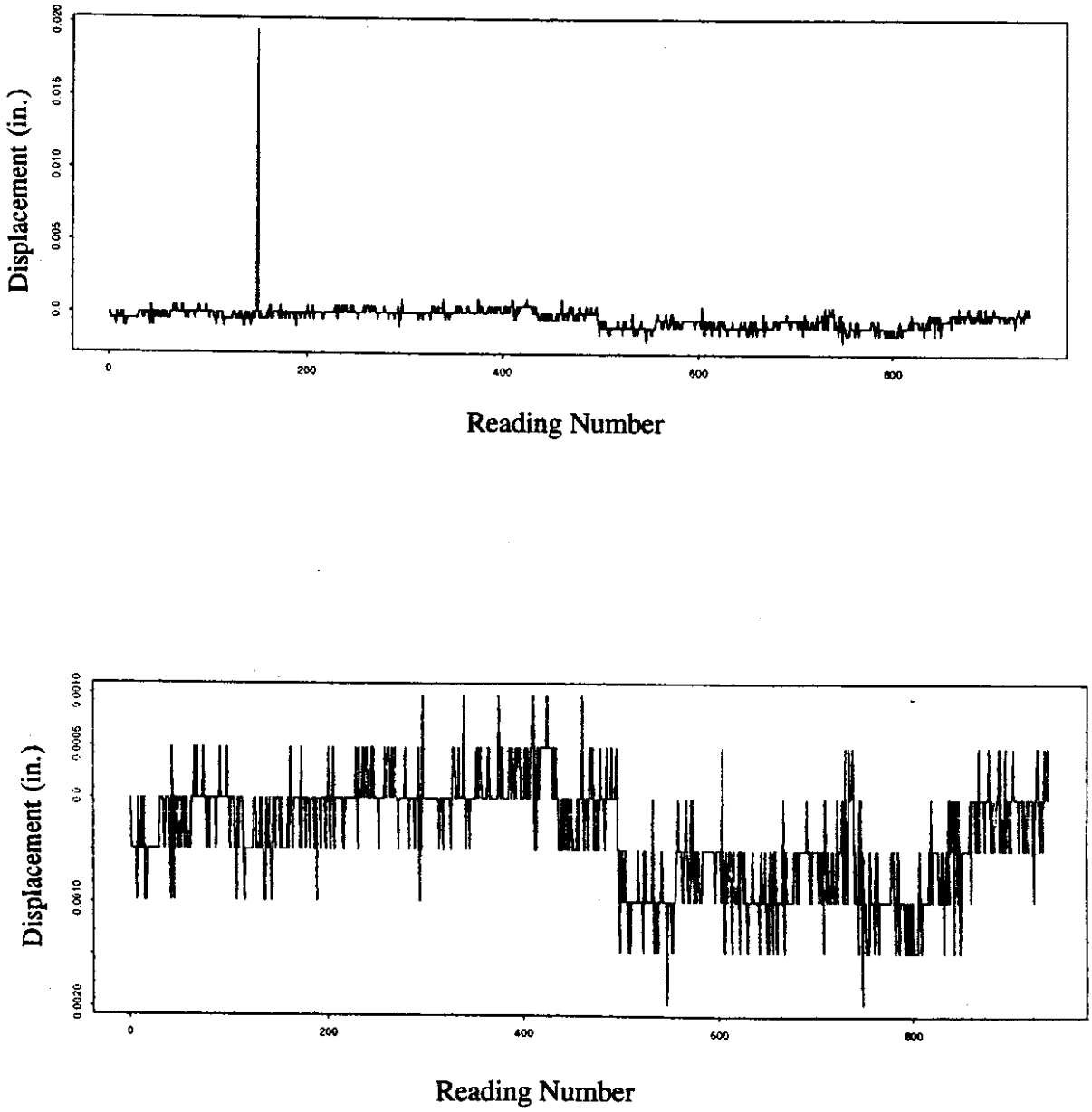

Figure 6.3. Measured and Corrected Displacements for WNB1T

An operator blunder affected three values of the pump pressure. During the test, an operator accidentally reversed a switch that controlled the polarity of the pump pressure potentiometers. This sign error was corrected.

An operator error during half-cycle B2N2 created another series of meaningless data points. At one point during unloading, the rams were retracted without sufficiently moving the prestressing chucks. Consequently, for a short time, the prestressing chucks (instead of the rams) carried the cable tension; although the pump pressure was reduced, the structure was not unloaded. This data can be easily identified in Figure 6.1 in the form of nearly vertical lines at a displacement of approximately minus 5 inches. The affected readings (readings 658 to 663) were removed; this purging created a gap in some of the response histories. In other response histories, such as the one shown in Figure 6.4, the purged data were replaced with values that were interpolated from the remaining adjacent data points.

6.3 CORRECTION TO ACCOUNT FOR ABUTMENT RESISTANCE

The researchers modified the structure's measured response to account for the resistance that the abutment-isolation system provided. As described in Section 4.3, the researchers estimated that a 18-kip force was necessary to overcome the isolation system's resistance. The structure's force-displacement behavior, shown in Figures 6.1 and 6.4, was consistent with this estimate. For both directions of loading, the force-displacement curve rises almost vertically to a force of approximately 18 kips before significant displacement begins.

To obtain additional corroboration of the friction estimate, the researchers compared the measured deck deflection with the deflection calculated for two 15-kip loads. The researchers modeled the deck with a linear finite element program (SAP90 (12)) as a simply-supported beam with 15-kip loads applied at the bents and with 15-kip reactions at the endwalls. The pier and railing stiffnesses were neglected. The pier deflection was calculated to be 0.0092 inches.

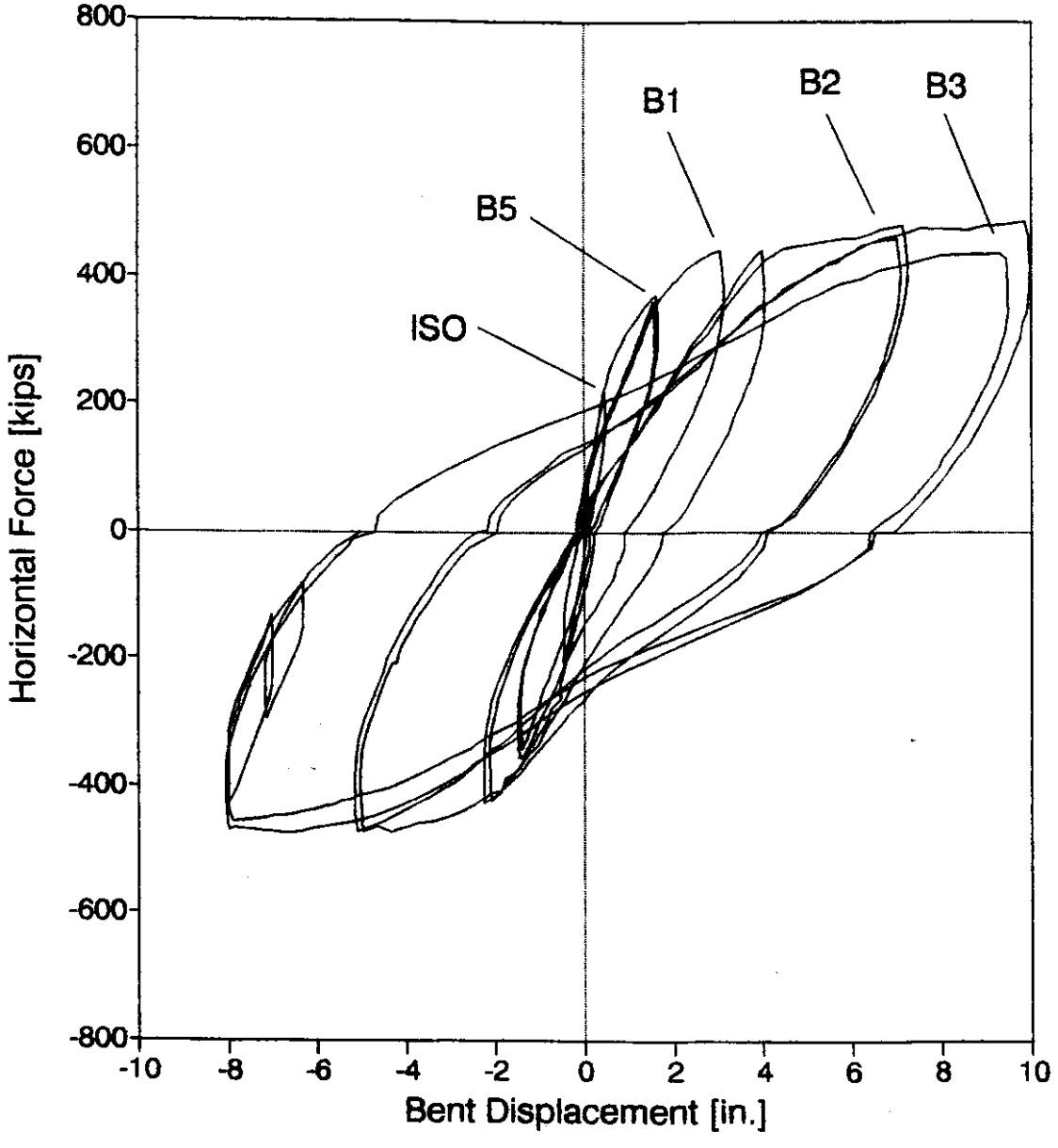

Figure 6.4. Force-Deflection Response, Corrected for Operator Error

The researchers compared the calculated deck deflection with the difference between the measured pier and the endwall displacements (Figure 6.5). Only the first 250 readings are presented in Figure 6.5 because the endwall instruments ran out of stroke after that point. Figure 6.5 shows that, within a cycle, the difference between the pier and endwall displacements was consistent with the calculated elastic deflection. The remarkable agreement between the instruments also increased the confidence that could be placed in the individual histories. Though one spike is approximately 0.07 inches high, it should be noted that the maximum structural displacement during these cycles was 1.5 inches.

A simple model that accounted for the abutment's resistance was used to correct the measured response. Figure 6.6(a) illustrates a structure that is subjected to a lateral load. For convenience, it is assumed that the structure exhibits elastic, perfectly-plastic behavior (Fig 6.6 (b) and (c)). Figure 6.6(d) shows the same structure, but with the addition of a Coulomb-friction element to model the isolation system. The hysteretic response of this system is shown in Figure 6.6(f).

A comparison of the two load-displacement curves shows the effect of friction (Figure 6.6). First, the force on the structure increases to a force equal to the frictional resistance (μN) before the structure displaces. Second, at peak loading, the applied force decreases by $2\mu N$ before the structure displaces in the reverse direction. Third, the unloaded structure contains residual forces in the spring and friction elements; the magnitude of these opposing forces is μN. A close examination of the recorded force-displacement behavior, shown in Figure 6.4, reveals that the measured response was similar to that of the simple model.

The effect of the isolation-system friction was removed from the measured loads to obtain the behavior of the bents as follows:

- during loading, the applied force was set equal to zero when the total force on the structure was less than the friction force;

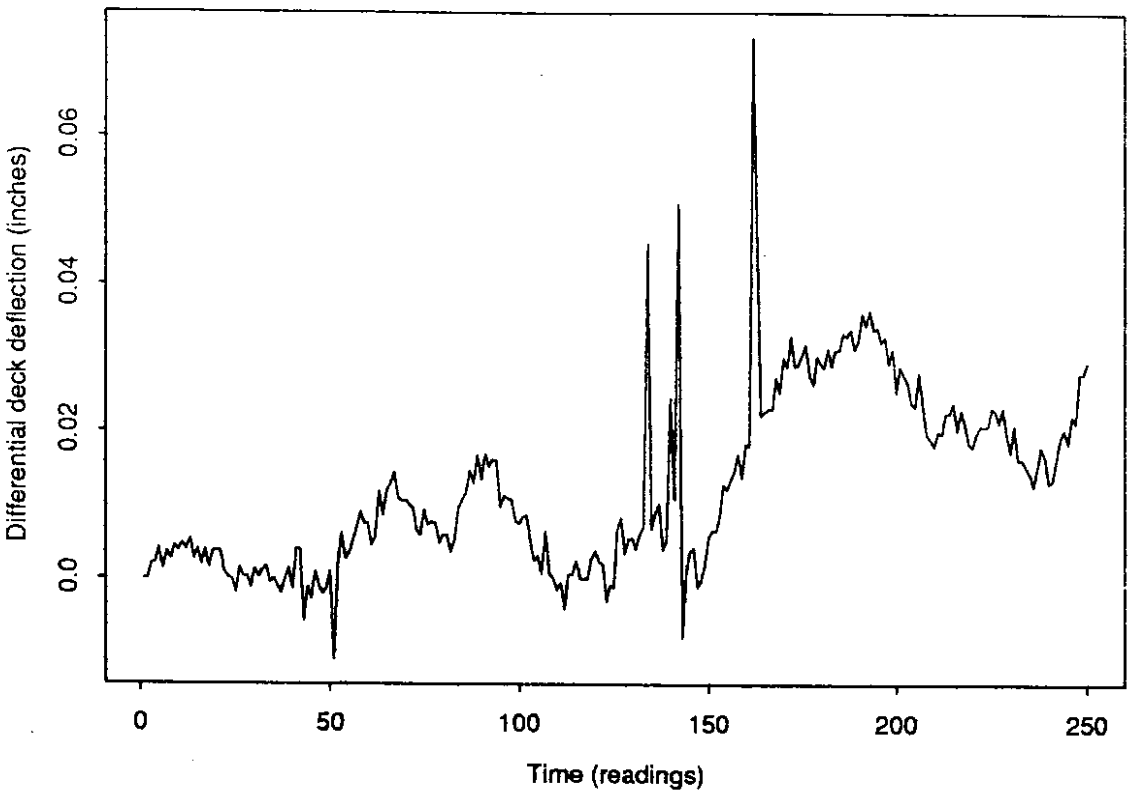

Figure 6.5. Deck Deflection

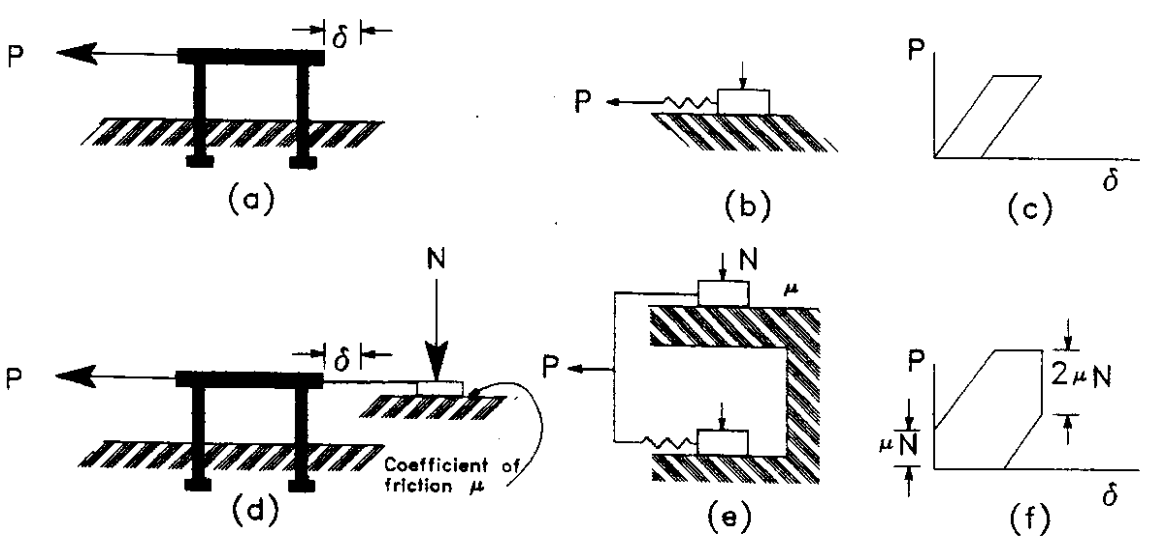

Figure 6.6. Simple Model of Pier-Isolation System Interaction

- during loading, the friction force was subtracted from the applied force when the total force on the structure exceeded the friction force; and
- during unloading, the frictional force was added to the applied force.

The modifications had the effect of lowering the loading portion of the curve and raising the unloading portion by an amount equal to μN. This lowering and raising is analogous to correcting the model curve in Figure 6.6 from 6.6(f) to 6.6(c). The difference between the original force displacement behavior and the corrected behavior is shown in Figure 6.6 for the large displacement cycles (half-cycles B3S1, B3N1, B3S2, and B3N2).

This correction was not completely effective for the unloading portion of the hysteresis plots. As shown in Figure 6.7, the unloading curves still exhibited small jumps for some cycles at the zero force level. These jumps in the unloading curve may have been caused by creep in the isolation system, and to a lesser extent, in the piers. During loading, the force was increased at such a rate that the total force on the structure exceeded 18 kips within a few minutes of the beginning of the half cycle. In contrast, during unloading, delays often lasted 30 minutes to 2 hours, during which the researchers recycled the jacking frames. These delays may have been sufficient for the structure and isolation devices to relax.

6.4 CURVATURE CALCULATION

The instruments installed at the tops and the bottoms of the columns were designed to measure the relative rotations of the column cross sections. The procedure that the researchers followed to convert the measured displacements to rotations was based on the geometry shown in Figure 6.8. Using the displacements measured by opposing instruments, I_1 and I_2, the relative rotation, θ, of the plane connecting the instruments was calculated with the following equation:

$$\theta = 2 \text{ ATAN } \frac{(I_1 - I_2)}{2D} \qquad (6.1)$$

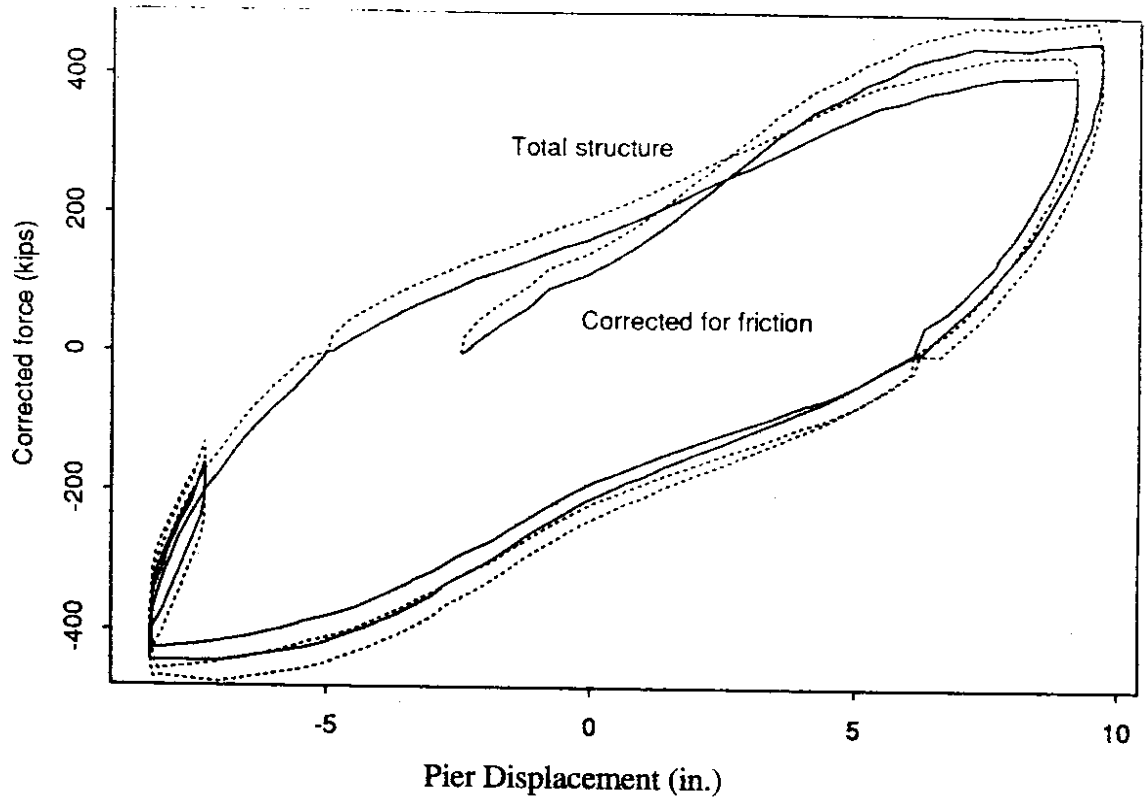

Figure 6.7. Effect of Friction Correction on Pier Hysteresis

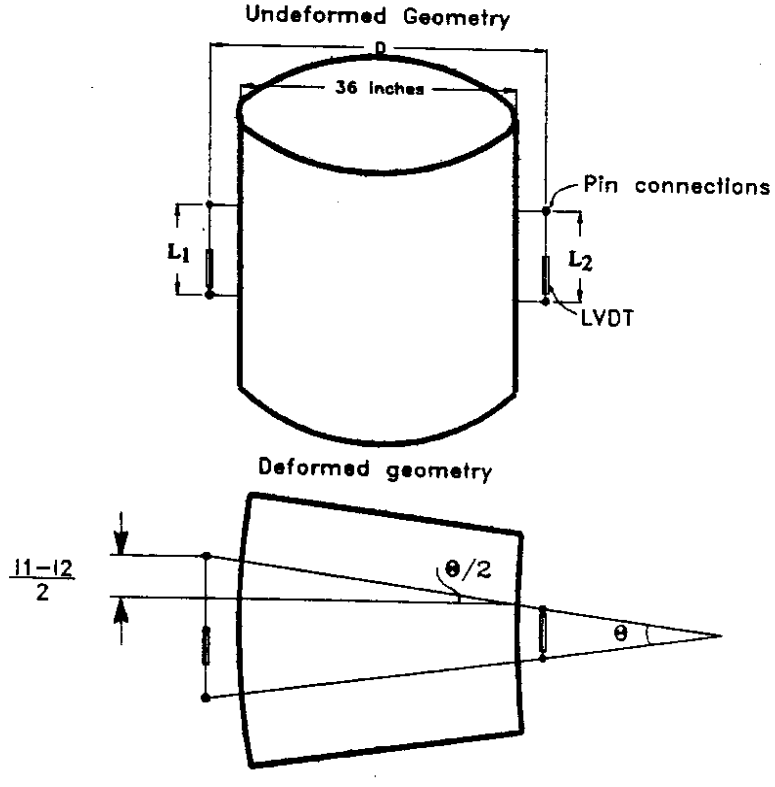

Figure 6.8. Geometry of Column-Curvature Instrument Pairs

where D is the distance between the instruments. The average curvature of the column, Φ, was calculated with the following relationship:

$$\Phi = 2\,\mathrm{ATAN}\,\frac{(I_1/L_1 - I_2/L_2)}{2D} \tag{6.2}$$

where L_1 and L_2 are the gauge lengths for the instruments.

CHAPTER 7

LATERAL-LOAD RESPONSE

During Phase II, the piers were subjected to transverse displacements of 1.5, 3, 6, and 9 inches, which corresponded to drift ratios of 0.5, 1, 2, and 3 percent, respectively (Figure 1.4). This chapter presents the piers' response to the applied loads, as documented by displacement and curvature response histories, as well as sketches and photographs.

7.1 RESPONSE HISTORIES

The measured response histories can be grouped into the following categories:

- pier translation,
- crossbeam curvature,
- column curvature, and
- footing rotation and translation.

As described in Section 6.3, the response histories were corrected to remove the influence of the isolation system's resistance. Though over 60 channels of data were recorded during the tests, only representative plots are presented in this section. Additional individual response histories, along with their naming conventions, are presented in Appendix C.

Pier Translation

The researchers constantly monitored the applied forces and the piers' transverse motion. A hysteresis curve for corrected applied load versus average pier displacement is shown in Figure 7.1. Maximum lateral displacements were corroborated by the less precise measurements of an electronic distance meter. The piers resisted an applied force of approximately 400 kips, which corresponded to approximately one third of the bridge's weight. Although the structure's stiffness decreased with repeated, cyclic loading, its lateral-load resistance degraded only minimally, even at a drift ratio of 3 percent. The

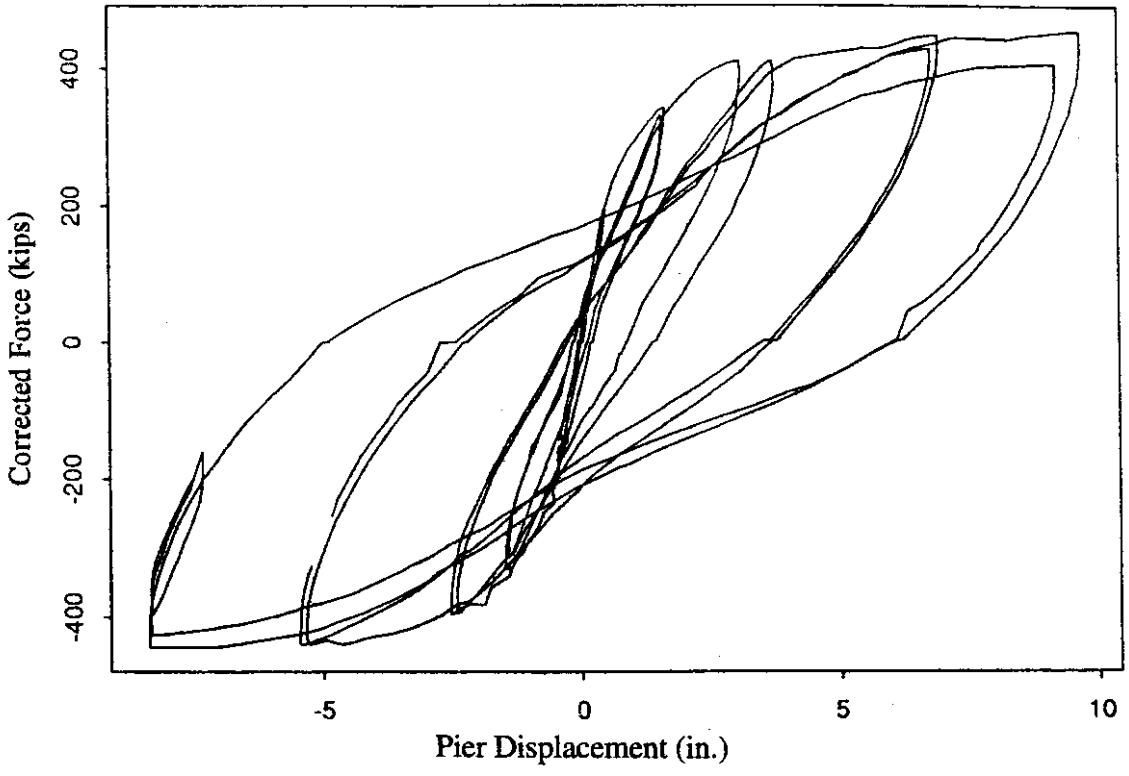

Figure 7.1. Corrected Force-Displacement Response for Piers

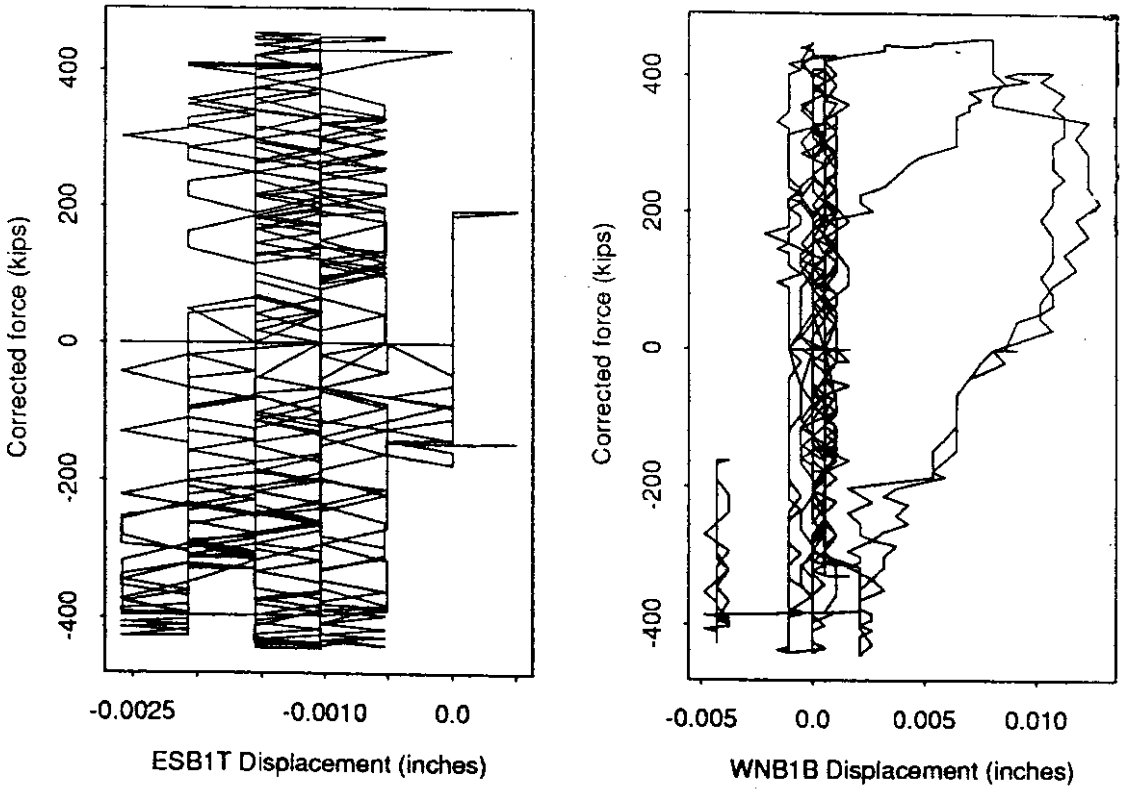

Figure 7.2. Measured Displacements for Crossbeam Instruments

shear and axial-load capacities did not degrade sufficiently that either a shear or axial-force failure occurred.

In Phase II, the abutment displacements were not closely monitored beyond the first few cycles because the pier and abutment displacements were nearly identical. The abutment displacement histories were used only to estimate deck deflection during the first few inches of displacement (Section 6.3) because larger displacements exceeded the abutment instruments' stroke.

Crossbeam Curvature

The crossbeam instruments were installed to measure the relative rotations of crossbeam cross sections near the columns (Figures 5.2 and 5.5). Figure 7.2 shows the displacement history for an east bent crossbeam instrument located near the south column (ESB1T). The displacements at this location produced voltages that were on the order of the least count of the analog-to-digital converter. No movement larger than 0.0025 inches was recorded. This history was typical of the crossbeam-instrument histories.

Figure 7.2 also shows the only crossbeam-instrument history with significant displacements (WNB1B). This instrument, located on the crossbeam near the northwest column, detected a 0.01-inch displacement during the last two loading cycles. This recorded displacement was consistent with the observation that a hairline crack opened in this location.

Column Curvature

The instruments installed at the tops and the bottoms of the columns worked in pairs to measure the relative rotations of the column cross sections; average column curvatures were calculated with Equation 6.2. Figure 7.3 shows the curvature histories for the three instrumented segments at the top of the northwest column. As expected, the curvature was largest for the top 3 inches of the column, and the curvature decreased as the distance from the crossbeam increased. This trend was consistent throughout the

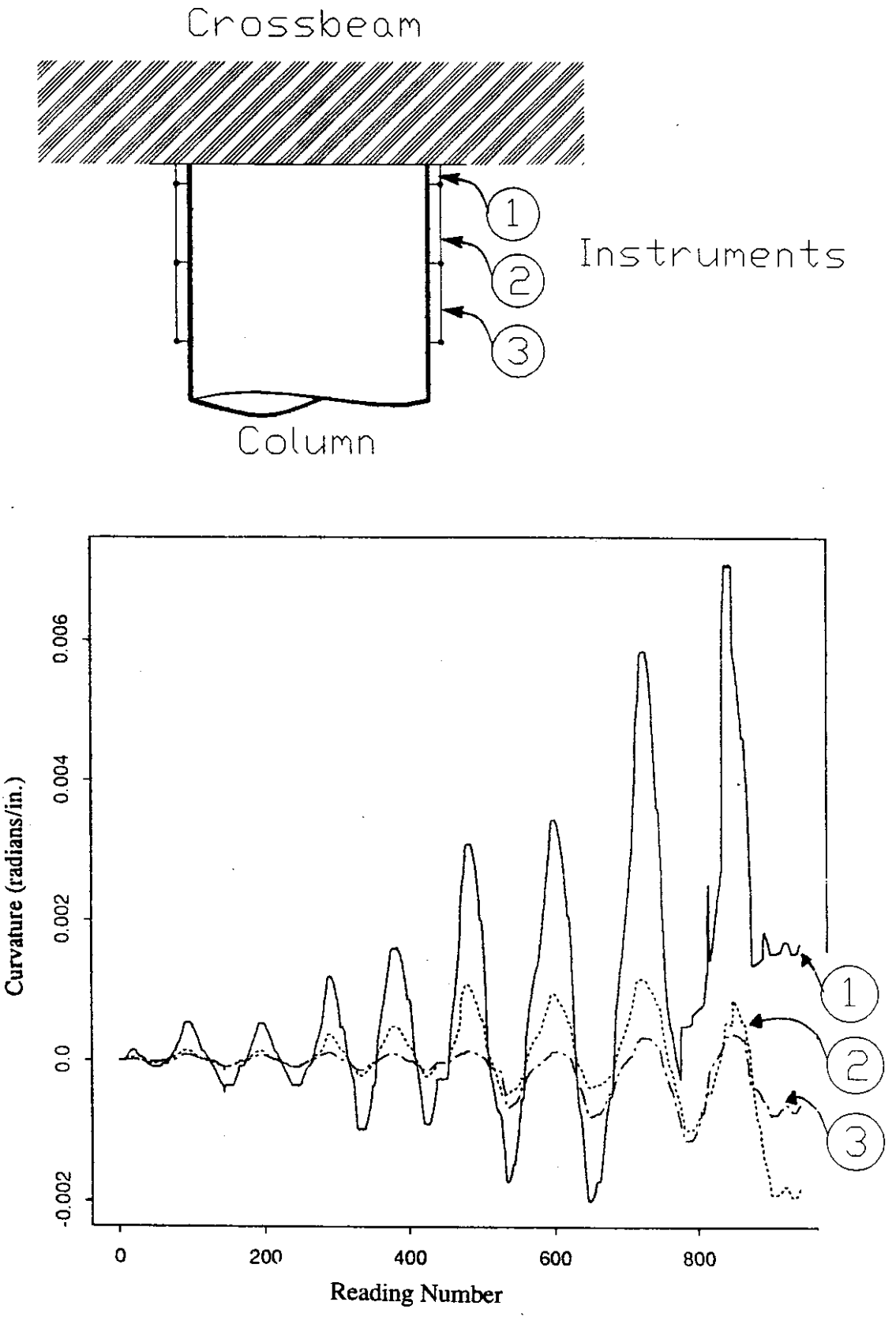

Figure 7.3. Curvature Histories for Northwest Column

tests. The three curvature histories reported in Figure 7.3 (WNCT1, WNCT2, and WNCT3) were combined to produce a hysteresis plot for the top 27 inches of the west pier's north column (Figure 7.4(a)). The measured column curvatures are consistent with the direction of the applied load.

Peak curvatures for each cycle are plotted in Figure 7.5 for the west pier's north and south columns. With the exception of the last two cycles, the curvatures consistently increased in successive cycles. The maximum curvatures measured during the last two cycles were not consistent with the measurements in previous cycles. It is likely that extensive spalling of the cover concrete affected these measurements.

The measurements were less reliable at the bottoms of the columns. Despite extensive efforts to protect the instruments in these locations, they suffered severely from falling rocks and soil. Figure 7.4(b) displays the curvature history for the only bottom-of-column instrument pair that was not significantly disturbed by the soil (WNCB3). This instrument pair measured curvatures for the column segment that ranged from 27 to 51 inches above the footing; these instruments were never buried in soil.

Footing Rotation and Translation

The footing rotation instruments were not greatly affected by falling soil because they were protected by wooden shelters. As shown in Figure 7.6, the voltages produced by the instruments were near the resolution of the analog-to-digital converter. To investigate the periodicity of the measurements, the researchers fitted a smooth curve to the data. The correlation between the fitted curves and the direction of applied loads suggests that some footing rotation was measured, but that it was very small, on the order of 0.1 degree.

The data from the footing translation instrumentation were severely affected by the soil and rocks that fell on the reference booms. The soil's effect was compounded by the researchers' movements; the researchers often disturbed the boom and the instruments when they entered the trench to record cracking patterns. Consequently, the measured

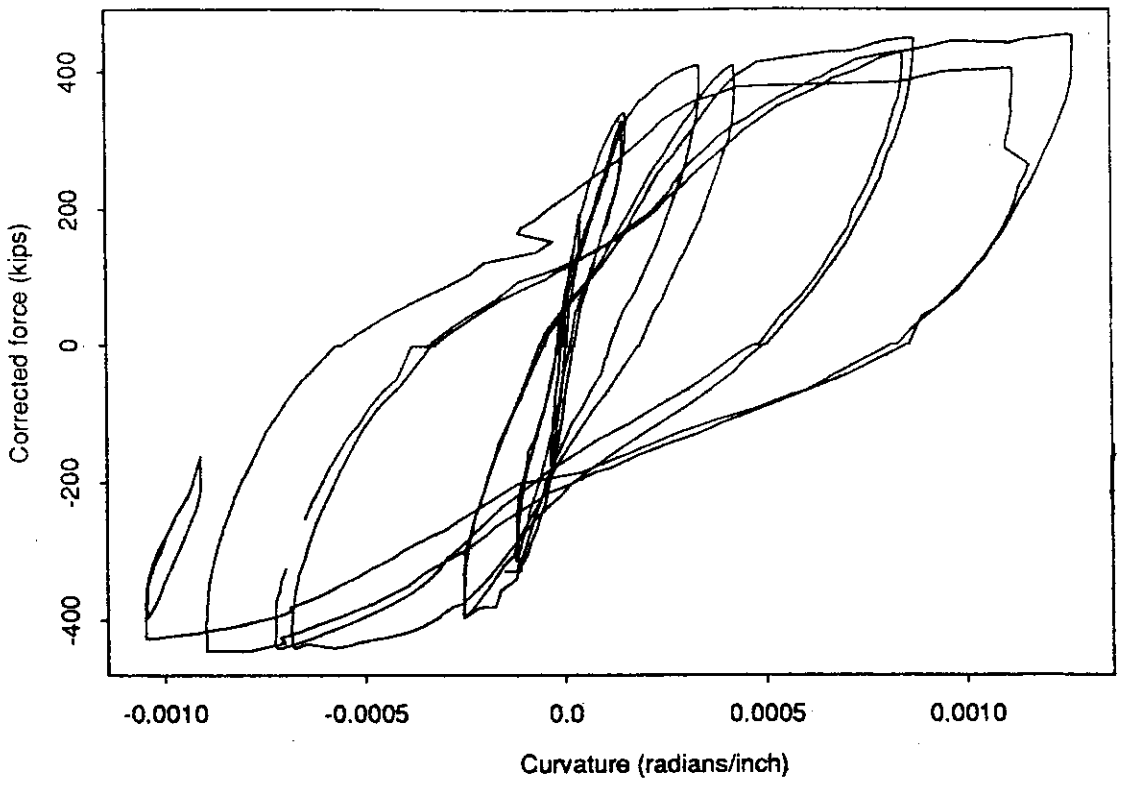

a) Top 27 Inches of NW Column

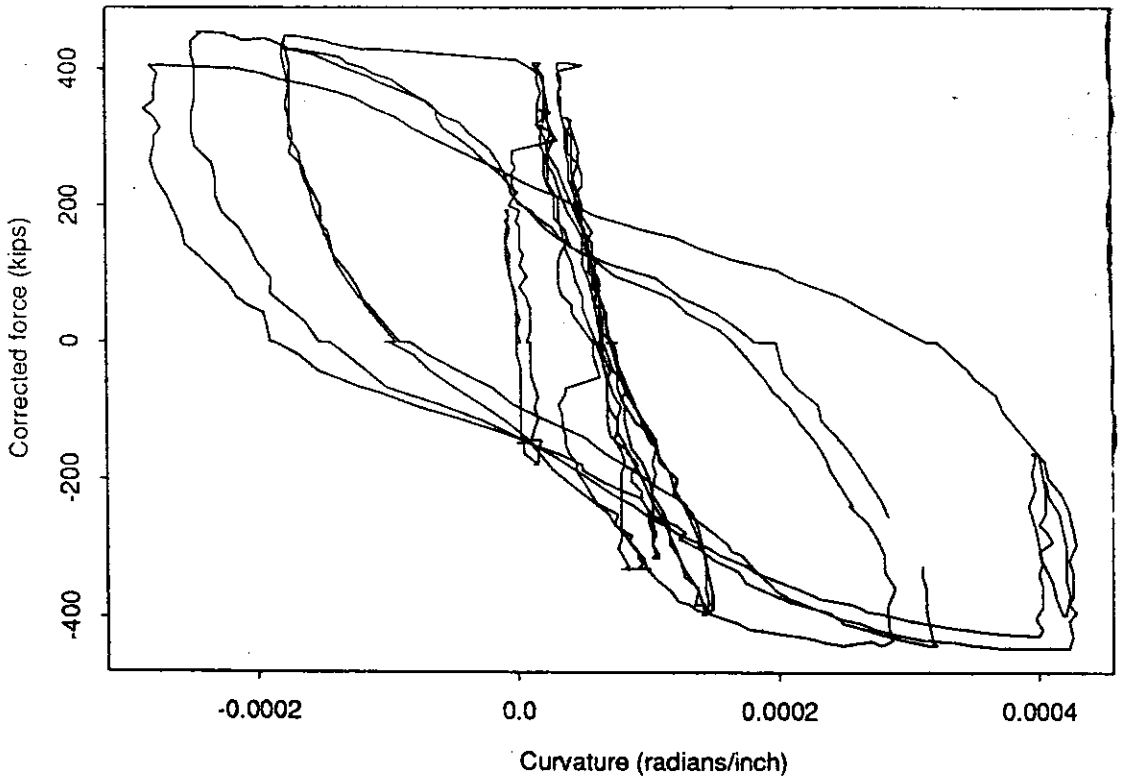

b) 27 to 51 Inches Above NW Footing

Figure 7.4. Force-Curvature Hysteresis Curves for Northwest Column

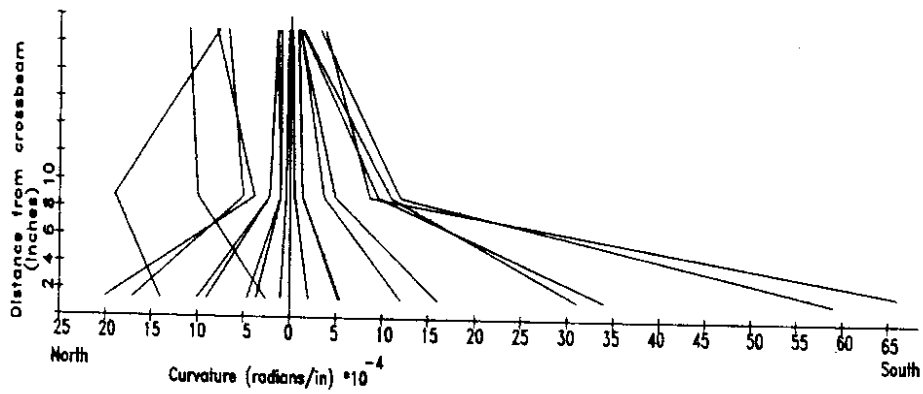

a) North Column

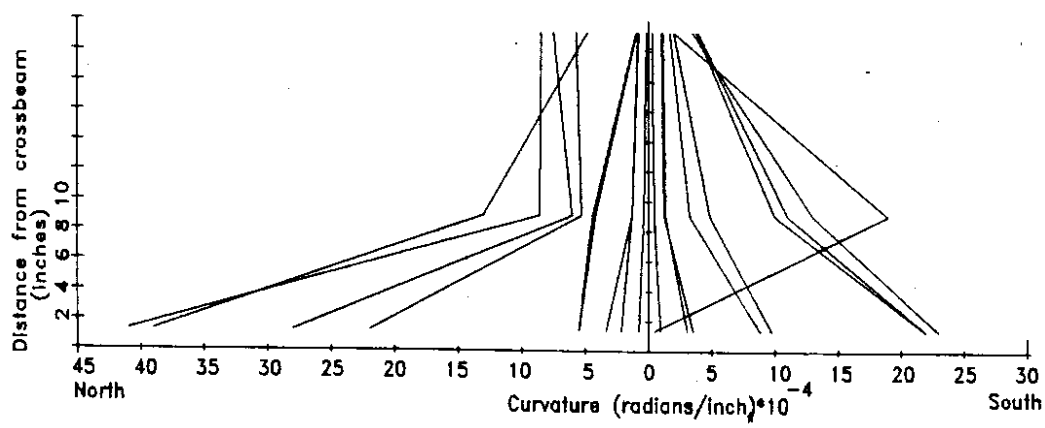

b) South Column

Figure 7.5. Maximum Curvatures for Top of West Pier Columns

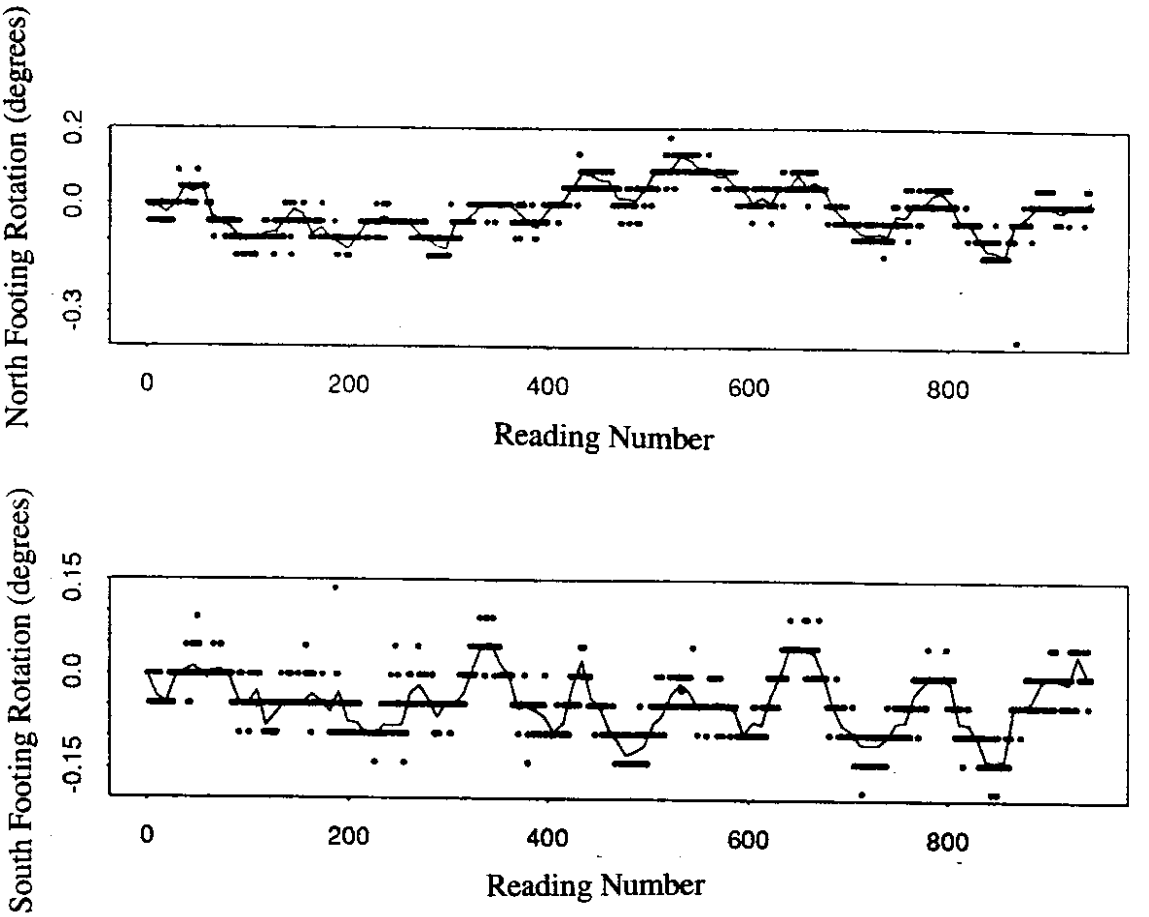

Figure 7.6. Footing Rotation Histories

response (Figures 7.7 and 7.8) was erratic and it was useful only in setting an upper bound on displacement. Given the variation within the typical cycles, it appears that the footing moved less than 0.05 inches during a typical cycle. This limit is consistent with the fact that no signs of footing translation were observed.

7.2 OBSERVED DAMAGE

At each peak displacement, the research team sketched crack patterns and the extent of spalling. To aid in making these sketches, the researchers marked a grid on the columns and data sheets. Damage was also documented by photographs and observations logs; observations of the columns' bottoms were restricted to the exposed east face.

Two factors caused the southeast column to appear more damaged than the other three columns. Before the tests began, the southeast column was cracked more than the other three columns; the southeast column was likely exposed to greater temperature variations during its lifetime. In addition, loose concrete was removed with a hammer from the southeast column throughout the test to determine the depth of damage. On the other columns, spalled concrete was removed only when the spalling threatened the instrumentation. In general, the northwest column was the least damaged.

Phase I Damage

Damage to the piers during Phase I had been limited to minor flexural cracking. (2) With the exception of a 0.02-inch wide crack at the top of the southeast column, all of the cracks had been 0.01-inches wide or less. No cracks had been visible at the bottom of the columns or on the crossbeams. As the columns had moved back and forth during testing, gaps had opened between the columns and the surrounding soil on the column tension side. During Phase I (cycle IIN1), the maximum separation between the columns and the surrounding soil had been 0.10 inches at a height of 10 feet above the footings. This gap had gradually tapered to zero at a height of 4 feet above the footing.

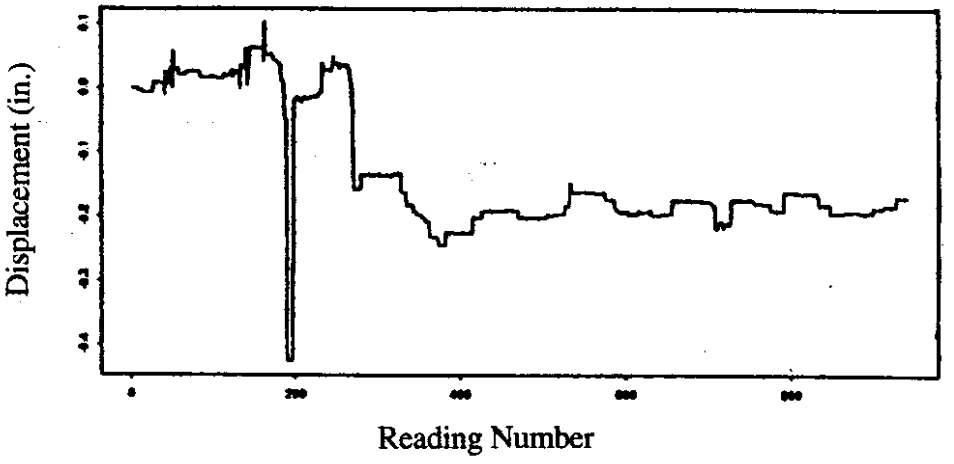

Figure 7.7. Southwest Footing Translation History

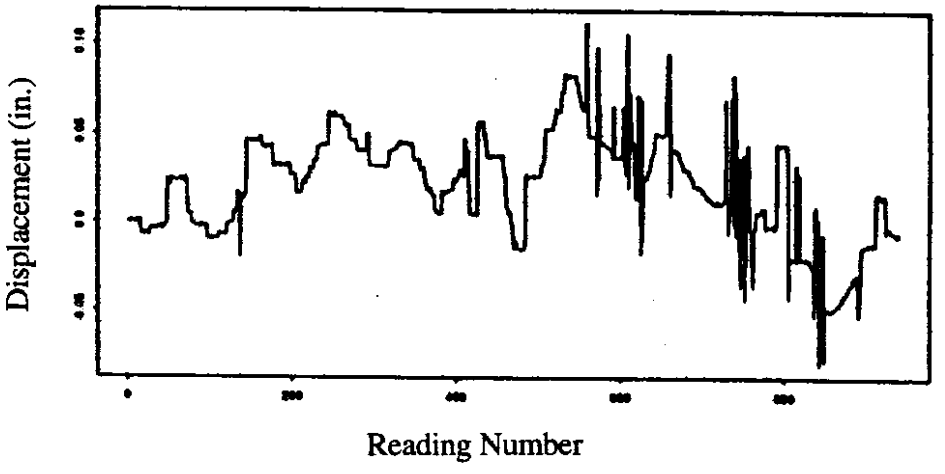

Figure 7.8. Northwest Footing Translation History

0.5 Percent Drift Ratio (B5)

At a displacement of 1.5 inches, equivalent to a drift ratio of 0.5 percent, the maximum crack size at the top of each column ranged from 0.02 to 0.04 inches (Table 7.1, half-cycle B5S1). Cracking extended 3 to 4 feet down the column face at approximately 12-inch spacings. The cracks coincided roughly with the hoop locations. Figures 7.9 and 7.10 show typical damage to the tops of the columns. No damage was discernible on the columns' compression faces. The damage at the bases of the columns was limited to a few hairline cracks at heights ranging from 2.5 to 5 feet above the footing.

After the direction of the load was reversed (half-cycle B5N1), the cracks that had opened in the previous half cycle closed completely. The crack patterns for the tension faces of the columns were similar to those observed during the previous half cycle. In addition, the research team observed minor flaking of the patching mortar on the column's compression face near the crossbeam. The damage did not increase significantly when the structure was subjected to a second cycle to a drift ratio of 0.5 percent (half-cycles B5S2 and B5N2).

1.0 Percent Drift Ratio (B1)

At a drift ratio of 1.0 percent, all of the columns had maximum crack sizes in the range of 0.08 to 0.12 inches (Table 7.1). The number of cracks on the tension face also increased, as shown in Figures 7.11 and 7.12. Note that Figure 7.11 shows photographs of the actual cracks; markers were not used to increase the crack's visibility. During the first excursion to a drift ratio of 1 percent (B1S1), the southeast column was the only column that had minor concrete flaking. Several new cracks appeared in the bottom of the west-pier columns, the largest crack being 0.01 inches wide. The movement of the columns wallowed out a hole in the surrounding soil.

The tensile crack patterns that formed when the load was reversed (B1N1) were similar to those that had formed in the previous half cycle. All of the columns had minor

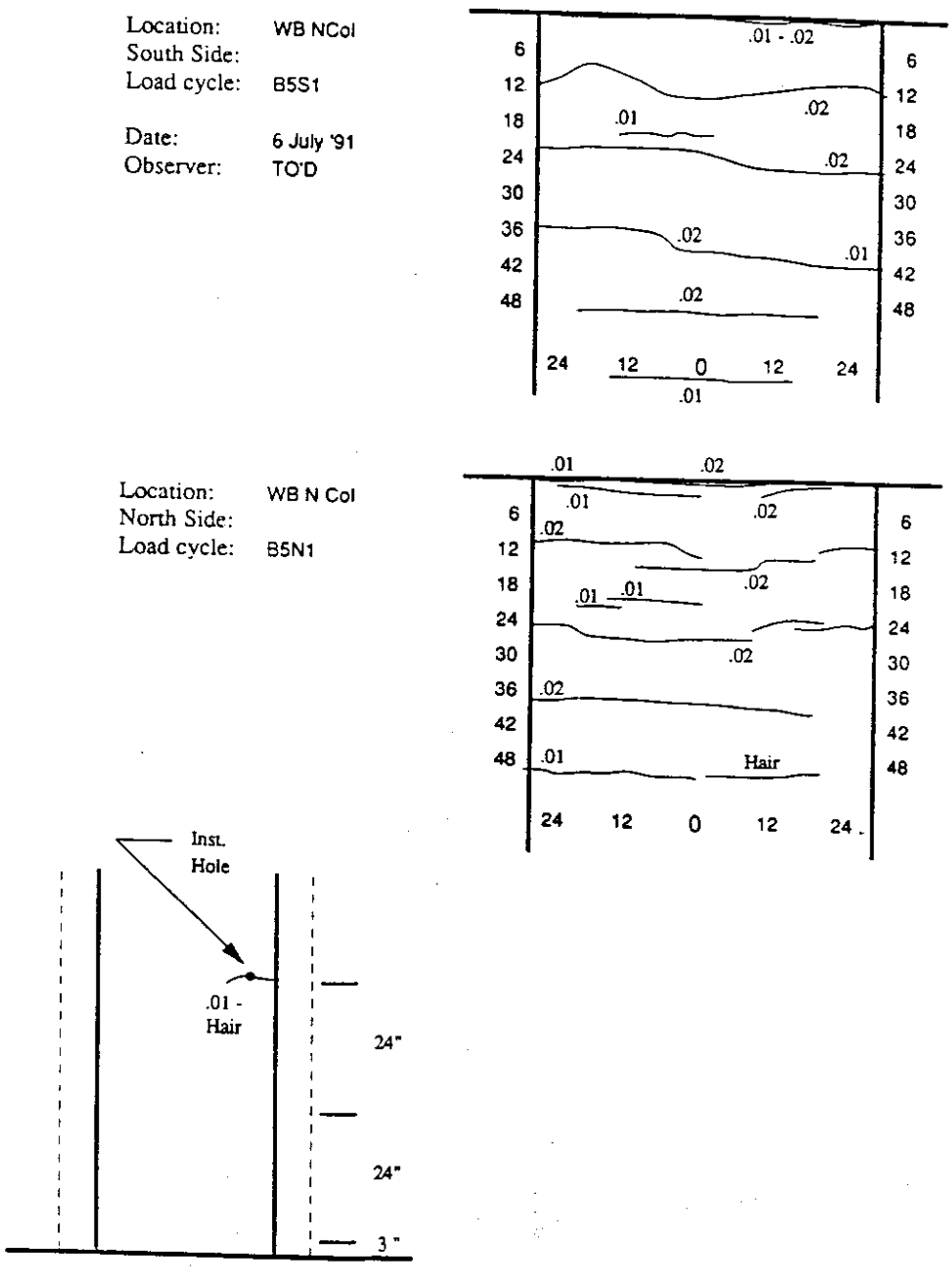

Figure 7.10. Sketch of Damage at 0.5 Percent Drift

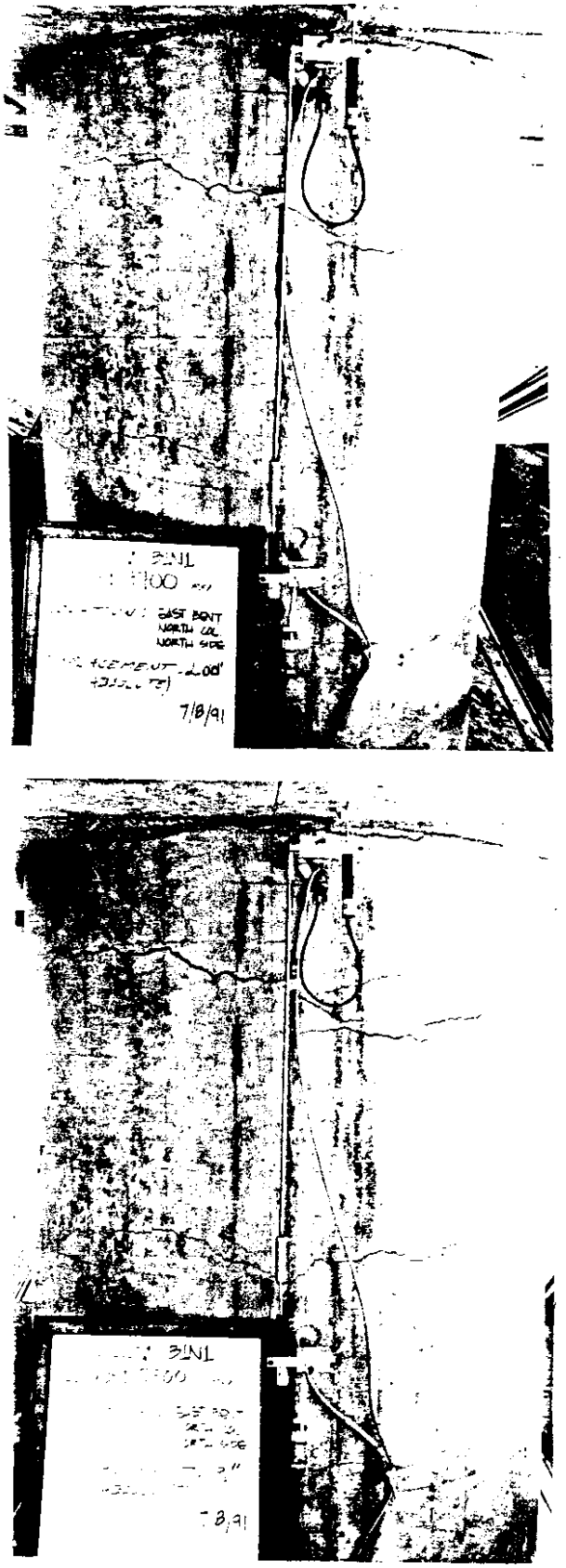

Figure 7.11. Photograph of Damage at 1.0 Percent Drift

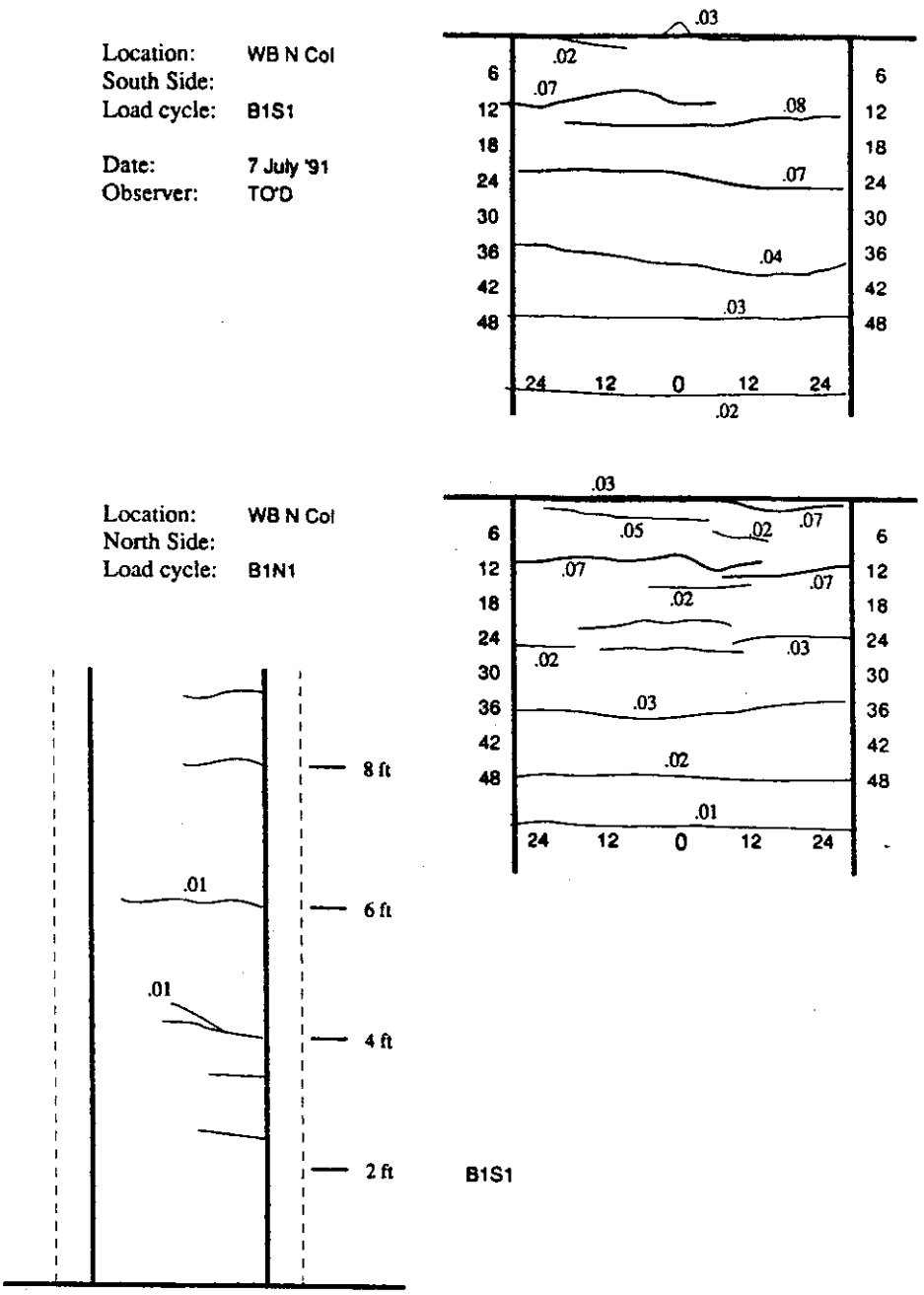

Figure 7.12. Sketch of Damage at 1.0 Percent Drift

flaking of the compression concrete. The southeast column, the column with the most damage, had a vertical crack on the compression face. In subsequent cycles at the same drift ratio (B1S2 and B1N2), some of the cracks did not close completely when the column face went into compression. In the last half cycle to a drift ratio of 1 percent (B1N2), the researchers tapped the cover on the tension side of the columns. On both the southwest and southeast columns, the researchers heard a change in pitch when the tapping moved up the columns. This change in pitch indicated that the cover concrete was beginning to detach from the core.

2.0 Percent Drift Ratio (B2)

At a 2.0 percent drift ratio, the maximum crack size ranged from 0.15 to 0.26 inches (Table 7.1). During the first excursion to a drift ratio of 2.0 percent, the onset of spalling was apparent on all of the columns. A semicircular piece of cover, with a radius of approximately 15 inches, was removed from the southeast column, but the steel was not visible in the first half cycle. At the base of the columns, the crack widths ranged from less than 0.01 inches to 0.05 inches. The largest cracks were in a region that was approximately 3 to 6 feet above the footing. At a height of about 10 feet, the gap between the soil and column was approximately 2 inches. The gap closed to approximately 0.10 inches at a height of about 2 feet above the footing.

Upon repeated loading to a drift ratio of 2 percent (B2N1, B2S2, and B2N2), all of the columns spalled on both sides (Figures 7.13 and 7.14). On the southeast column, two longitudinal reinforcing bars and a tie were visible. The repeated loading did not increase the damage at the base of the columns.

3.0 Percent Drift Ratio (B3)

At a 3.0 percent drift ratio, the largest displacement imposed on the structure, spalling was widespread in the top 2 feet of the columns, as shown in Figures 7.15 and 7.16. Large vertical cracks formed to accommodate the spalling. Diagonal cracking on the sides of the columns became much more pronounced. Bars buckled to the point that,

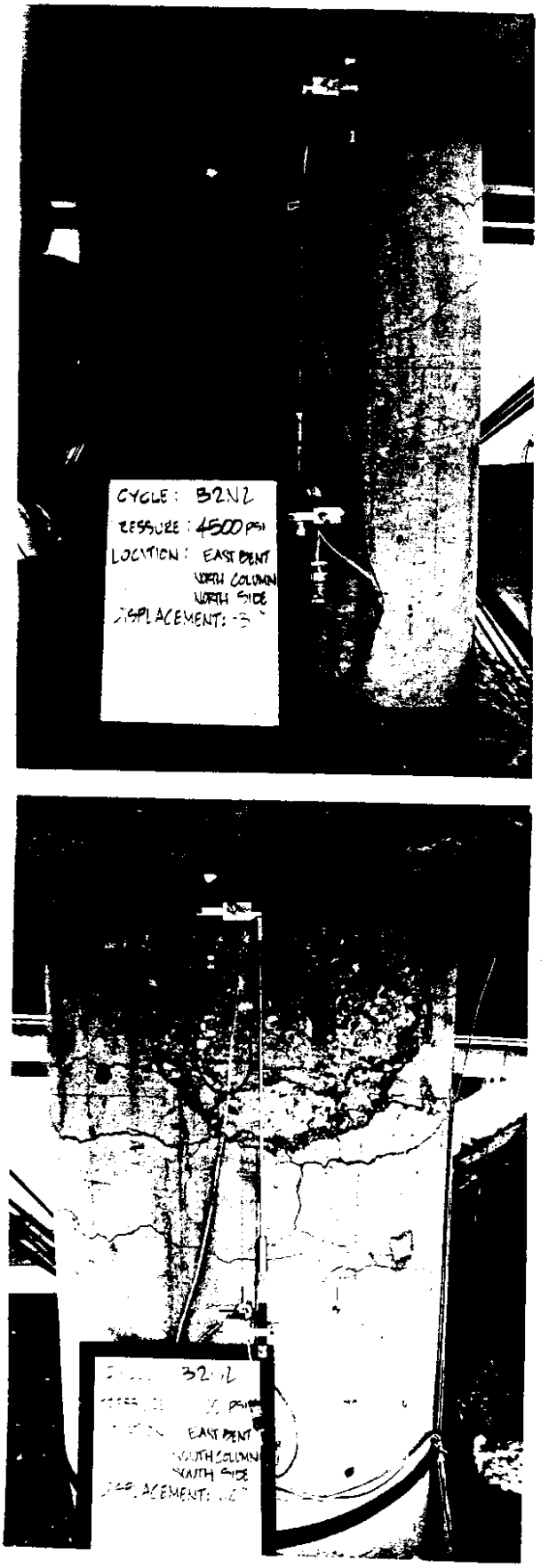

Figure 7.13. Photograph of Damage at 2.0 Percent Drift

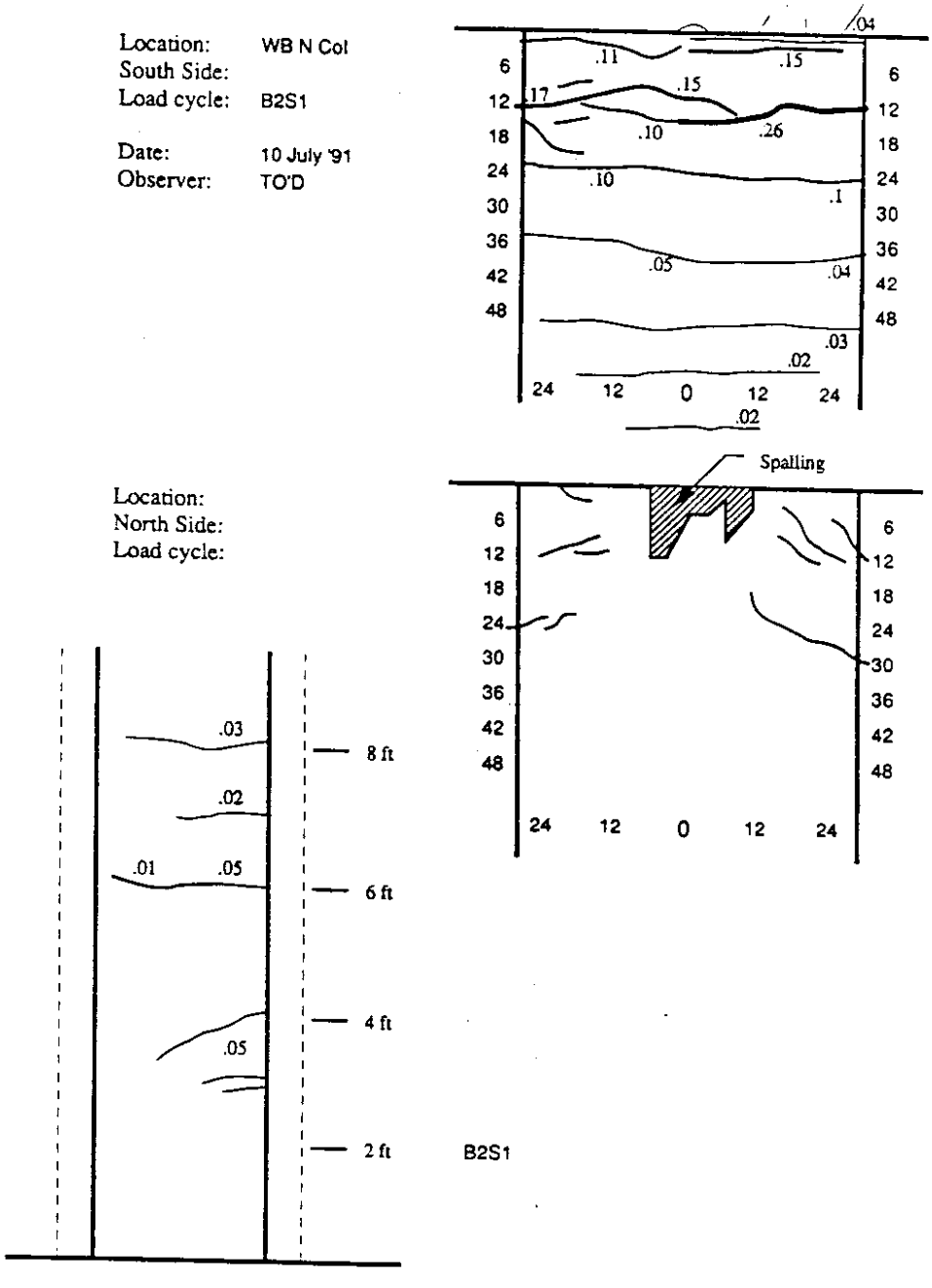

Figure 7.14. Sketch of Damage at 2.0 Percent Drift

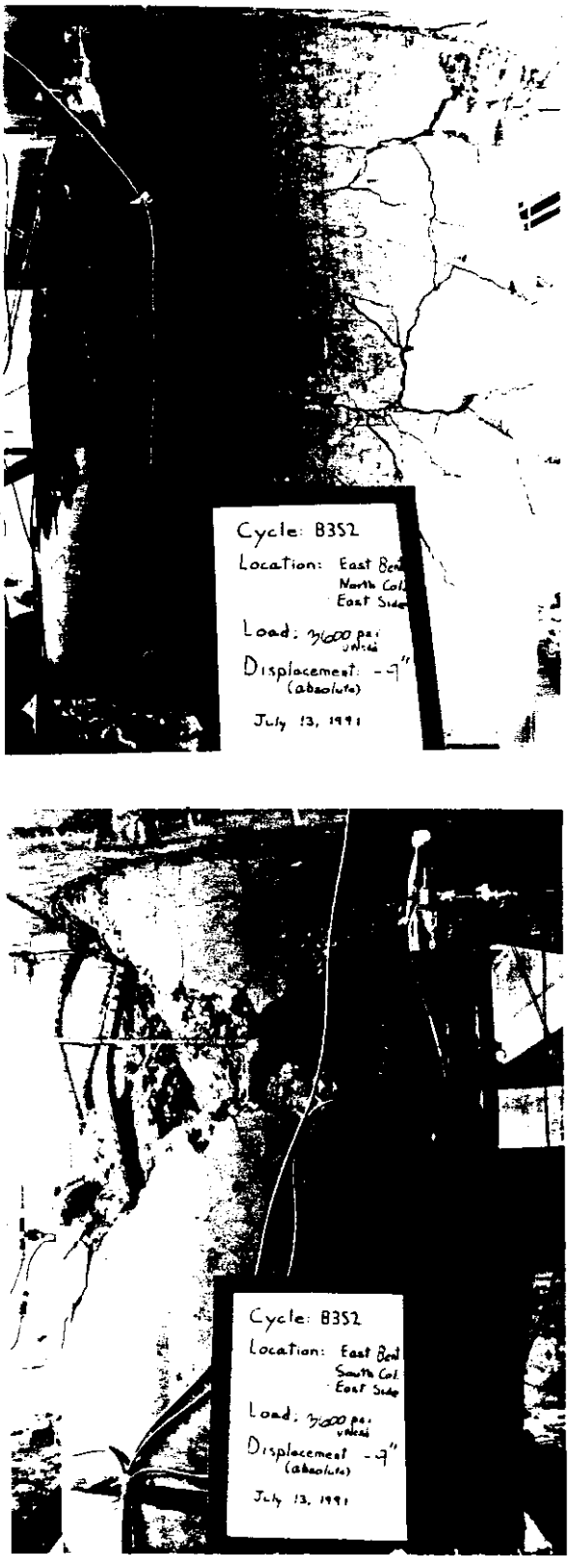

Figure 7.15. Photograph of Damage at 3.0 Percent Drift

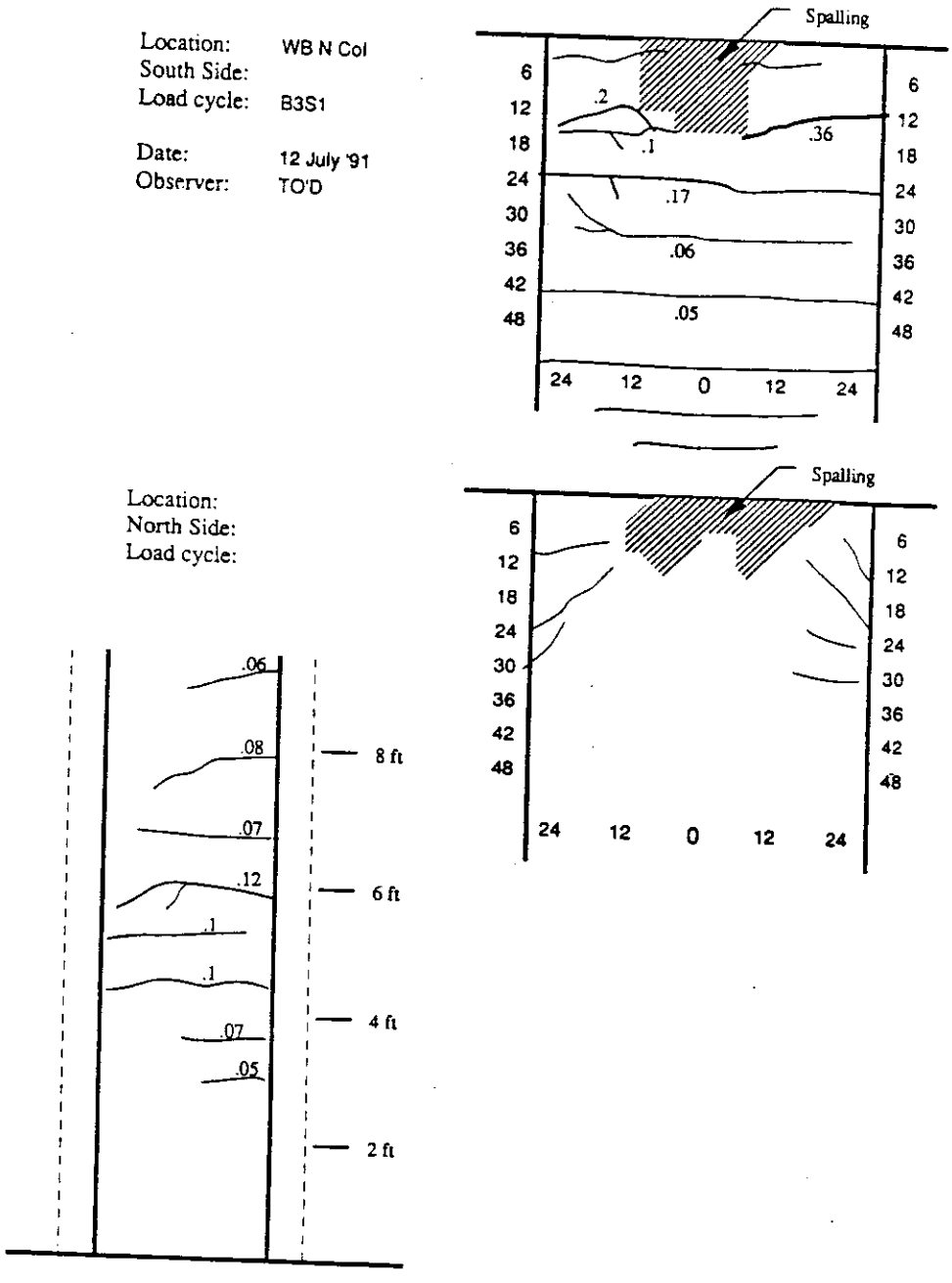

Figure 7.16. Sketch of Damage at 3.0 Percent Drift

on the southeast column, there was a gap between the longitudinal bar and the core. On the other columns, the buckling also occurred, but it was less drastic than on the southeast column.

At the end of the second cycle to a drift ratio of 3.0 percent, the spalling had spread, and all of the columns had some longitudinal bars that had buckled. On the lower portions of the columns, cracking was more widespread than at lower drifts; however the bottom was much less damaged than the tops of the columns (Figure 7.16). Despite the heavy damage to the columns, no footing damage was observed. Crossbeam damage was limited to minor cracking near the beam-column joint.

CHAPTER 8

ANALYSIS

The piers' measured response was compared with the responses calculated by the researchers (UW model), the California Department of Transportation (CALTRANS model), and the Washington State Department of Transportation (WSDOT model). The UW model was developed on the basis of the measured properties of the concrete, reinforcing steel, and soil. In contrast, the state engineers were supplied only with the information that would be routinely available to them in assessing a bridge's seismic vulnerability. Though the researchers did not modify the model to reproduce the measured response, they had the advantage of being aware of the measured response. The state agency engineers performed their analyses without knowing the measured response. Consequently, in comparison with the UW model, the CALTRANS and WSDOT models were more representative of standard practice.

8.1 DESCRIPTION OF UW MODEL

The researchers combined a series of linear models to perform step-by-step nonlinear analysis of a single column. At each step, the properties of the linear model were modified to be consistent with the columns' nonlinear moment-curvature relationship.

Linear Model

The linear analyses were performed with the SAP90 structural analysis program. (12) Each linear model consisted of 25 frame elements and 12 horizontal springs, as shown schematically in Figure 8.1. The springs modeled the soil's resistance over the bottom 13 feet of the column. Loads were applied at the top of the column.

The top of the column was fixed against rotation but was free to translate horizontally. This boundary condition was reasonable because the crossbeam/diaphragm combination was stiff and because no crossbeam rotation was measured. Similarly, the

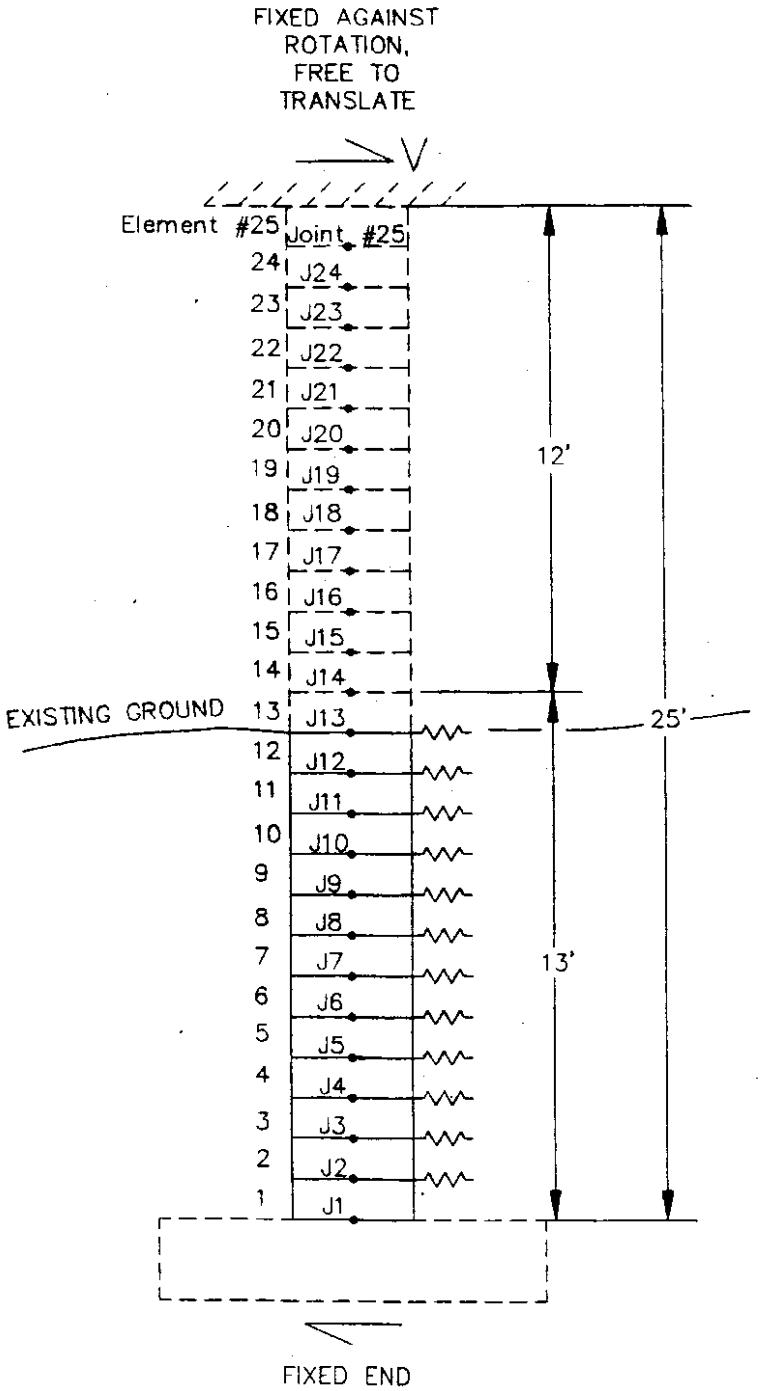

Figure 8.1. Analytical Model of Column

bottom of the column was fixed against rotation and translation. A typical input file is presented in Appendix D.

Moment-Curvature Relationships

The column's moment-curvature relationship was generated by a computer program (MPHI) that assumed that forces were in equilibrium and that sections that were plane before bending remained plane after bending. (13) As shown in Figure 8.2, the concrete's stress-strain relationship was modeled as a parabola below a strain of 0.002 and as a line for strains that exceeded 0.002. (14) The relationship was calibrated to be consistent with the measured compressive modulus, E_c, and the compressive strength, f'_c. The assumed stress-strain curve used to model the steel is shown in Figure 8.3.

The moment-curvature program did not account for confinement of the concrete. The effect of confinement was small because the confinement steel consisted of #3 hoops that were spaced at 1-foot intervals The corresponding spiral reinforcement ratio (volume ratio of confinement steel to confined concrete) was only 0.14 percent.. Furthermore, the hoops did not have hooks.

The moment-curvature relation was calculated for an axial load of 214 kips (210 psi), which corresponded to the tributary dead load for each column. The calculated moment-curvature relationship is shown in Figure 8.4. The column's ultimate moment was calculated to be 11,300 kip-inches.

Influence of Variations in Axial Load

Both the vertical component of the applied load and the overturning moment on the bridge modified the columns' axial load. Assuming that the maximum applied load in Phase II was distributed equally among the four columns, the vertical component of the maximum applied load was approximately 28 kips per column. The influence of this additional axial load can be estimated from Figure 8.5. The figure shows moment-axial load interaction diagrams calculated for nominal and actual material properties. A 28-kip

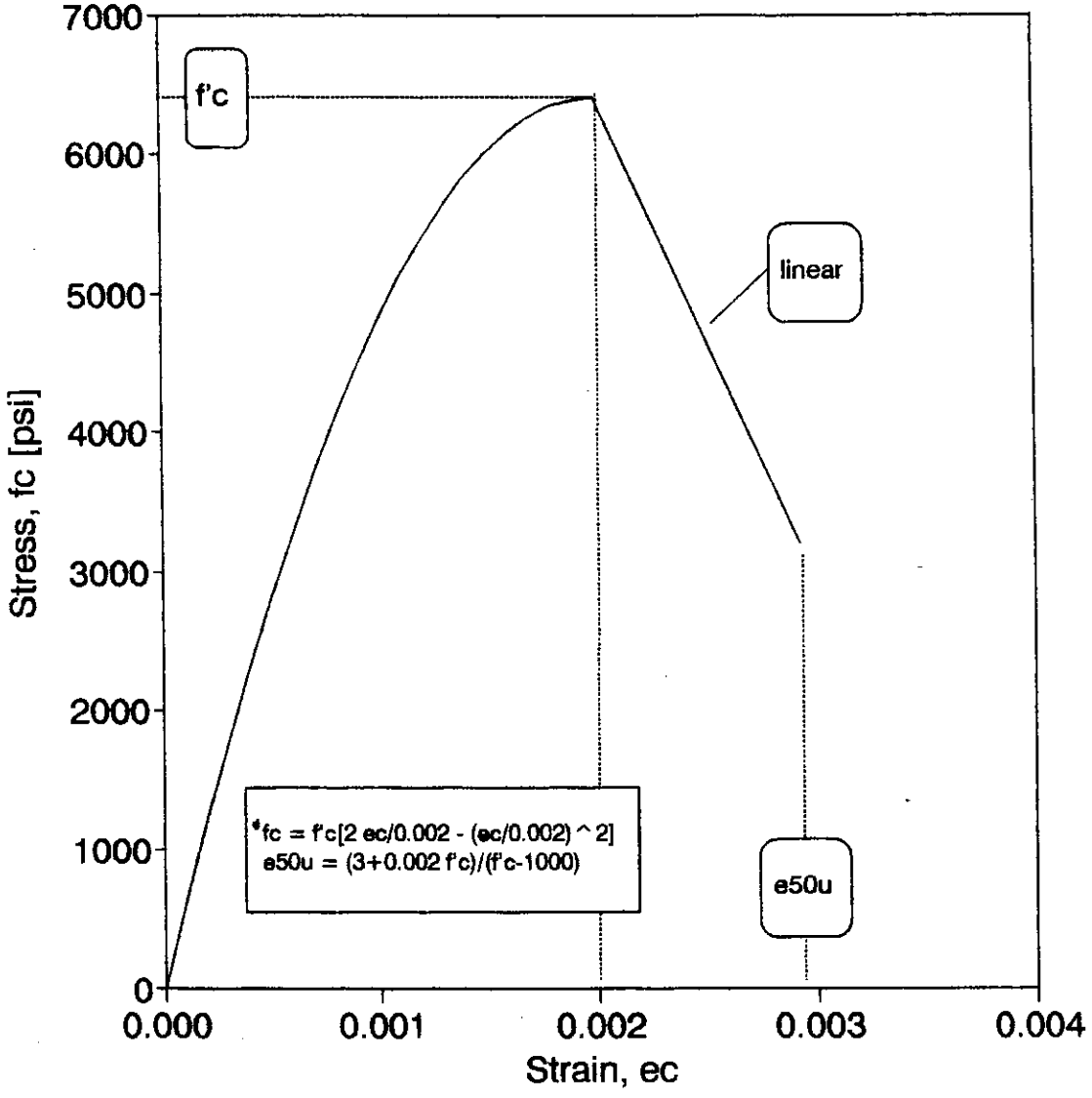

Figure 8.2. Assumed Stress-Strain Relationship for Concrete

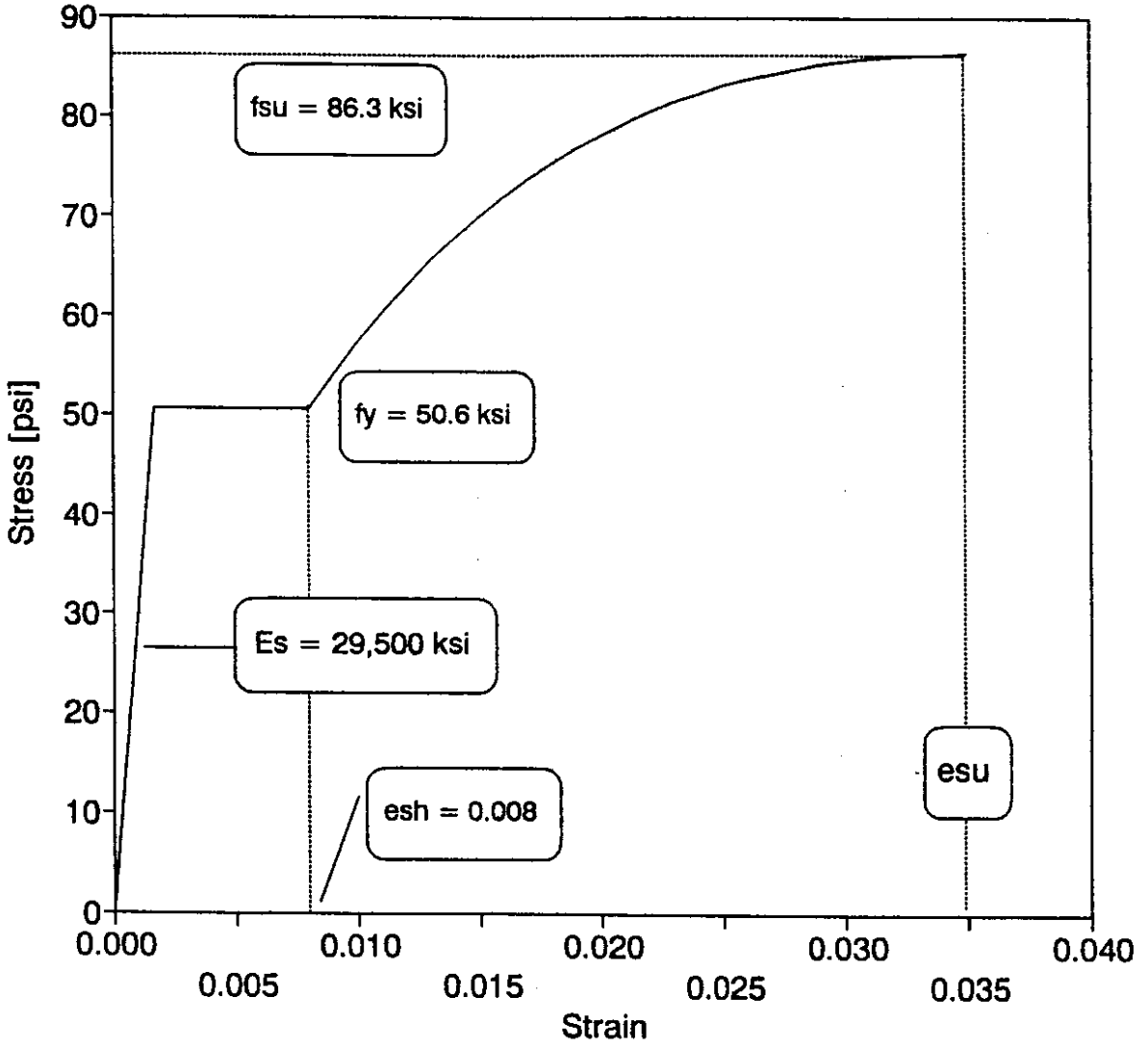

Figure 8.3. Assumed Stress-Strain Relationship for Steel

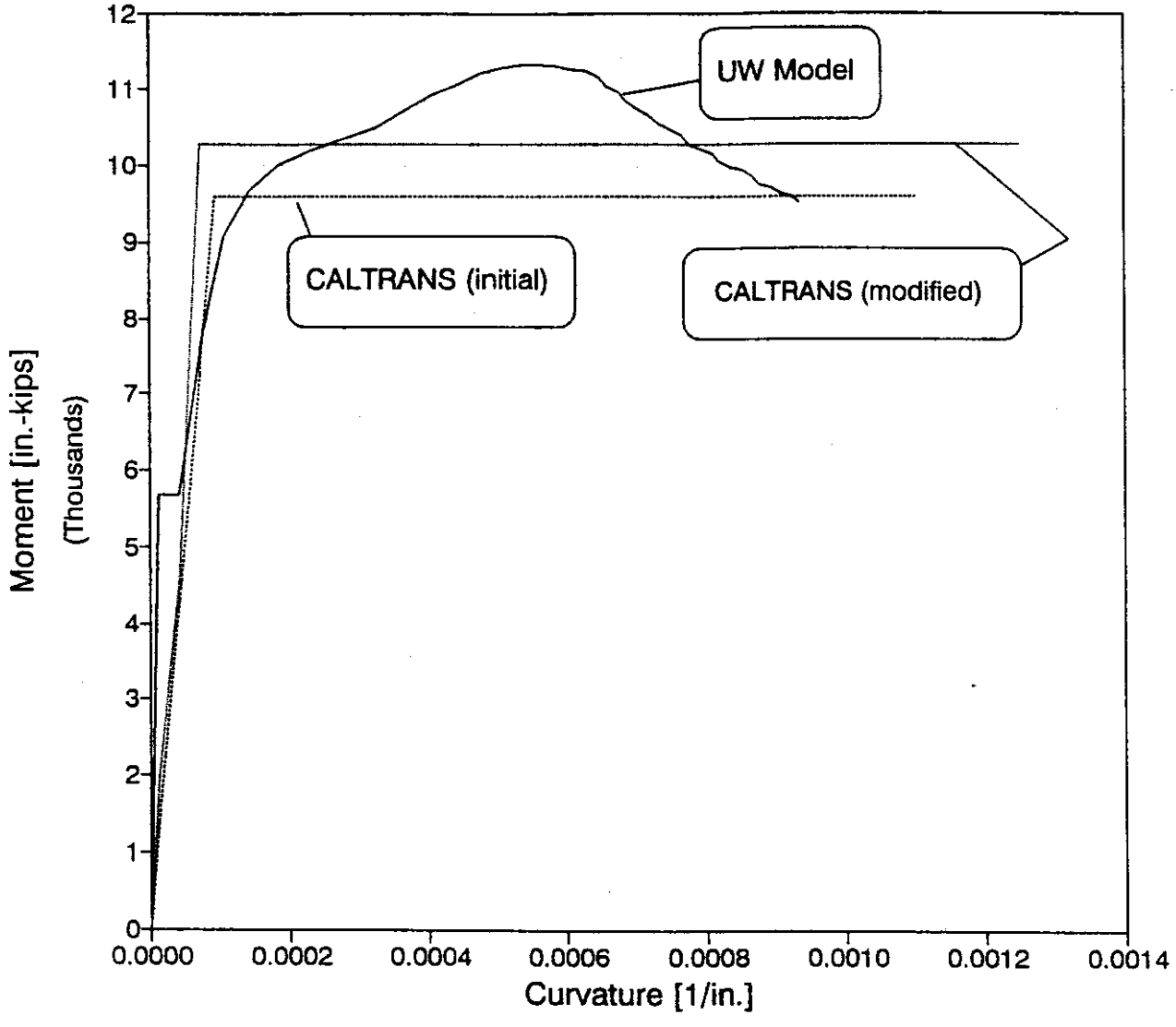

Figure 8.4. Column Moment-Curvature Diagram

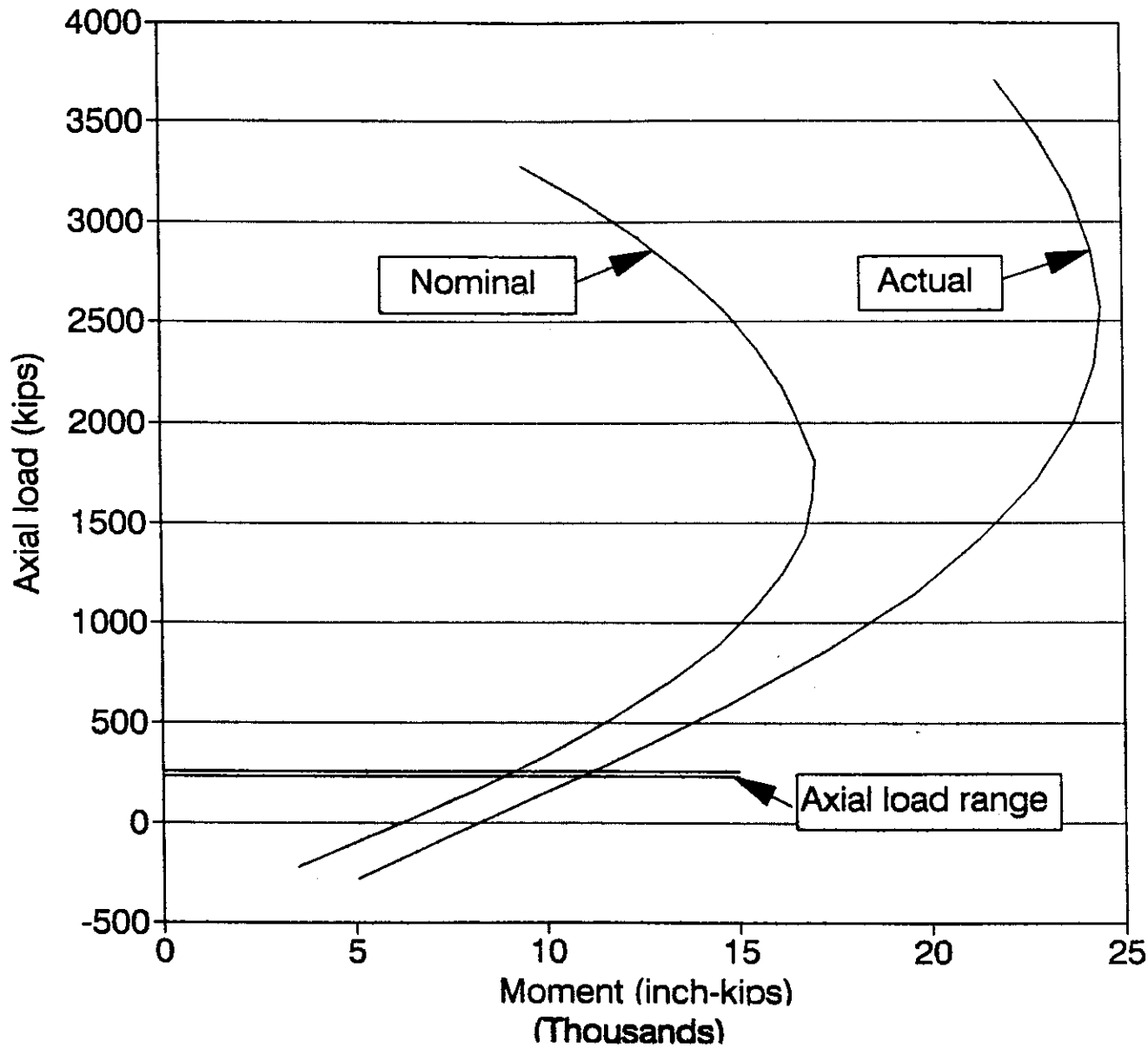

Figure 8.5. Column Moment-Axial Force Interaction Diagram

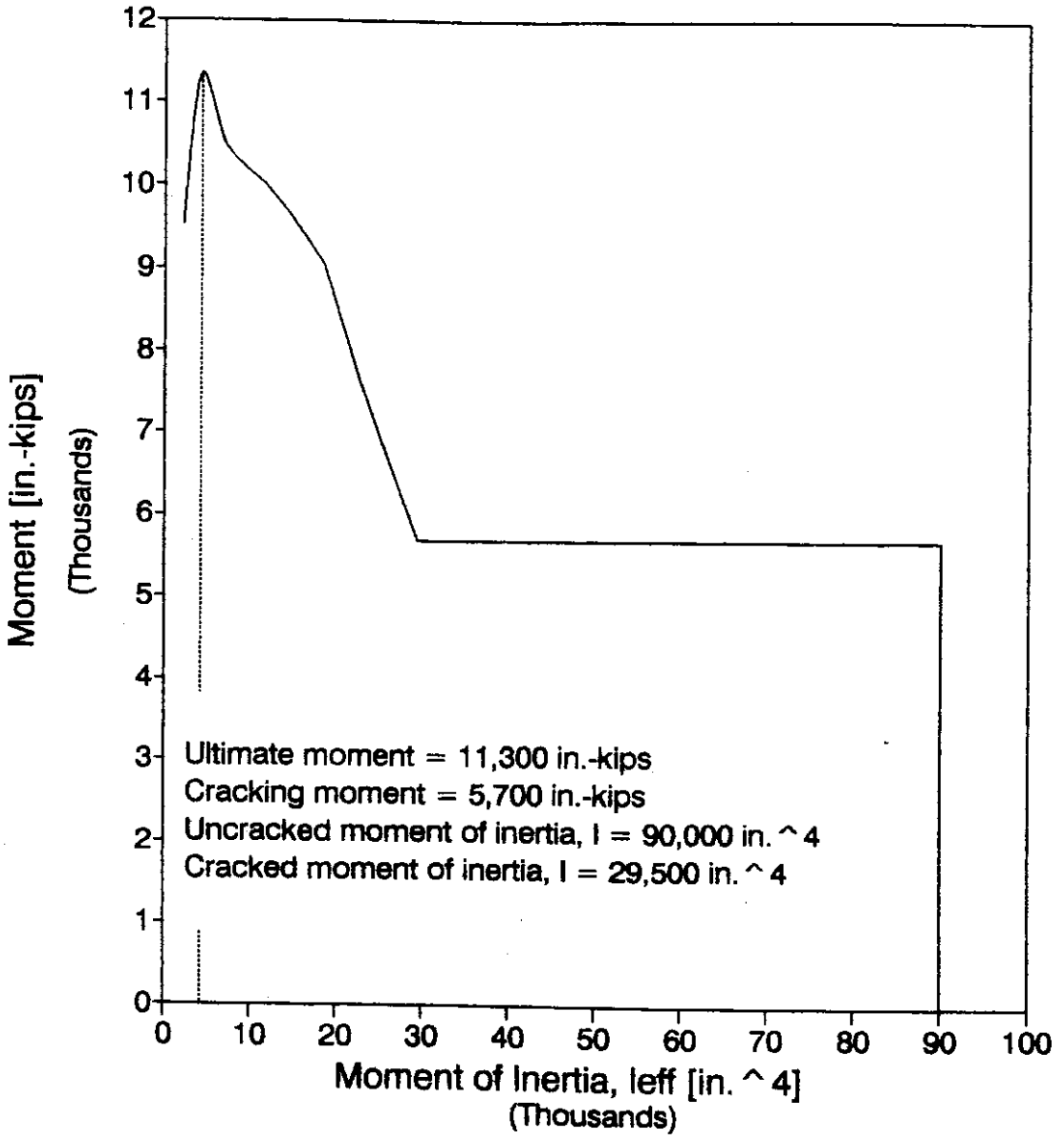

Figure 8.6. Column Moment-Effective Moment of Inertia Diagram

Soil Around the Base of the Column

Twelve linear springs at 1-foot intervals modeled the soil around the base of the columns. To establish the spring stiffnesses, the researchers followed a p-y curve approach for non-cohesive soils described by O'Neill and Murchison (15) and also described in the Phase I report (2). The stiffnesses were a function of the height above the footing and the maximum displacement at that height. In computing the secant stiffnesses, the researchers assumed that the maximum displacement varied linearly between the top of the column and the footings. The top of the column was assumed to displace 2 inches, and the footing was assumed to remain stationary.

Figure 8.7 shows a p-y curve for a spring located 6 feet above the footing. For that elevation, the secant stiffness was calculated at a displacement of 0.48 inches. The spring stiffnesses also varied according to the assumed angle of internal friction. Table 8.1 lists the soil spring secant stiffnesses for the other elevations and for internal angles of soil friction equal to 36, 38, and 41 degrees.

Analysis Procedure

To be consistent with the observed damage in Phase I, the top three elements were assumed to be cracked initially. Horizontal loads were applied to the top of the column in increments of 5 kips until the ultimate curvature, ϕ_{ult}, was reached in an element. At each stage of loading, the curvature and internal moment in each element were monitored. The element was assigned the cracked moment of inertia the first time the curvature in an element exceeded the cracking curvature. If the element had cracked already, the effective moment of inertia for that element, I_{eff}, was calculated from the moment-curvature relationship (Figure 8.4 and Equation 8.1). If the value of I_{eff} was within 5 percent of its previous value, the effective moment of inertia remained the same and the load was incremented. Otherwise, the curvature was used to determine a new effective moment of inertia for another iteration at the same load. If the calculated effective moment of inertia changed in any elements within an iteration, then the

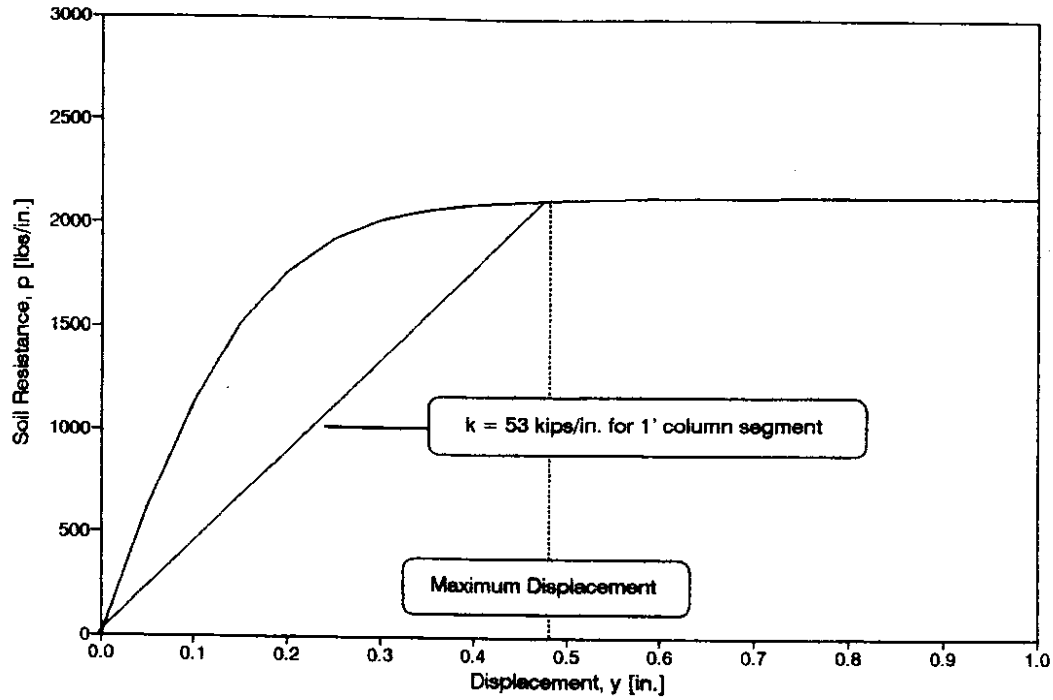

Figure 8.7. Example Calculation of Spring Stiffness (height = 6 ft, $\phi = 38°$)

Table 8.1. Soil Spring Stiffnesses

ϕ= 36	
Height Above Footing [ft.]	Soil Spring Secant Stiffness [kips/in]
1	238
2	194
3	146
4	103
5	70
6	46
7	29
8	18
9	10
10	5
11	2
12	0

ϕ= 38	
Height Above Footing [ft.]	Soil Spring Secant Stiffness [kips/in]
1	269
2	221
3	168
4	119
5	81
6	53
7	34
8	21
9	12
10	6
11	2
12	0

ϕ= 41	
Height Above Footing [ft.]	Soil Spring Secant Stiffness [kips/in]
1	414
2	322
3	228
4	153
5	100
6	65
7	42
8	26
9	15
10	7
11	3
12	0

Note:
Soil springs for 1' column segment

calculation was repeated with the new member properties. Iteration at each load level continued until effective moments of inertia in all elements changed less than 5 percent from the previous iteration.

The analysis stopped when the column reached its ultimate moment capacity. Consequently, the model did not account for moment redistribution that might continue to occur after the top of the column had reached its ultimate moment.

8.2 RESULTS FROM UW MODEL

Figure 8.8 shows the calculated load-displacement curves for a single column. The curves are superimposed on measured load-displacement curves from Phase II. The measured load-displacement curves for a column were calculated by subtracting 18 kips of friction (to account for the isolation system) from the applied load on the bridge and dividing this load by four (four columns). The first analysis neglected the soil's contribution to resistance. The other analyses included soil springs whose stiffnesses were based on three values of the soil's internal angle of friction. In addition to the measured value of 38 degrees, analyses were performed for 36 degrees and 41 degrees, the angles that O'Neill and Murchison give as the limiting values for dense sand. (15)

The model provided a good fit to the measured response, and the calculated load-displacement curves provided monotonic loading envelopes for the measured load-displacement curves from Phase II. Figure 8.8 shows that each load-displacement curve for angles of internal friction between 36 and 41 degrees was nearly the same. In comparison with the measured response, the model with no soil springs was too flexible and had a lower strength than was measured. For the model with the measured angle of internal friction, the column reached its calculated strength at an applied load of 100 kips and at a pier displacement of 2.7 inches. Because the analysis stopped when the column reached its ultimate curvature, the analysis did not estimate the system's displacement ductility.

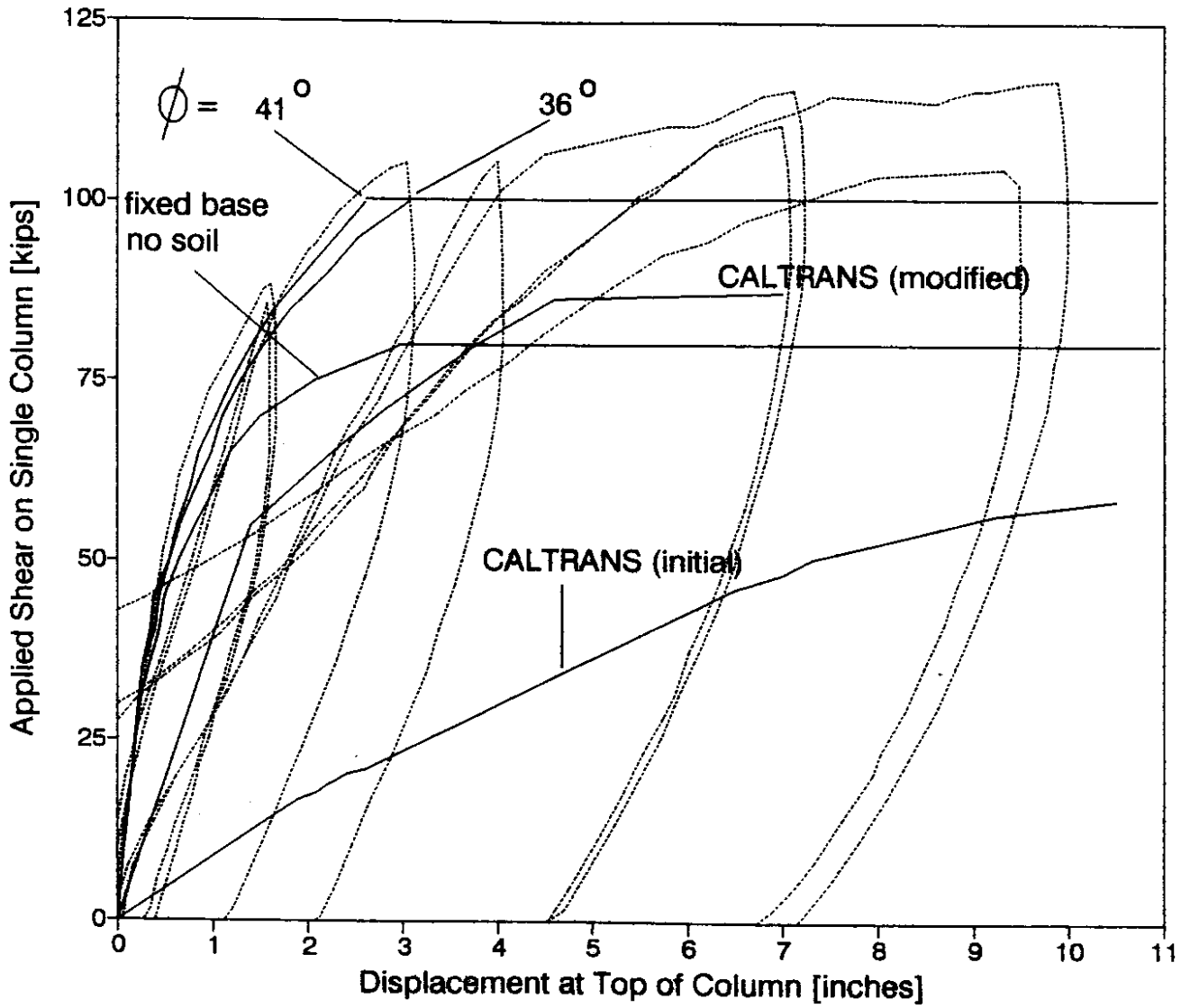

Figure 8.8. Calculated and Measured Response for Single Column

For the model with the calculated angle of internal friction of 38 degrees, the secant stiffness of the soil spring nearest the ground surface was approximately equal to zero (Table 8.1). The soil spring 1 foot below the ground surface provided approximately 95 percent of the ultimate soil resistance at a displacement of 2.7 inches at the top of the column. The soil spring nearest the column footing provided only 3 percent of the ultimate soil resistance at this displacement.

The shear distribution throughout the column at four load levels is shown in Figure 8.9. For load levels of 25, 50, and 75 kips, the shear at the bottom of the columns remained constant at approximately 20 kips; the soil's contribution to resistance steadily increased with increasing load. At 100 kips, the shear reversed to minus 20 kips. In a sense, the column was pivoting about the soil springs, and the soil resisted 120 percent of the applied load.

Figures 8.10 and 8.11 show the column moment and curvature distributions. At all load levels, the largest curvature occurred in the top element. The maximum curvature below the ground surface occurred at the footing level for the 25-, 50-, and 75-kip load levels. At 100 kips, the maximum curvature below the ground surface occurred approximately 4 feet above the footing. This curvature distribution is consistent with the observed cracking. At the maximum load, the curvature 1 foot above the footing (1.3×10^{-4} /inches) was less than 25 percent of the curvature in the top element. The calculated curvatures at the top of the column (Figure 8.11) were significantly smaller than the measured curvatures. This discrepancy was attributed to two factors. First, the column element was one foot long in the analysis, whereas the curvatures were measured over a three-inch length. Second, the analysis did not consider pull-out of the reinforcing bar from the beam.

Figure 8.12 shows the effective moment of inertia throughout the column. At 25 kips applied load, no new cracking occurred; the top three elements had been cracked at the beginning of the analysis. As the load increased, the extent of cracking in the

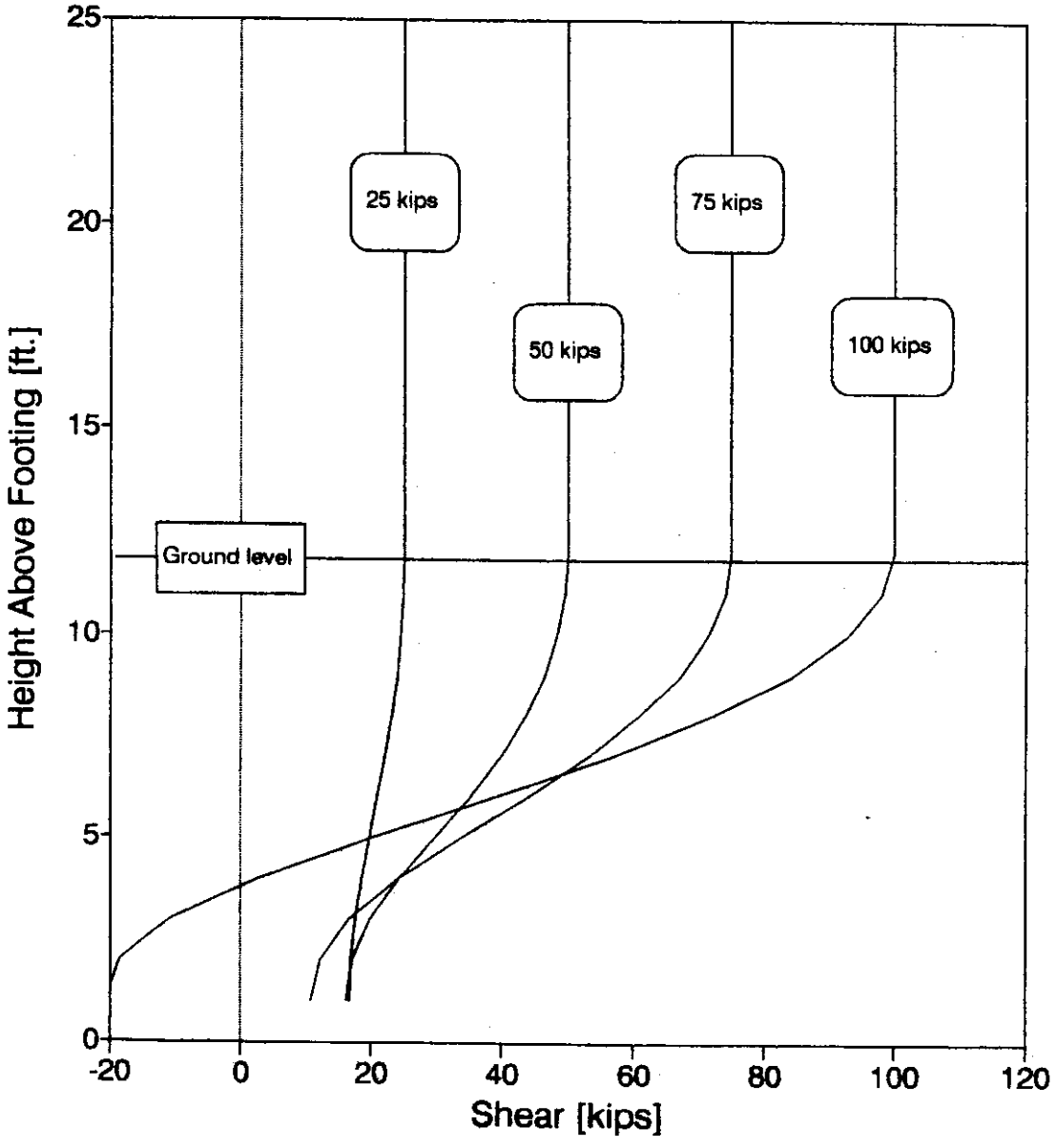

Figure 8.9. Column Shear Distribution ($\phi = 38°$)

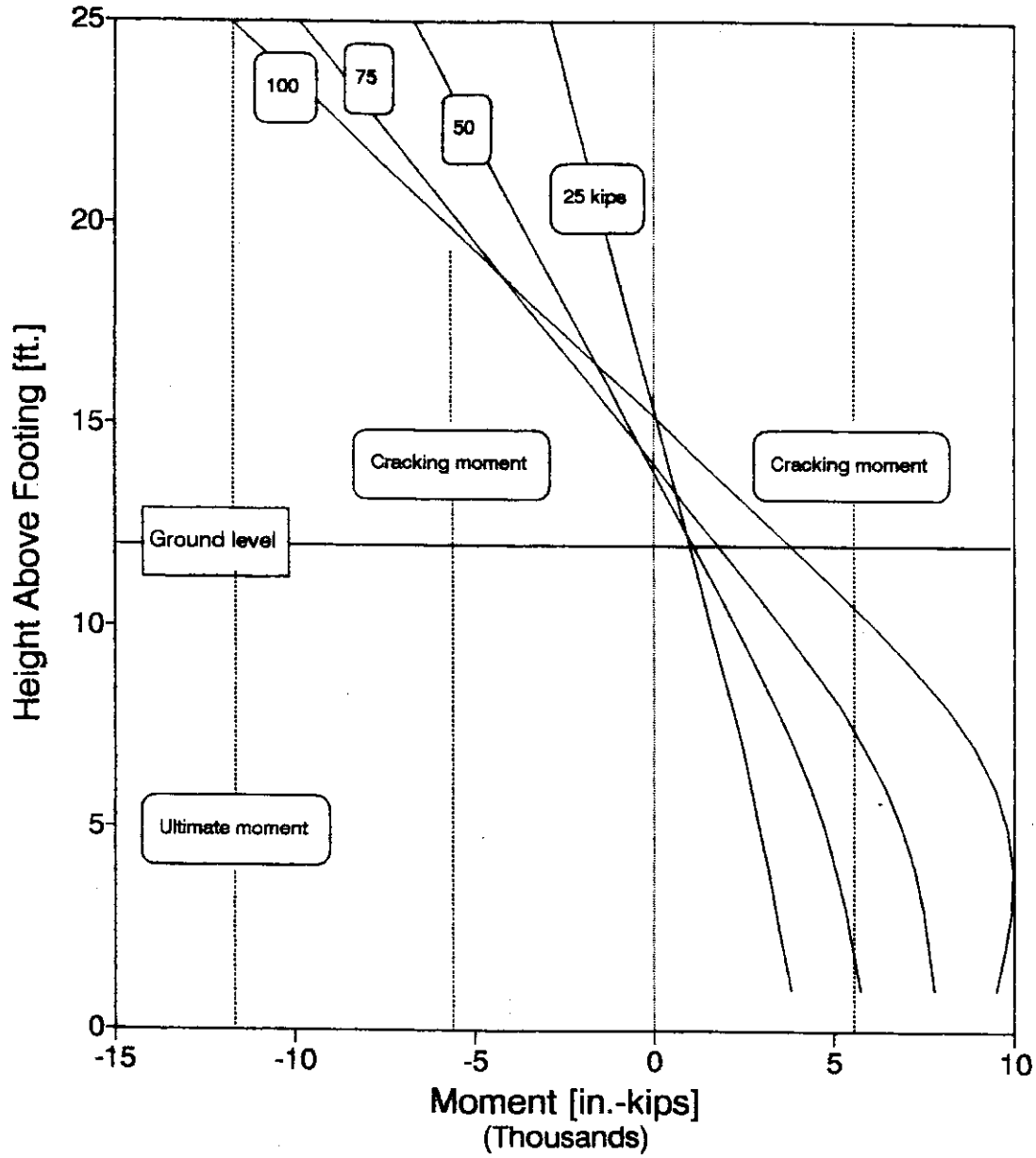

Figure 8.10. Column Moment Distribution ($\phi = 38°$)

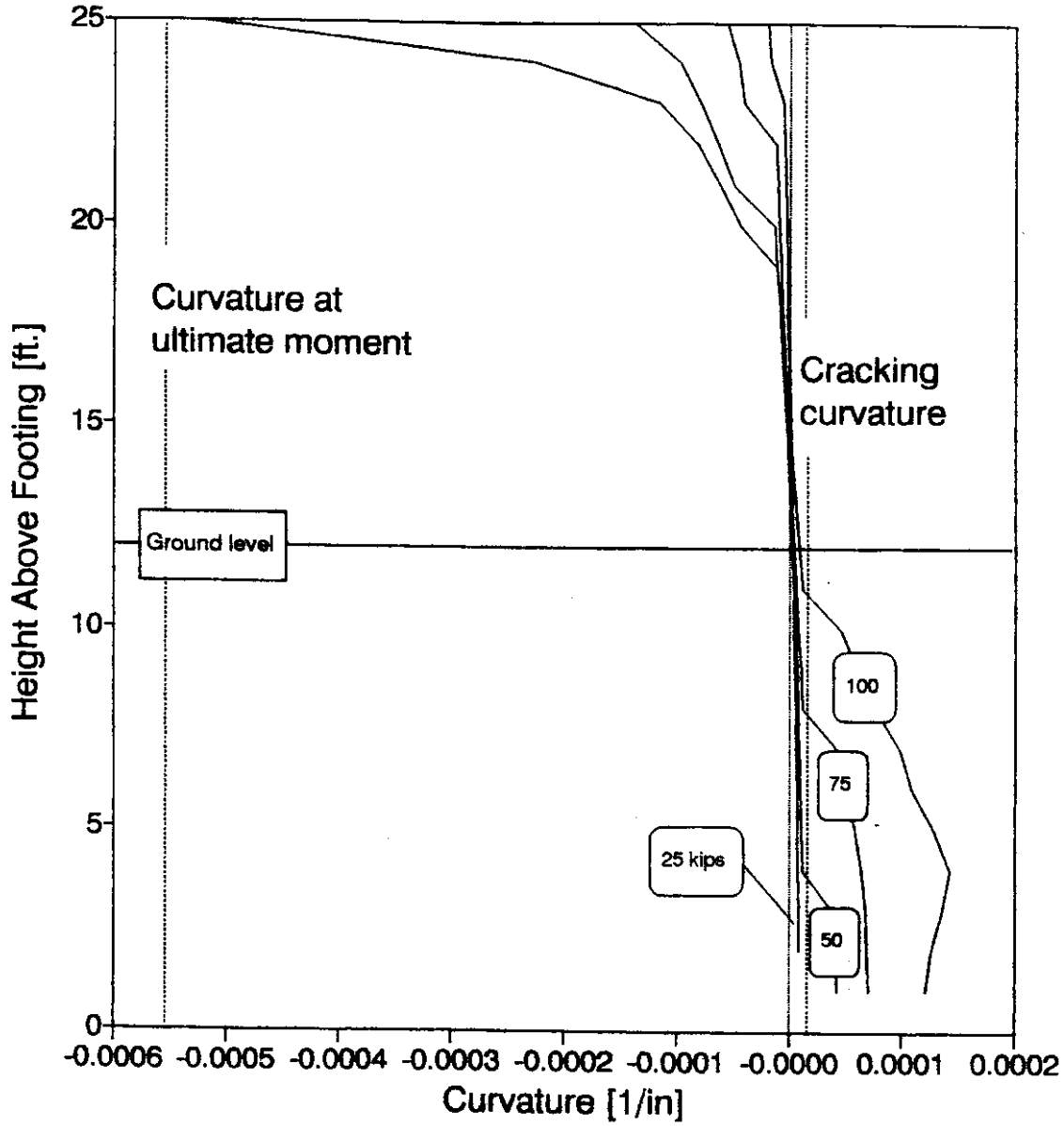

Figure 8.11. Column Curvature Distribution ($\phi = 38°$)

bottom of the column increased. At a load of 50 kips, the bottom three elements were cracked. At 100 kips, every element below the ground surface and within the top 5 feet of the column cracked. At 100 kips, the effective moment of inertia in the element directly above the footing was reduced to 17,000 inches^4.

8.3 EVALUATION OF UW MODEL

The calculated response was similar to the observed response in many ways. As shown in Figure 8.8, the load-displacement curve for the piers was well predicted. The discrepancy at large pier displacements may have been due to the fact that the analysis did not continue beyond the ultimate curvature; additional moment redistribution likely occurred in the field. In addition, the abutment contribution may have increased in later cycles when the TIVAR pads slipped off of the supporting stainless steel.

The initial cracking pattern in the model agreed closely with the observed crack patterns. This agreement was to be expected because the top 3 feet of the model was assumed to be cracked to account for Phase I damage. As the load increased, the consistency remained good. For example, the curvature was much larger at the top of the column than at the bottom. This size difference was consistent with the observed damage and the instrument records. As the load increased, cracking spread upwards in the bottom of the column. At the maximum load, the maximum calculated curvature in the bottom half of the columns occurred 4 feet above the footing level. This behavior was consistent with the observed crack patterns.

The only clear discrepancy between the calculated response and the measured response was that the model predicted cracking at the bottom of the column where no cracking was observed in the field. Model cracking at the base of the column extended from the footing level up to an elevation of 10 feet. In the piers, cracks were observed in a 2- to 8-foot region above the footings.

Possible explanations for the discrepancies are as follows:

- the soil springs were too flexible,
- the assumed modulus of rupture for the concrete was too low,
- the footings rotated or translated, and
- minor cracking occurred in the field but was not observed.

Because of the limitations of the footing instrumentation, the footings may have translated and rotated a small amount. Though the instrumentation did not detect any footing movement, the footings may have rotated as much as 0.1 degree without being detected. A 0.1 degree angle corresponds to a drift ratio of 0.18 percent. To estimate the effect of a footing rotation of 0.1 degree, a simple calculation was performed. The moment needed to rotate the end of an uncracked bridge column 0.1 degree with the other end fixed was calculated to be approximately 9,000 kip-inches, which is over 75 percent of the calculated moment capacity of the column. In this case, footing flexibility would strongly influence crack patterns.

The moment induced at the ends of an uncracked bridge column by displacing the bottom of the column horizontally 0.01 inches is approximately 300 kip-inches. This moment is small enough that undetected horizontal displacement of the bridge column would be expected to have a negligible effect on column behavior.

8.4 CALTRANS MODELS

The California Department of Transportation (CALTRANS) developed two nonlinear models of a single bent. CALTRANS used idealized moment-curvature relations for a bent crossbeam and columns to model a bent in a step-by-step nonlinear analysis. CALTRANS assumed that the compressive strength of the concrete was 5,200 psi and that the yield stress of the reinforcing steel was 44 ksi. On the basis of the bridge's deadweight, the moment capacity was calculated for an axial load of 200 kips.

Initially, the engineers assumed elasto-plastic behavior for the columns, in which the moment capacity of 9,600 kip-inches was attained when the curvature reached the

yield curvature, ϕ_y, equal to 9.5 x 10^{-5} /inches. The ultimate curvature, ϕ_u, was 1.1 x 10^{-3} /inches. The moment-curvature diagram is shown in Figure 8.4.

From the soil blow count numbers, N, the bridge plans, and an empirical relation, the compressive modulus of the soil was calculated to be 1,755 psi. From this compressive modulus, translational and rotational soil springs for the footings were calculated with several empirical equations for elastic settlement and eccentric loads. Unlike CALTRANS' model of the entire bridge (2), soil springs were used around the base of each column in the pier model. On the basis of an assumed average modulus of subgrade reaction for a dense sand, the soil spring stiffnesses were calculated by treating the column as a beam on an elastic foundation. CALTRANS used the stiffnesses of the footing springs and the modulus of subgrade reaction around the base of the column to generate soil springs. The soil springs began with an initial stiffness that was reduced at a softening displacement. These soil spring values are listed in Table 8.2.

The model was loaded until a collapse mechanism formed. The load-displacement curve for one column is shown in Figure 8.8. The figure shows that the initial CALTRANS model was much more flexible than the measured response of the bridge bent. The soil springs failed immediately near the ground surface and the failure region progressed downward as the load increased. All soil springs failed at an applied load of approximately 50 kips on one column and a displacement of 6.5 inches. The top element of the columns yielded next at a displacement of approximately 7 inches. Finally, at a displacement of 10.5 inches and a load of 60 kips, the bottom element reached its moment capacity and the pier formed a mechanism. The maximum average rotation at the footings was approximately 0.7 degrees. Maximum average horizontal and vertical displacements at the footings were 4.4 inches and 0.2 inches, respectively.

After the initial CALTRANS analysis had been compared with the measured response, a second analysis was performed by CALTRANS. In performing the modified analysis, the engineers were informed of the soil properties listed in Table 2.1.

Table 8.2. Comparison of UW, CALTRANS, and WSDOT Models

INPUT PARAMETERS					
Item	Measured	UW	CALTRANS (initial)	CALTRANS (modified)	WSDOT
Concrete strength, f'c	6,400 psi	6,400 psi	5,200 psi	5,200 psi	4,000 psi
Yield strength of steel, fy	50.6 ksi	50.6 ksi	44 ksi	44 ksi	60 ksi
Column Axial Load		214 kips	200 kips	200 kips	200 kips
Column flexural capacity		11,300 in.-kips	9,600 in.-kips	10,280 in.-kips	14,040 in.-kips
Yield Curvature		8.2 x 10^-5/in.	9.5 x 10^-5/in.	7.2 x 10^-5/in.	
Ultimate curvature		5.6 x 10^-4/in.	1.1 x 10^-3/in.	1.25 x 10^-3/in.	
Soil springs around column (stiffness per 1 foot of column)		0 kips/in. at surface, 269 kips/in. at footing	Pre-softening: 0.0 kips/in. at surface, 1.8 kips/in. at footing Post-softening (>1.0") 0.0 kips/in. at surface, 0.5 kips/in. at footing	Pre-softening: 0.0 kips/in. at surface, 98 kips/in. at footing Post-softening (>1.0") 0.0 kips/in. at surface, 41 kips/in. at footing	
Rotational spring at base of footing		Fixed	Pre-softening: 7.6 x 10^5 in.-kip/rad Post-softening (>.008 rad) 1.1 x 10^6 in.-kip/rad	1.7 x 10^6 in.-kip/rad	
Translational spring at footing		Fixed	Pre-softening: 12.8 kips/in. Post-softening (>1.0") 9.6 kips/in.	Pre-softening: 596 kips/in. Post-softening (>1.0") 307 kips/in.	
Vertical spring at footing		Fixed	Pre-softening: 283 kips/in. Post-softening (>1.0") 233 kips/in.	Fixed	

CALCULATED RESPONSE					
Lateral strength of column	110 kips	100 kips	60 kips	85 kips	85 kips
Displacement at first yield		0.81 inches	6.5 inches	1.21 inches	
Ultimate displacement	> 9 inches		10.5 inches	7 inches	

The moment-curvature relationship was computed using the COL6 program. As shown in Figure 8.4, the modified moment-curvature relationship was similar to the initial relationship. The p-y curves were generated with the program COM624. The resulting soil springs were much stiffer than those computed in the initial model. The computed force displacement relationship for the column (Figure 8.8) still underestimated its resistance. However, the computed response of the modified model was much better than the response of the initial model.

8.5 WSDOT MODEL

The WSDOT did not perform nonlinear analysis, but instead, only estimated the lateral strength of a column. Assuming a concrete strength of 4,000 psi and a steel yield strength of 60 ksi, WSDOT constructed an axial force-moment interaction diagram. For a dead load axial force of 200 kips, the moment capacity of the column was 14,040 kip-inches. Assuming a column with two fixed ends and an effective height of 28.2 feet, the applied load that would cause the column to reach its strength was calculated to be 85 kips. The column's displacement ductility was not evaluated.

8.6 COMPARISON OF MODELS

Table 8.2 compares input parameters and calculated responses from the UW, CALTRANS, and WSDOT models. The initial CALTRANS model was much more flexible than the UW model and the actual piers. The flexibility in the initial CALTRANS model was due primarily to the low stiffness of the soil springs around the base of the column. The soil springs near the footing were nearly 150 times stiffer in the UW model than in the initial CALTRANS model. The excessive flexibility of initial CALTRANS' soil springs was most apparent in the excessive footing translation of 4.4 inches. Table 8.2 shows also that the springs in the modified CALTRANS model were much stiffer than the springs in the initial model.

The column's strength was influenced not only by the soil springs, but also by the assumed steel properties. The column's measured strength was approximately 110 kips. The UW, CALTRANS (initial), and WSDOT strength estimates were 91, 55, and 77 percent, respectively, of the measured strength. The strength of the WSDOT model was low because the effective column height was overestimated. The strength of the WSDOT model would have been even lower if the WSDOT model had not overestimated the steel's yield strength. If WSDOT had assumed a yield stress of 50 ksi, the calculated strength would have been reduced to 64 percent of the measured strength.

CHAPTER 9

RECOMMENDATIONS

Although the differences between a static test and an earthquake must be acknowledged, this study serves as the basis for recommendations in several areas. The information gained in developing and implementing the test program will help researchers plan other large-scale tests. The tests provided a rare opportunity to measure a structure's lateral-load resistance and to estimate the damage that would occur in similar piers. The analyses that were associated with the tests provided the opportunity to evaluate commonly used analytical models.

9.1 LIMITATIONS OF THE STUDY

Before listing this study's recommendations, it is prudent to discuss the difficulties inherent in predicting the seismic response of other bridges on the basis of this study's results. The confidence with which one can extrapolate from the tests to an actual earthquake depends both on the extent to which the piers are typical and on the extent to which the tests were similar to actual earthquakes.

The piers that were tested were similar in many ways to piers in other highway bridges. It is still common to build bridges in which cast-in-place columns support precast girders that, in turn, support a cast-in-place slab. The proportions of the bridge are also typical for the interstate system. Further, it was standard practice before 1971 to provide little confinement reinforcement, to permit short lap splices at the footing construction joint, and to omit top footing reinforcement.

The Phase II study is particularly relevant to bridges in which the abutment resistance does not dominate the bridge's seismic behavior. In many bridges, the abutment is configured in such a way that it is unlikely to generate large forces. In other bridges, the superstructure's flexibility would limit the force that would be transmitted to

the abutments. The superstructure is particularly flexible if the bridge is long or if it has expansion joints.

These piers also had characteristics that made them atypical. For example, the top-of-footing elevation was 32 feet below the elevation of the fill at the abutments, while the pier was only 41 feet from the abutment. Consequently, the 2:1 slope intersected the columns at approximately mid-height, and the columns were embedded in 12 feet of compacted fill. This embedment increased the footing stiffness and decreased the rotational demand on the column splices. Many bridge footings are nearer the ground surface.

The cast-in-place pier diaphragms added greatly to the crossbeam's strength and stiffness. The crossbeam's large strength prevented it from being damaged and forced the yielding to occur only in the columns. The crossbeams' stiffness also increased the rotational demand at the top of the columns. If a similar pier had been tested without the diaphragms, the crossbeam would likely have been damaged more. At a given drift ratio, it is also likely that the damage to the top of the column would have decreased.

The limitations of the testing method also need to be acknowledged. The loading rate, which was essentially static, was much lower than the rates that occur during earthquakes. Furthermore, since the researchers applied load only in the transverse direction, the influence of longitudinal and vertical motions was not considered.

9.2 RECOMMENDATIONS FOR PERFORMING FUTURE TESTS

The loading system concept implemented for these tests should be considered for future tests. This system successfully applied 800-kip, transverse, cyclic loads, as well as 9-inch displacements to the piers. The deadmen proved to be an economical means of providing reactions to the large horizontal loads. Prestressing strands proved to be an economical means of transferring the tensile loads among the load train components. The system would have been improved greatly if the researchers had used center-hole jacks instead of solid rams. If center-hole jacks with the ability to take up stroke had been

used, the jacking frames could have been replaced with transfer beams, and the loading operation would have been less tedious. Unfortunately, the researchers' contractual arrangements made it difficult to use center-hole jacks.

Isolation of the superstructure from the abutments should also be considered in future tests. By isolating the superstructure, the researchers were able to subject the piers to much larger displacements than would have been possible if the researchers had not reduced the abutment resistance. The isolation system was inexpensive and was quickly installed. The system could have been improved by increasing the length of the stainless-steel plates; the 24-inch length was insufficient to support the TIVAR blocks for repeated cycles to 9 inches.

The instrumentation plan should be considered for future tests, but with some modifications. The deck instrumentation concept worked well, particularly in Phase II, because the displacements were large. For smaller displacements, the influence of wind and temperature variations on cable elongation would need to be considered. (2) It was also helpful to verify the measured displacements with an electronic distance meter (EDM), but a more precise check could have been obtained with a survey transit.

The top-of-column instrumentation provided credible, consistent measurements of column curvature. In contrast, despite great efforts to shelter the bottom-of-column instruments, they were repeatedly disturbed by falling soil. A better system would need to be devised to protect the instruments below ground. In addition, the sensitivity of the footing instrumentation would need to be increased.

9.3 RECOMMENDATIONS DERIVED FROM MEASURED RESPONSE

These tests should serve as benchmarks against which to evaluate analytical procedures. In addition, the WSDOT retrofit program priorities should be consistent with the damage observed during the tests. The tests also demonstrated that the compacted soil surrounding the columns protected the splice detail from large rotational demands.

The tests also revealed the stiffness, strength, and toughness of the piers. Despite their deficiencies, the piers repeatedly resisted a lateral load equal to one third of the bridge's weight. Though the tops of the columns were heavily damaged at a drift ratio of 3 percent, the stiffness and toughness did not degrade drastically. Quite significantly, neither the shear capacity nor the axial-load capacity deteriorated sufficiently to threaten the safety of the bridge.

On the basis of the observed damage, the researchers concluded that the most vulnerable elements of the piers were the tops of the columns. Consequently, of the deficiencies listed in Section 1.1 and shown in Figure 3.1, only the poor confinements of the hinge region affected the structure's response. The footings and the footing-level splice did not deteriorate significantly because the compacted fill reduced the rotational demands on these elements. Under different circumstances, for instance, a weaker and more flexible crossbeam and less fill around the columns, more damage might have occurred during the Phase II tests.

The vulnerability of the undisturbed structure, including the abutments, was discussed in the Phase I report. (2) The Phase II tests provided the opportunity to estimate the bridge's seismic vulnerability after the abutment resistance was removed. Such a vulnerability assessment is relevant to bridges in which the piers are similar to the test bridge, but in which the abutment's contribution to resistance is negligible. To estimate the isolated bridge's vulnerability it is useful to model the isolated bridge as a single-degree-of-freedom, elasto-plastic system that yields at a force equal to one third of its weight and at a displacement equal to 2 inches (Figure 7.1). It is further assumed that the ground motion has a dynamic amplification factor of 2.75, and that the nonlinear displacements are equal to the linear displacements.

One can estimate displacements, and hence damage, associated with a particular earthquake intensity. A ground motion with an effective peak acceleration of 0.2g would produce a displacement of approximately 2.75 x 0.2 x 2 / (1/3) = 3.3 inches, which

corresponds to a drift ratio of roughly 1 percent. As documented in Section 7.2, the damage at this drift ratio was minor and consisted of minor flaking of the concrete and flexural cracks. At an effective acceleration of 0.3g, the estimated displacement increases to 5 inches (1.7 percent). During the tests, the tops of the columns began to spall at this drift ratio. The corresponding drift ratio for an effective acceleration of 0.4g is 2.2 percent. During the tests, spalling and the onset of bar buckling was apparent at this drift ratio.

9.4 RECOMMENDATIONS DERIVED FROM ANALYSES

The large discrepancies among the analytical models confirmed the difficulties of predicting a bridge's nonlinear response to lateral loads. The difficulties stemmed mainly from uncertainties in steel strength, in the stiffness of the spread footings, and in the resistance provided by the soil around the columns. The differences among the models are important because they may determine whether a retrofit is needed. For example, it would not have been necessary to retrofit the bottom of the columns because the soil redistributed the rotational demands. Using realistic material strengths and performing soil tests can reduce the discrepancy between measured response and analysis. Given that soil tests are expensive, the influence of the soil on the distribution of column damage should be studied further to determine when geotechnical tests are required.

ACKNOWLEDGMENTS

The writers are grateful for the effort and support of many people and organizations. University of Washington (UW) students S. Clark, G. Hjartarson, R. Mah, and C. Wang helped prepare and conduct the static tests. The loading system was fabricated by Concrete Technology Corporation under the direction of S. Moustafa and N. Peshtaz. Professor D. McLean of Washington State University provided instrumentation to supplement that available at the University of Washington.

University of Washington professors S. Kramer and R. Holtz provided valuable advice on the geotechnical aspects of this project. H. Coffman of the Washington State Department of Transportation (WSDOT), as well as J. Gates, T. Cartner, and G. Reyes-Gutierrez of the California Department of Transportation (CALTRANS) performed independent analyses of the piers. This report was prepared with the assistance of UW graduate student S. Ryter and TRAC staff members S. MacLachlan, A. O'Brien, E. Nachmanson, R. Porter, and D. Wright.

The project was funded primarily by the WSDOT and the Federal Highway Administration. E. Henley served as the technical contact at the WSDOT Office of Bridges and Structures. R. Wang and C. Clark were supported by the National Science Foundation through the Research Experience for Undergraduates Program. Captain T. O'Donovan was supported by the U.S. Army Corps of Engineers, and G. Hjartarson was supported by the Valle Foundation at the UW.

REFERENCES

1. Noson, L.L., Qamar, A. and Thorsen, G.W., "Washington State Earthquake Hazards," Information Circular 85, Washington Division of Geology and Earthquake Resources, Olympia, Washington, 1988.

2. Eberhard, MacLardy, J. M., Marsh, M.L., and Hjartarson, G., "Lateral-Load Response of a Reinforced Concrete Bridge," Technical Report WA-RD 305.1, Washington State Department of Transportation, Olympia, Washington, August 1993.

3. "Standard Specifications for Road and Bridge Construction," State of Washington Department of Highways, Olympia, Washington, 1964.

4. "Standard Specifications for Highway Bridges," The American Association of State Highway Officials, Washington, D.C., 1961.

5. "1987 Annual Book of ASTM Standards," American Society for Testing and Materials, Philadelphia, Pennsylvania, 1987.

6. "Building Code Requirements for Reinforced Concrete, (ACI 318-89)" American Concrete Institute, Detroit, 1989.

7. Forstie, D.A. and Schnormeir, R., "Development and Use of 4 by 8 inch Concrete Cylinders in Arizona," *Concrete International*, American Concrete Institute, pp. 42-45, July 1981.

8. Mirza, S.A. and MacGregor, J.G., "Variability of Mechanical Properties of Reinforcing Bars," Proceedings ASCE, *Journal of the Structural Division*, vol. 105, no. ST5, pp. 921-937, May 1979.

9. Ovesen, N.K. and Stromann, H., "Design Methods for Vertical Anchor Slabs in Sand," Proceedings, Specialty Conference on Performance of Earth and Earth-Supported Structures, American Society of Civil Engineers, vol. 2.1, pp. 1481-1500, New York, 1972.

10. Campbell, T.I. and Kong, W.L., "TFE Sliding Surfaces in Bridges," Technical Report Number ME-87-06, The Research and Development Branch, Ontario Ministry of Transportation and Communications, July 1987.

11. Becker, R.A., Chambers, J.M. and Wilks, A.R., *The S Language*, Wadsworth & Brooks/Cole, Pacific Grove, California, 1988.

12. Wilson, E.L. and Habibullah, A., "Sap90 Users Manual," Computers and Structures, Berkeley, California, 1989.

13. Park, R. and Paulay, T., *Reinforced Concrete Structures*, Wiley and Sons, New York, 1975.

14. Kent, D.C. and Park, R., "Flexural Members with Confined Concrete," Proceedings ASCE, *Journal of the Structural Division*, vol. 97, no. ST12, 1971.

15. O'Neill, M.W. and Murchison, J.M., *An Evaluation of P-Y Relationships in Sands*, A report to the American Petroleum Institute (PRAC 82-41-1), May 1983.

APPENDIX A

BRIDGE PLANS

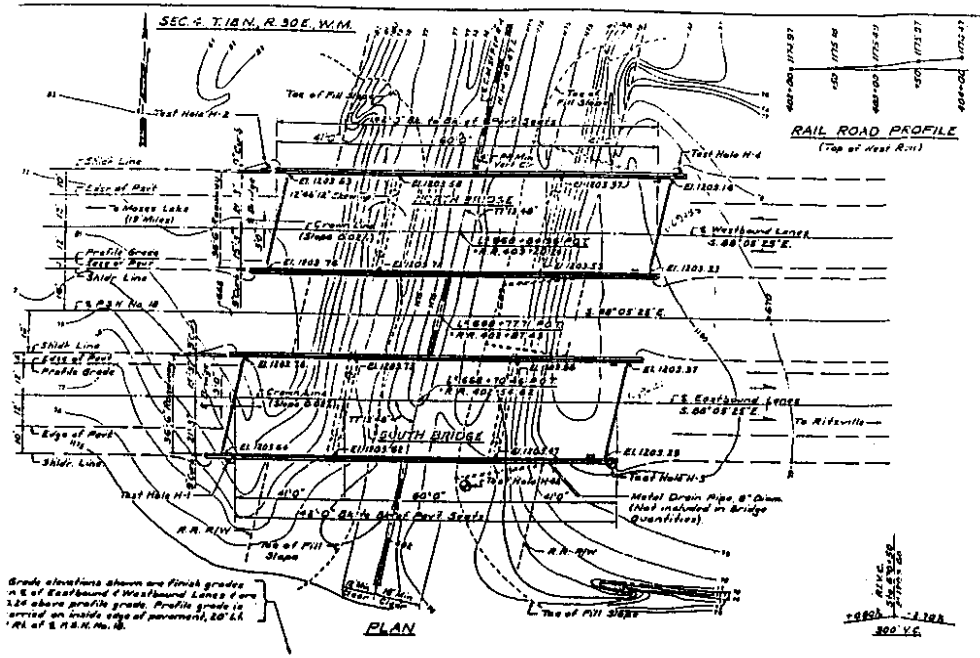

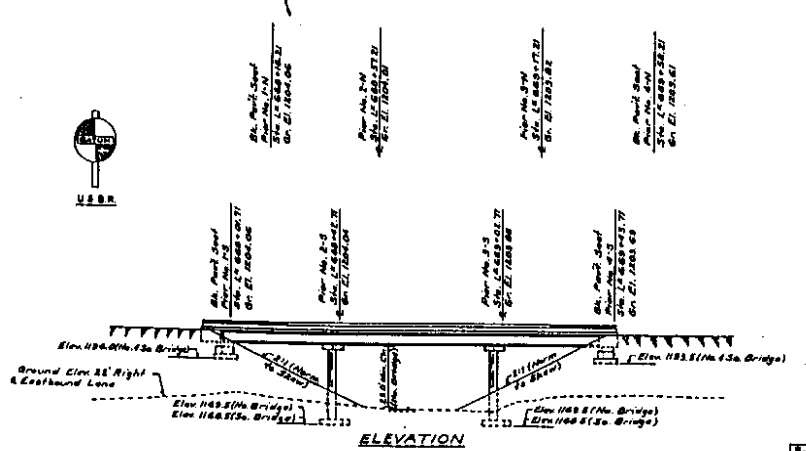

GENERAL NOTES

All material and work shall be in accordance with the requirements of the State of Washington, Department of Highways, Standard Specifications for Road and Bridge Construction, dated 1963.

Footing elevations are subject to change depending upon foundation material encountered. Reinforcing steel for the footings, columns and walls shall not be cut until the final footing elevations have been determined in the field.

The concrete in the footings of all piers and the walls at Piers No. 1 & 4 shall be Class B mix. All other concrete shall be Class AX mix except the concrete in the prestressed girders shall be as set forth in the 'Special Provisions.'

The roadway slab shall be placed in one continuous pour after the falsework for Piers No. 2 & 3 has been removed.

Falsework supporting the girder ends shall not be released at any pier until all concrete, except that in the curb, and railbase has been in place in all spans the required length of time and has developed sufficient strength as outlined in the Standard Specifications. Falsework shall be carefully released to prevent impact or undue stresses in the structure.

The maximum design soil pressure per square foot is two and three quarter (2.2) tons for Piers No. 1 & 4 and three (3) tons for Piers No. 2 & 3.

APPROXIMATE QUANTITIES

Structure Excavation,	205	Cu. Yds.
Mechanical Tamper	30	Hours
Bridge Railing, Type-R,	811	Lin. Ft.
Prestressed Concrete Girders-CHESPIR RR OXing	1,645	Lin. Ft.
Concrete, Class AX,	480	Cu. Yds.
Concrete, Class B,	185	Cu. Yds.
Steel Reinforcing Bars,	143,000	Lbs.
Bridge Drain,	4	Only
Water Reducing Additive,	440	Dollars

LOADING: HS-20
2-24K AXLES @ 4' CTRS.

PSH 18 (SR 90)
RAUGUST TO WARDEN ROAD
GRANT COUNTY
C.M. ST. P. & P. R.R. OVERCROSSING

LAYOUT

WASHINGTON STATE HIGHWAY COMMISSION
DEPARTMENT OF HIGHWAYS
OLYMPIA, WASHINGTON

Aug. 8, 1966

DATE	REVISION	BY	APPRD
9-8-66	Approval Date Added	WCB	
9-1-66	Wall 1 Piers No 1 & 4 - Quantity Class B Concrete	YI	LWR

NP 188.51 WPS
90/237 SYN
786

SHEET 61 OF 86 SHEETS

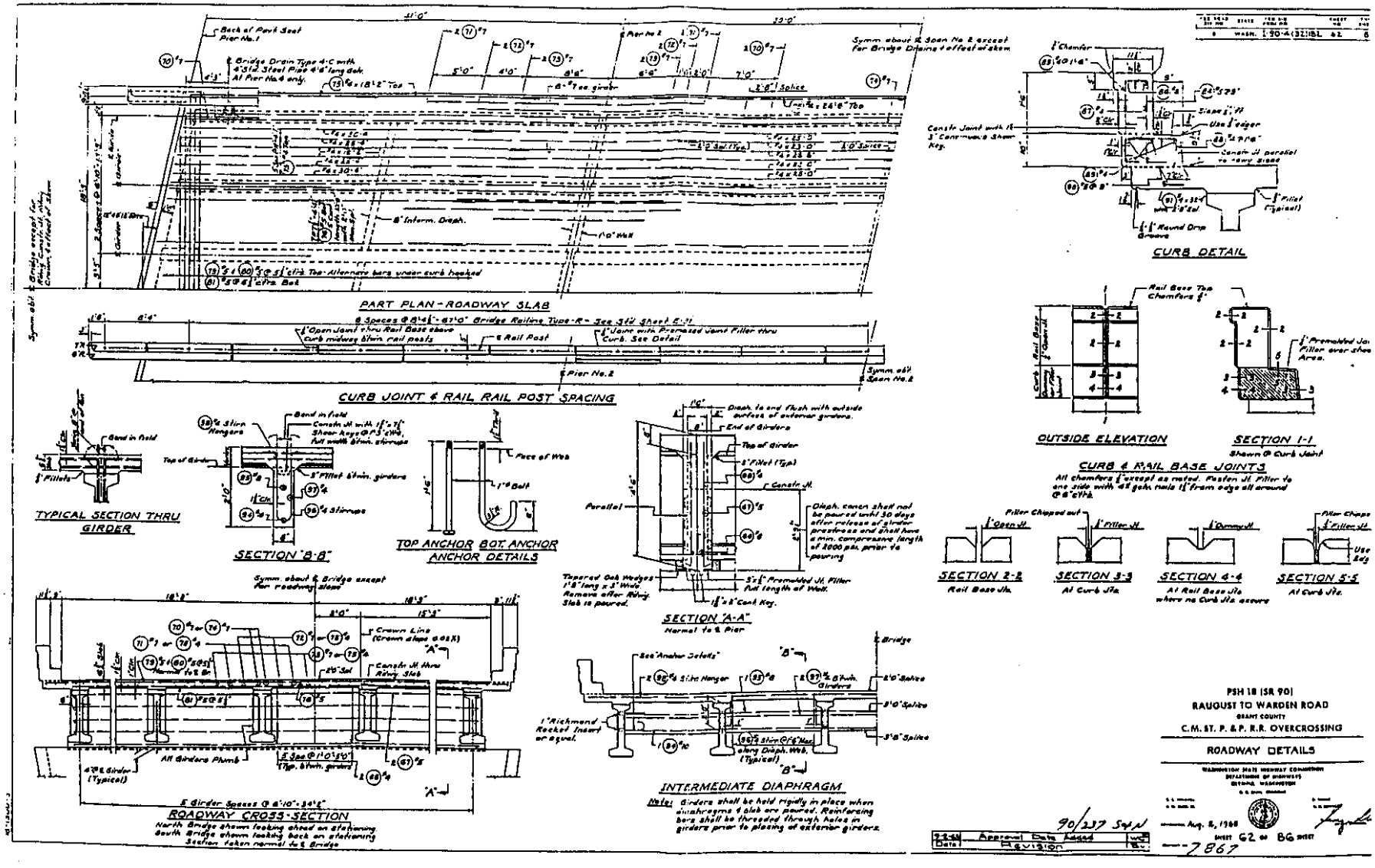
PART PLAN - ROADWAY SLAB
CURB JOINT & RAIL RAIL POST SPACING
CURB DETAIL
OUTSIDE ELEVATION
SECTION 1-1
CURB & RAIL BASE JOINTS
TYPICAL SECTION THRU GIRDER
SECTION "B-B"
TOP ANCHOR BOT. ANCHOR ANCHOR DETAILS
SECTION "A-A"
SECTION 2-2
SECTION 3-3
SECTION 4-4
SECTION 5-5
ROADWAY CROSS-SECTION
INTERMEDIATE DIAPHRAGM
PSH 18 (SR 90)
RAUGUST TO WARDEN ROAD
GRANT COUNTY
C.M. ST. P. & P. R.R. OVERCROSSING
ROADWAY DETAILS

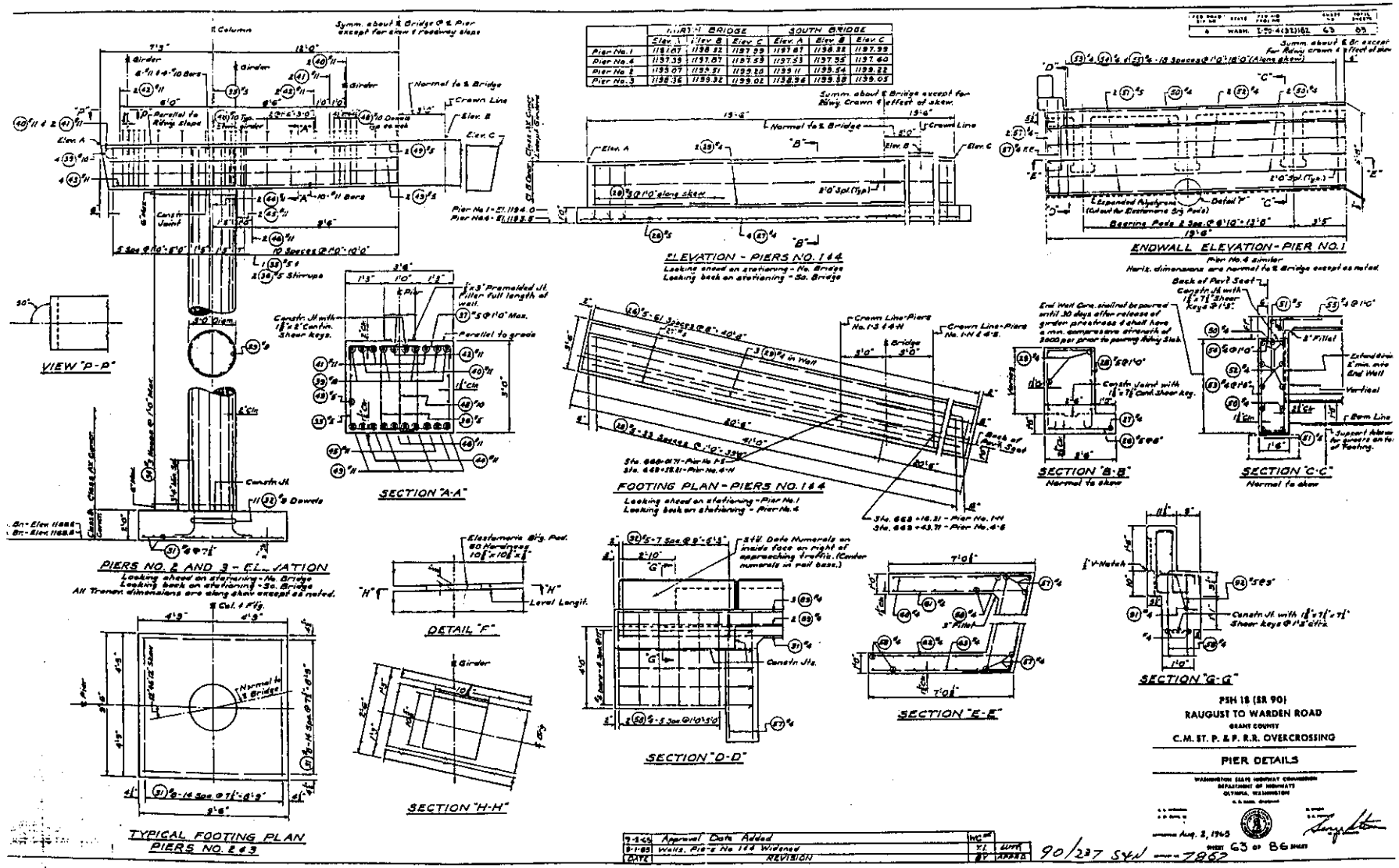
NORTH BRIDGE
SOUTH BRIDGE
Pier No. 1
Pier No. 4
Pier No. 2
Pier No. 3
ELEVATION - PIERS NO. 1 & 4
ENDWALL ELEVATION - PIER NO. 1
VIEW "P-P"
PIERS NO. 2 AND 3 - ELEVATION
SECTION "A-A"
SECTION "B-B"
SECTION "C-C"
FOOTING PLAN - PIERS NO. 1 & 4
SECTION "D-D"
SECTION "E-E"
DETAIL "F"
SECTION "G-G"
SECTION "H-H"
TYPICAL FOOTING PLAN PIERS NO. 2 & 3
PSH 18 (SR 90)
RAUGUST TO WARDEN ROAD
GRANT COUNTY
C.M. ST. P. & P. R.R. OVERCROSSING
PIER DETAILS
WASHINGTON STATE HIGHWAY COMMISSION
DEPARTMENT OF HIGHWAYS
OLYMPIA, WASHINGTON
Aug. 2, 1965
SHEET 63 OF 86 SHEETS
90/237 SW
7862
7-1-64 Approval Date Added
9-1-65 Walls, Pier-s No 1 & 4 Widened
DATE REVISION

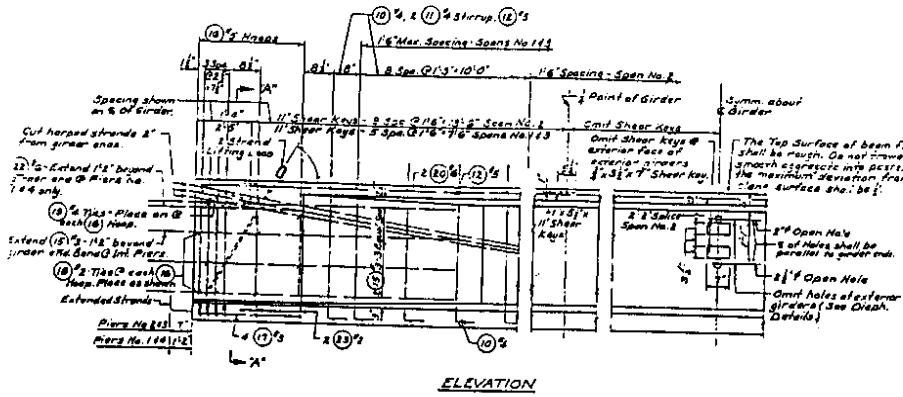

ELEVATION

GIRDER SECTION AT ℄ SPAN

SECTION "A-A"
Prestressing strands not shown.

END ELEVATION

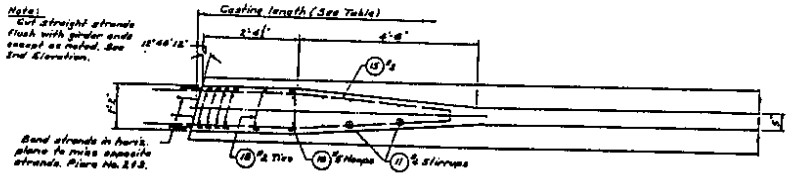

SECTION THRU END BLOCK

Note: Lifting loop angle ⊕ shall be determined by the type of lifting equipment used, 3'-4" minimum. If the lifting loops extend thru the roadway slab they shall be cut off, prior to pouring of roadway slab.
All lifting strands are of same size material and strength as prestressing strands.
Wrap lifting loops so that each strand will carry its share of the total load. Extend lifting loops to within 3" of bottom of the beam.
Lifting loops other than shown may be used provided they meet the approval of the Engineer.
Girder shall be maintained in an upright position at all times.

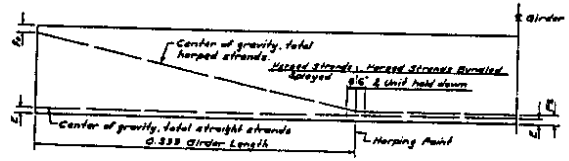

LOCATION OF CENTER OF GRAVITY OF STEEL AREAS

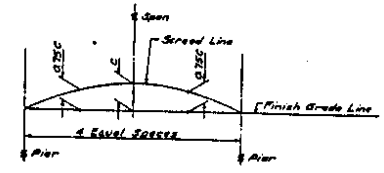

SCREED CAMBER FOR GIRDER DEFLECTION
For (C), see Table

Span	Casting Length (Along Slope)	Harped No. of Strands	Harped Jacking Force	Straight No. of Strands	Straight Jacking Force	Total Number Strands	Location of C.G. Steel Area (inches) Z	F1	F2	Defl. C (In.)	Wt. of Girl. Sec. (lb./in. ft)	Wt. of End Blk. Sec. (lb./in. ft)	Total Girder Weight
1 & 3	59'-3"	3	87^k	6	173^k	9	12	3	2¾	4	369	682	17,700
2	59'-3"	5	145^k	12	347^k	17	2¾	3	3¼	8	369	682	24,800

Prestressing strands shall be ½" diam. and shall have a minimum ultimate strength of 270,000 psi.
Each strand shall be jacked to give an initial tensile force of 28,500 lbs. per strand.

PSH 18 (SR 90)
RAUGUST TO WARDEN ROAD
GRANT COUNTY
C.M. ST. P. & P. R.R. OVERCROSSING

GIRDER DETAILS

WASHINGTON STATE HIGHWAY COMMISSION
DEPARTMENT OF HIGHWAYS
OLYMPIA, WASHINGTON

Approved Aug. 2, 1966

SHEET G4 OF 86 SHEETS

90/237 Sheet 7967

Date	Approval Date Added	Initials
5-2-68	Revision	WC

BAR LIST

All dimensions are out to out.

MARK	LOCATION	NO	SIZE	LENGTH	BENDING DIAGRAM
10	Bot. Flange Girder	1052	4	1'-5"	Stn
11	Stirrups, Girder	2184	4	4'-11"	
12	Top Flange, Girder	1092	5	1'-10"	Stn
15	Girders - Longit. @ Ends	576	5	Varies	
16	" - End Block Recess	432	5	10'-3"	
17	" - Longit. @ End Block Recess	240	5	21'-6"	Stn
18	" - End Block Ties	720	2	1'-8"	
19	" - " - "	360	4	1'-7"	
20	" - Top - Full Length	96	6	Varies	Stn
23	Girder - Ties @ Piers No. 1 & 4	48	6	31'-0"	Stn
22	" - Bot. Flange in End Block	864	5	2'-8"	
26	Footing - Longit. - Piers No. 1 & 4	248	5	31'-2"	Stn
27	" - Transv. " " 1 & 4	31	4	21'-4"	Stn
28	End Wall - Vertical - Piers No. 1 & 4	160	5	Varies	
29	" " - Horiz. " " " 1 & 4	48	4	20'-10"	Stn
31	Footing - Intermediate Piers	240	8	31'-2"	Stn
32	" - Dowel - Intermediate Piers	88	8	6'-8"	
33	Column - Longit. " "	88	9	Varies	Stn
34	" - Hoops - "	804	3	9'-8"	
35	Cross-Beam - Shrn - "	146	5	9'-8"	
36	" " - " - "	280	5	3'-9"	
37	" " - Top Ties - "	136	5	4'-3"	
33	Cross-Beam - Ties - Intermediate Piers	16	10	40'-6"	
40	" " " " "	16	11	15'-7"	Stn
41	" " " " "	16	11	14'-7"	Stn
42	" " " " "	16	11	13'-7"	Stn
43	" " " - Bot. - "	16	11	37'-2"	Stn
44	" " " " "	8	11	24'-0"	Stn
45	" " " " "	8	11	21'-0"	Stn
46	" " " " "	8	11	18'-0"	Stn
48	Hinge Bars - Intermediate Piers	180	10	7'-8"	
49	Cross-Beam - Side - " "	16	8	37'-6"	Stn
50	Horiz. - End Diaph. - Piers No. 1 & 4	84	4	30'-10"	Stn
51	" " " " " " 1 & 4	32	5	30'-10"	Stn
52	" " " " " " 1 & 4	48	4	21'-10"	
53	Vert. " " " " " 1 & 4	182	4	11'-11"	
54	Pav't. Seat - Ties " " " 1 & 4	182	4	2'-3"	
55	Slab - Concrete Ties " " 1 & 4	182	4	4'-6"	
57	Vert. - End Diaph. - Piers No. 1 & 4	24	4	6'-1"	Stn
58	" - Wing Wall " " 1 & 4	96	4	4'-7"	Stn
60	Horiz. - Wing Wall - Piers No. 1 & 4	20	4	7'-3"	
61	" " " " " 1 & 4	20	4	7'-2"	
62	" " " " " 1 & 4	20	4	7'-11"	
63	" " " " " 1 & 4	20	4	7'-3"	
66	End Wall - Horiz. - Piers No. 2 & 3	48	6	21'-0"	Stn
67	" " " " " 2 & 3	40	5	36'-10"	
68	" " - Vert. " " 2 & 3	240	4	4'-2"	
70	Slab - Top - Longit. - Piers No. 2 & 3	48	7	61'-10"	Stn
71	" " " " " " 2 & 3	48	7	23'-6"	Stn
72	" " " " " " 2 & 3	48	7	20'-6"	Stn
73	" " " " " " 2 & 3	48	7	15'-0"	Stn
74	" " " " " "	24	7	21'-4"	Stn
75	" " " " " "	584	4	Varies	Stn
76	" - Bot. " " "	440	5	30'-0"	Stn
79	Slab - Top - Transv.	852	5	Varies	Stn
80	" " "	612	5	Varies	
81	" - Bot. "	844	5	Varies	Stn
84	Rail Base - Vert.	820	6	3'-0"	
85	" " "	412	4	3'-3"	
86	" " - Horiz.	182	6	Varies	Stn
87	" " "	182	4	Varies	Stn

MARK	LOCATION	NO	SIZE	LENGTH	BENDING DIAGRAM
88	Curb - Transv.	612	4	1'-7"	
89	" - Longit.	2201	4	Varies	Stn
90	" - Ties	760	5	2'-3"	
91	" " - Hanger	20	4	32'-6"	Stn
92	" "	641	5	2'-7"	
94	Intermed. - Diaph. - Bot.	12	10	18'-1"	Stn
95	" " " - Web	12	8	18'-3"	Stn
96	" " " - Stirrups	150	4	4'-1"	
97	" " " - Web - Btwn. Girders	601	4	6'-6"	Stn
98	" " " - Stirrup Hangers	36	4	20'-10"	Stn

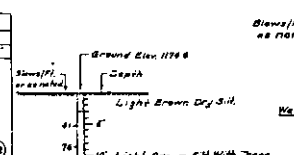

TEST HOLE H-4A

Approx. Sta. L^a 668+87 - 63.5 Rt. ℄

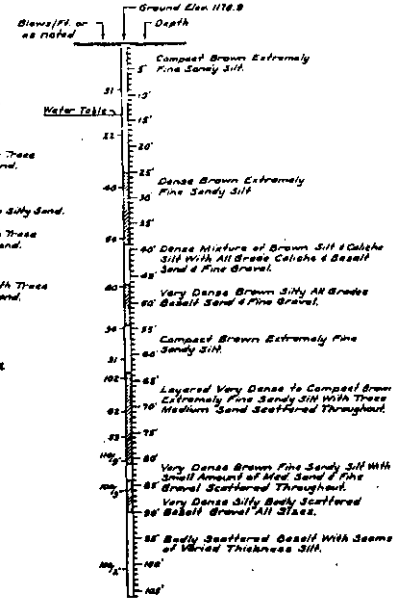

TEST HOLE H-4

Sta. L^a 669+66 - 55' Lt. ℄

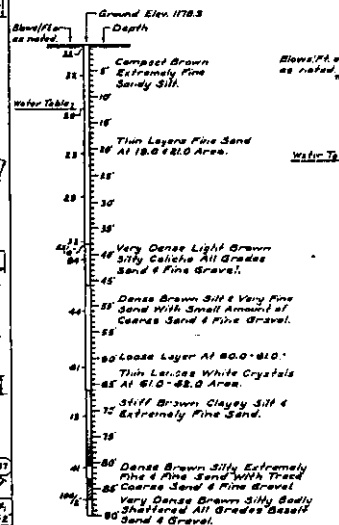

TEST HOLE H-1

Sta. L^a 667+96 - 55' Rt. ℄

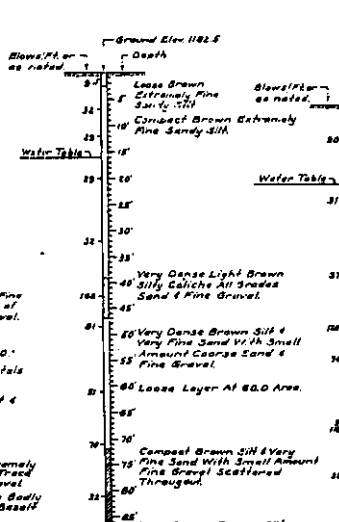

TEST HOLE H-2

Sta. L^a 668+18 - 55' Lt. ℄

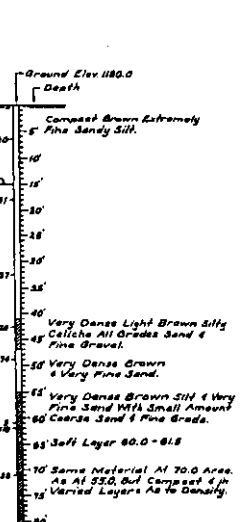

TEST HOLE H-3

Sta. L^a 669+42 - 55 Rt. ℄

DATE	REVISION	BY	APPRD
9-2-65	Approval Date Added	WCB	
8-1-63	Bor. No. 66 On Alen Test Hole H3	YI	APPD

90/237 S4N

PSH 18 (SR 90)
RAUGUST TO WARDEN ROAD
GRANT COUNTY
C.M. ST. P. & P. R.R. OVERCROSSING

BAR LIST AND TEST HOLES

WASHINGTON STATE HIGHWAY COMMISSION
DEPARTMENT OF HIGHWAYS
OLYMPIA, WASHINGTON

Aug. 2, 1968

SHEET 65 OF 86 SHEET

7867

APPENDIX B

EXCERPTS FROM DESIGNER'S CALCULATIONS

OFFICE OF BRIDGE ENGINEER

Project _____ Sheet No. 27 of _____ sheets

S. H. No. _____ Made by _____ Date _____ Check by _____ Date _____

	TOP			BOTTOM		
	P	M_L LONGITUD	M_T TRANSVERSE	P	M_L	M_T
DEAD Load	221.7		47.2	250.0		13.5
LL+I Max P	178.2		60.5	178.2		17.3
" Max M_T	105.7		184.1	105.7		52.7
T&S Transv			12.0			11.4
" Longit					44.8	
Eq Transv			155.2			117.9
" Longit					230.	
Wind			201.0			152.7
Group I Max P	399.9		107.7	390.3 / 428.2		26.3 / 30.8
Max M_T	327.4		231.3	355.7		66.2
Group II	177.4		198.6	200.0		133.0
Group IV M_L	261.9		185.0	284.6	37.4	53.0
Group VII	166.3		134.4	187.5		98.6
	166.3		35.4	187.5	172.5	10.1

Use 11-#9 bars in column 1% Min Steel.

Allow Soil Pressure = 6 K/ft²

Wt/ft² fig = (0.5)(.16) = .24

Wt/ft² OB = (8')(.12) = 1.02

1.26 6 - 1.26 = 4.74

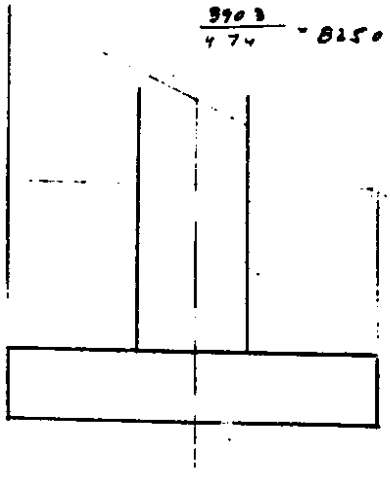

$\frac{390.3}{4.74} = 82.50$ Try 9.5 x 9.5 ft Area = 90.25 ft² $S = \frac{9.5^3}{6} = 142.9$ ft³

		P	M_L	M_T
Group I	W =	390.3		26.3
	Wt. Ftg = (9.5)(2)(.16) =	28.9		
	OB = (4.5)(9.5)(.12) =	48.7		
	$OB_2 = \frac{(8.5)^3}{4}(.12) =$	25.7		
		493.6	50	26.3

S.P. $\frac{493.6}{90.25} \pm \frac{50}{142.9} \pm \frac{26.3}{142.9} = 6.00$ K/ft²

OFFICE OF BRIDGE ENGINEER

Project C M S1 P & P R R O X I N G Sheet No. 27 of ____ sheets

S. H. No. 18 Made by YI Date 1-12-65 Check by ____ Date ____

Wind

$A = 4'-2" + 9" + 1\frac{1}{6}" + 6" = 6.92'$

$L = (40.5' + 0.5(60) = 70.5 ft.$

$P = (.05)(70.5')(6.92) = 24.393 K$ $\Delta = .0249'$

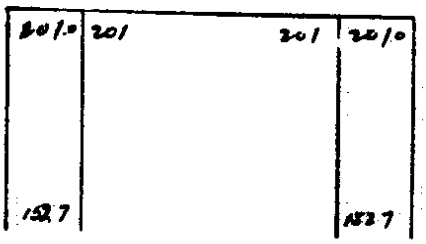

Transverse Earthquake

DL 613.64 + 14.13 = 627.77 K

$\Delta = (627.77)(.0922) = .5788$

$T = 1.12\sqrt{.5788} \cdot (1.12)(.761 = .851$

$C = \frac{.025}{.851} = .0294$ use .03

$EQ = (627.77)(.03) = 18.83 K$

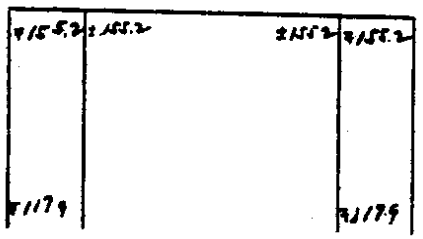

WASHINGTON STATE HIGHWAY COMMISSION
OFFICE OF BRIDGE ENGINEER

Project _____ Sheet No. 25 of _____ sheets

S. H. No. _____ Made by _____ Date _____ Check by _____ Date _____

Max M_u Neg = 9755 ft-k

$d = 36 - 2 - .774 = 33.226$"

$A_s = \frac{(9755)(12)}{(.90)(.87)(33.226)} = 45.78$" Try 10-#11

$\rho = \frac{45.6}{(96)(33.226)} = .01118$ $\phi = .8856$

$f_s = \frac{(9755)(12)}{(15.6)(.8856)(33.226)} = 19.75$ ksi

$M_R = \frac{3.0}{12}(88)(33.226)A_s$

$= 49.7 A_s$

10-#11	760 ft-k
8-#11	608 ft-k
6-#11	456 ft-k
4-#11	304 ft-k
2-#11	152 ft-k

Max Neg Mom @ ℄ Column = -7469 ft-k

$d = 36 + 2.393 - 2 - .774 = 35.619$"

$A_s = \frac{(7469)(12)}{(20)(.85)(35.619)} = 14.30$" Try = 6-#11 & 4-#10 $A_s = 14.96$ in²

$\rho = \frac{14.96}{(96)(35.619)} = .0049$ $J = 0.89$

$f_s = \frac{(7469)(12)}{(14.96)(.89)(35.62)} = 19.6$ ksi

Neg Mom @ face of equiv col = 562 ft-k

$d = 33.23$"

$\frac{4bx^2}{2} = (14.00)(8)(33.23 - x)$

$21x^2 + 115.52x = 3838.7296$

$x^2 + 5.50x = 182.796$

$(x + 2.75)^2 = 190.359$

$x + 2.75 = 13.797$

$x = 11.047$

$I_c = \frac{(96)(11.05)^3}{3} = 18874$ in⁴

$I_s = (14.96)(8)(22.18)^2 = 56890$

75704 in⁴

$f_c = \frac{(562)(12)(11.047)}{75,704} = .985$ ksi

$f_s = \frac{(562)(12)(8)(22.18)}{75,704} = 15.81$ ksi

Remaining Mom

4-#10 & 6-#11	$A_s = 10.46$	$M_R = 711$ ft-k
4-#10 & 4-#11	= 11.32	559 ft-k
4-#10 & 2-#11	= 8.20	404 ft-k
4-#10	= 5.08	250 ft-k

Max V = 275 k

$v = \frac{275}{(96)(.89)(33.23)} = .284$ ksi 300 o.k.

$V_c = (.108)(96)(.85)(33.23) = 132$ k

$V' = 275 - 132 = 142$ k

$s = \frac{(4)(.31)(12)(.85)(33.23)}{142} = 7.6$"

APPENDIX C

RESPONSE HISTORIES

APPENDIX C

RESPONSE HISTORIES

This appendix presents displacement and curvature response histories that supplement the data presented in Chapter 7. The appendix also describes the convention used to identify the instrument locations.

Figures C.1 and C.2 show the relationship between the total applied force to each pier and the displacement of the pier. The average pier response for each individual cycle is presented in Figures C.3 to C.6. Figures C.7 to C.11 document the curvature histories for the columns. In the curvature figures, the top plots show curvatures measured at the highest elevation. The bottom plots present curvatures that were measured further down the column.

The instruments were identified by six alphanumeric characters. The first letter, E or W, designated whether the instrument was located on the East or West half of the bridge. For the instrumentation that measured column and beam rotation, the second letter, N or S, designated whether the instrument was located near the North or South column. The third letter was C or B according to whether the instrument measured Column or Beam rotation; the fourth letter, T or B, denoted that the instrument was installed at the Top or Bottom of a Column. The following number, 1, 2, or 3, indicated the location of the instrument with respect to the end of the column of beam. The number 1 was given to instruments nearest the end of the member, and the number 3 was given to the instruments furthest from the end. The final letter, n or s, varied according to whether the instrument was mounted on the north or south face of the column.

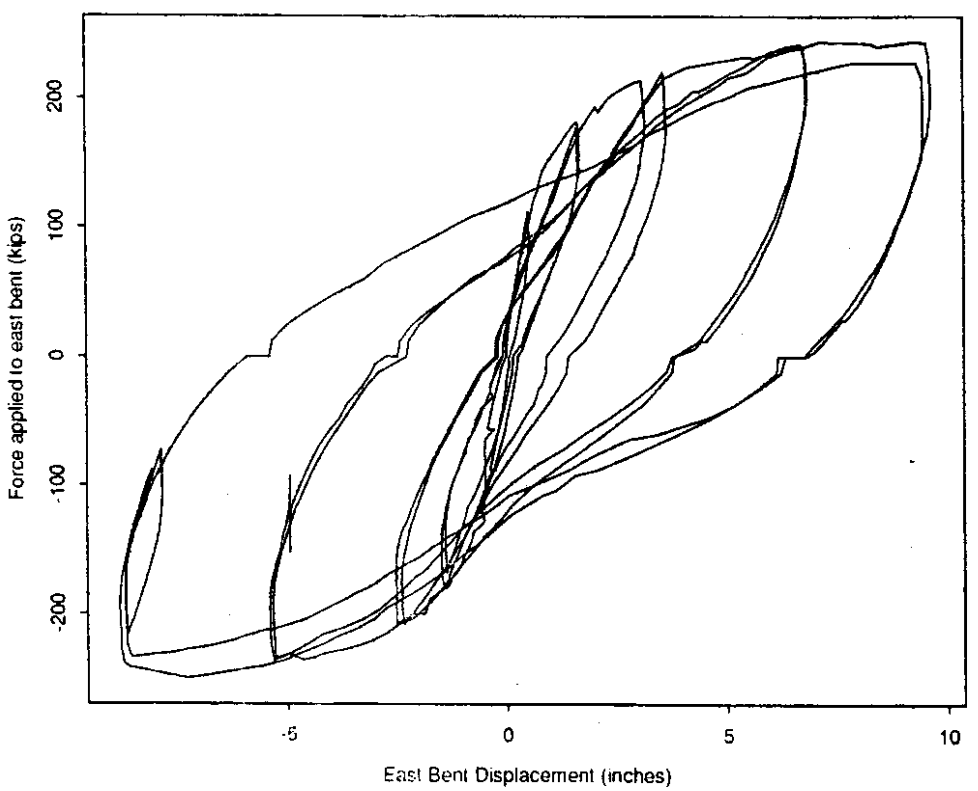

Figure C.1. Applied Force Versus Displacement for East Pier

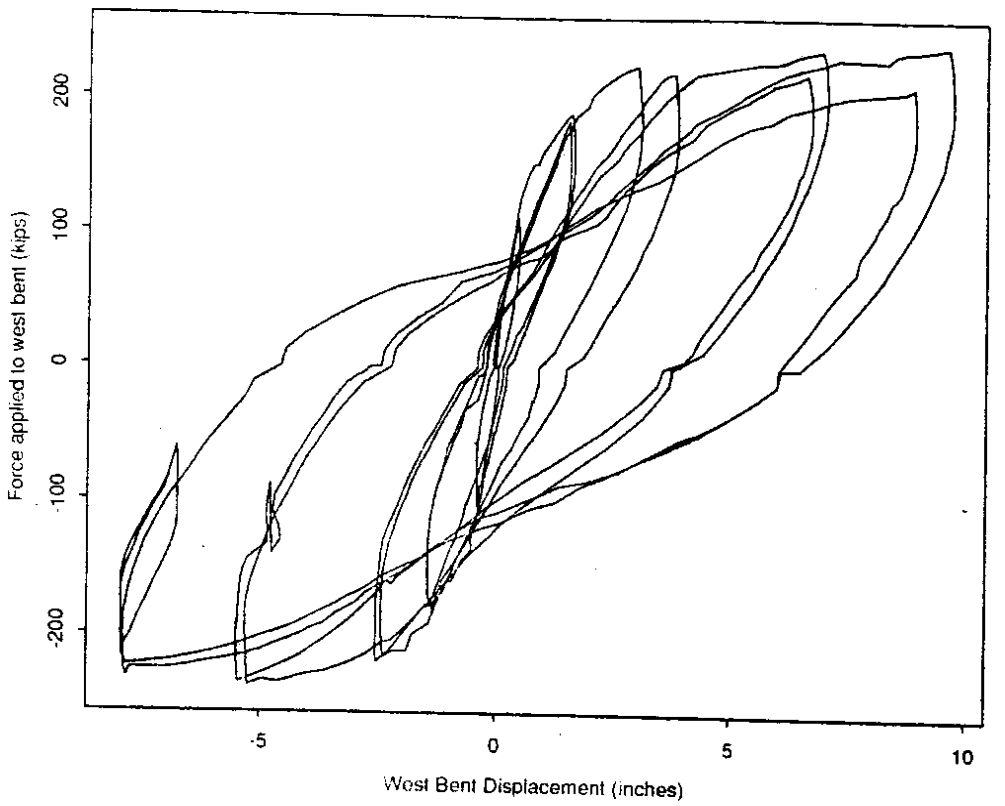

Figure C.2. Applied Force Versus Displacement for West Pier

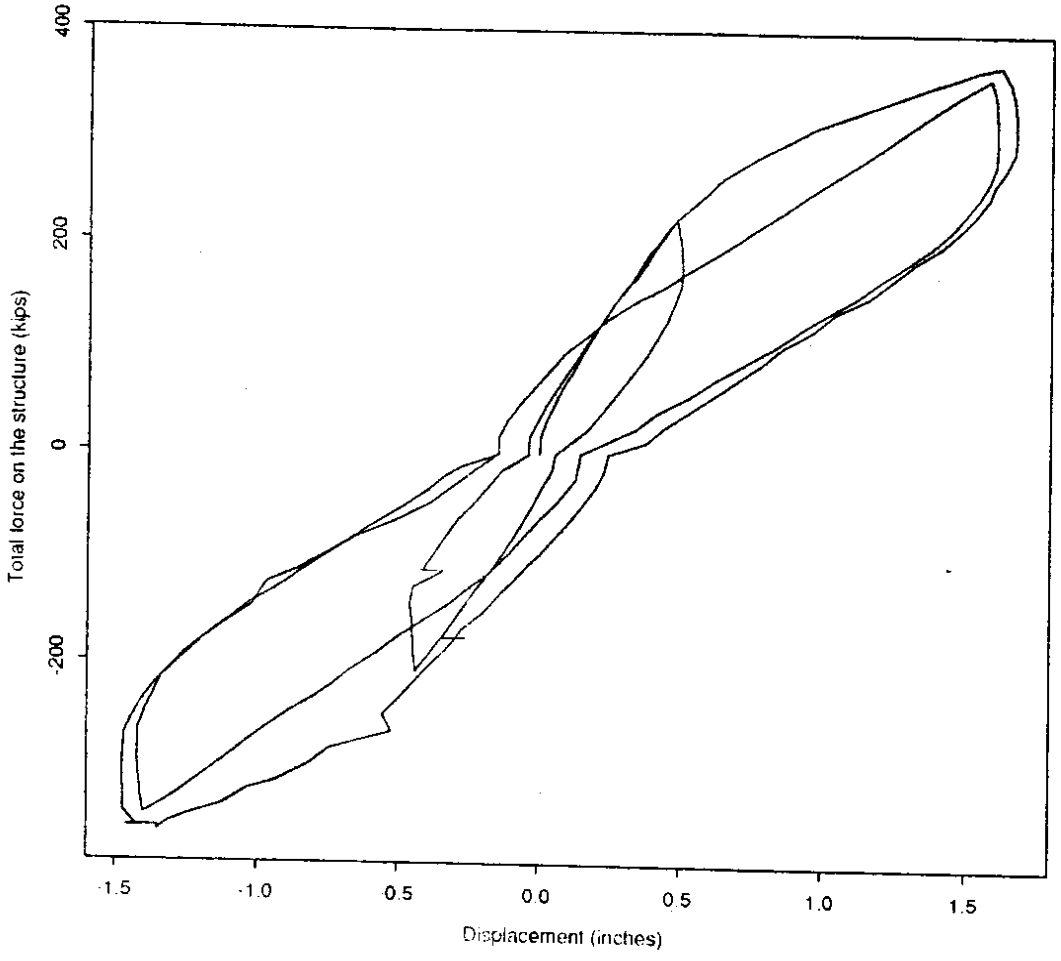

Figure C.3. Applied Force Versus Average Pier Displacement, Cycles ISO and B5

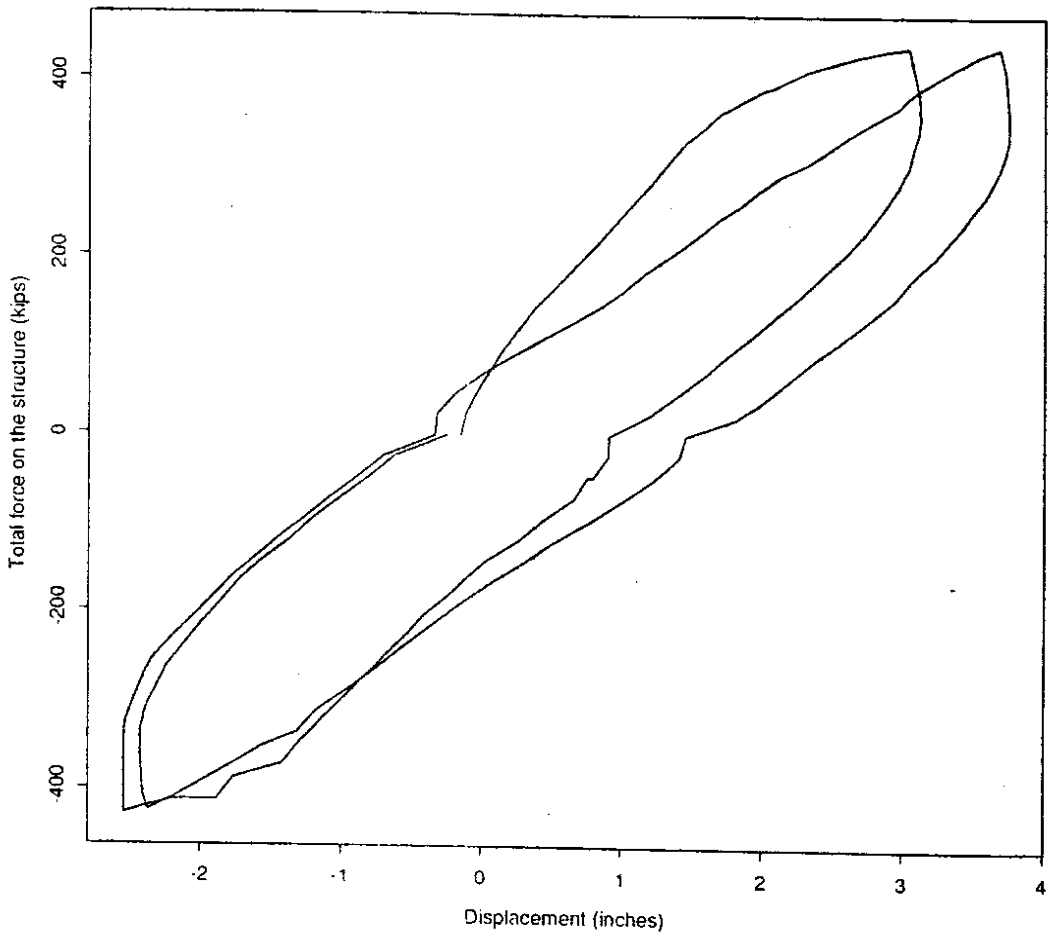

Figure C.4. Applied Force Versus Average Pier Displacement, Cycle B1

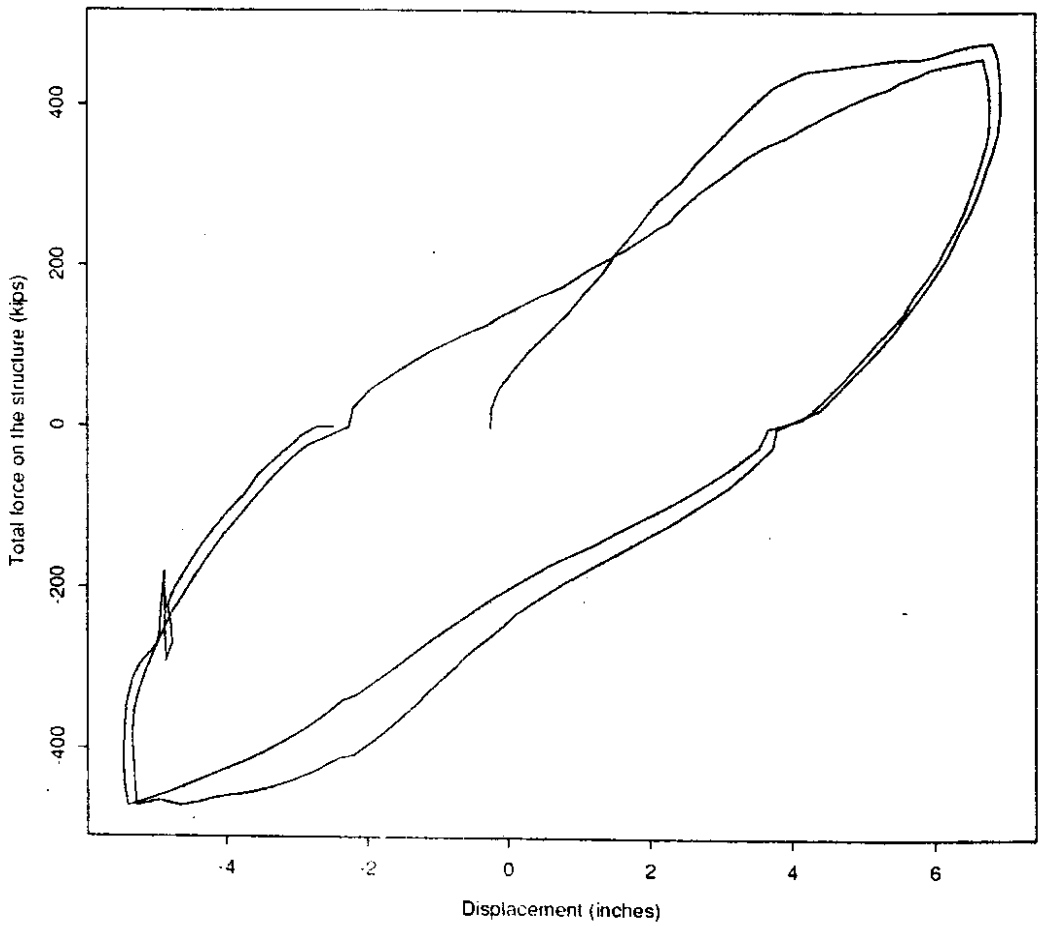

Figure C.5. Applied Force Versus Average Pier Displacement, Cycle B2

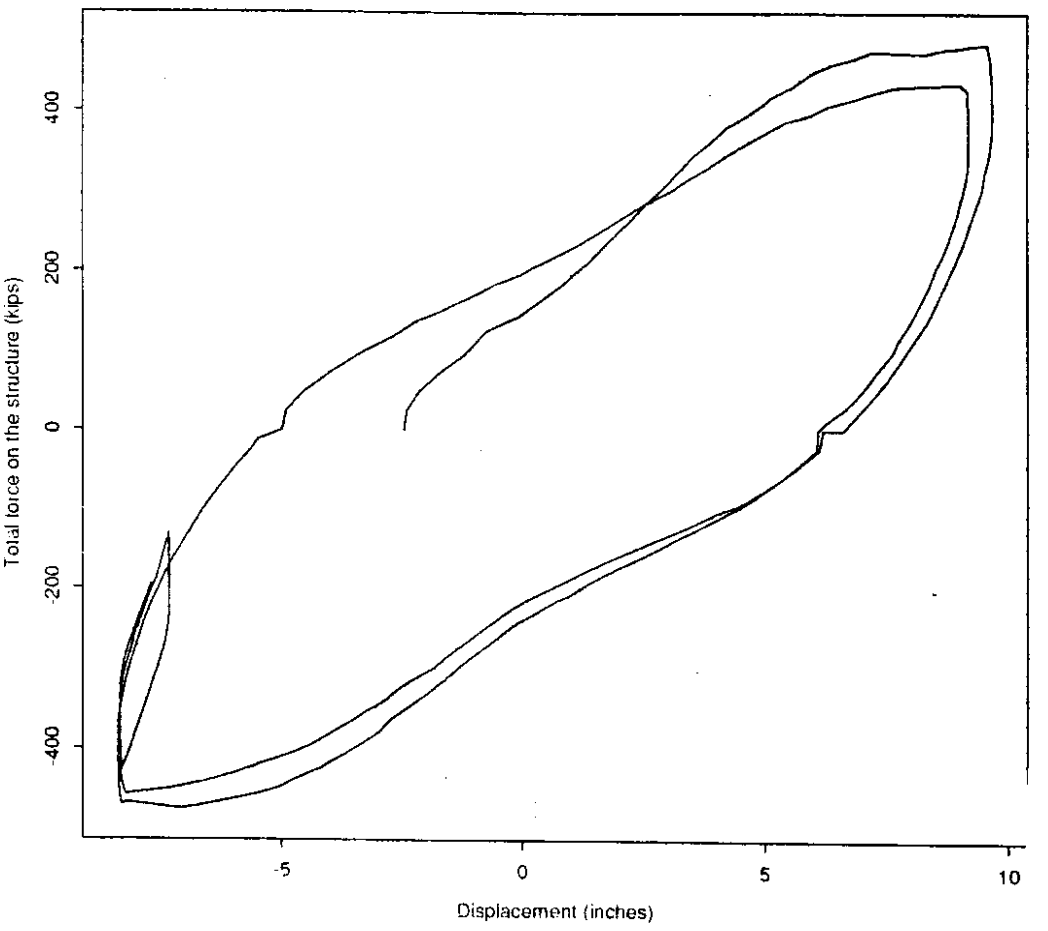

Figure C.6. Applied Force Versus Average Pier Displacement, Cycle B3

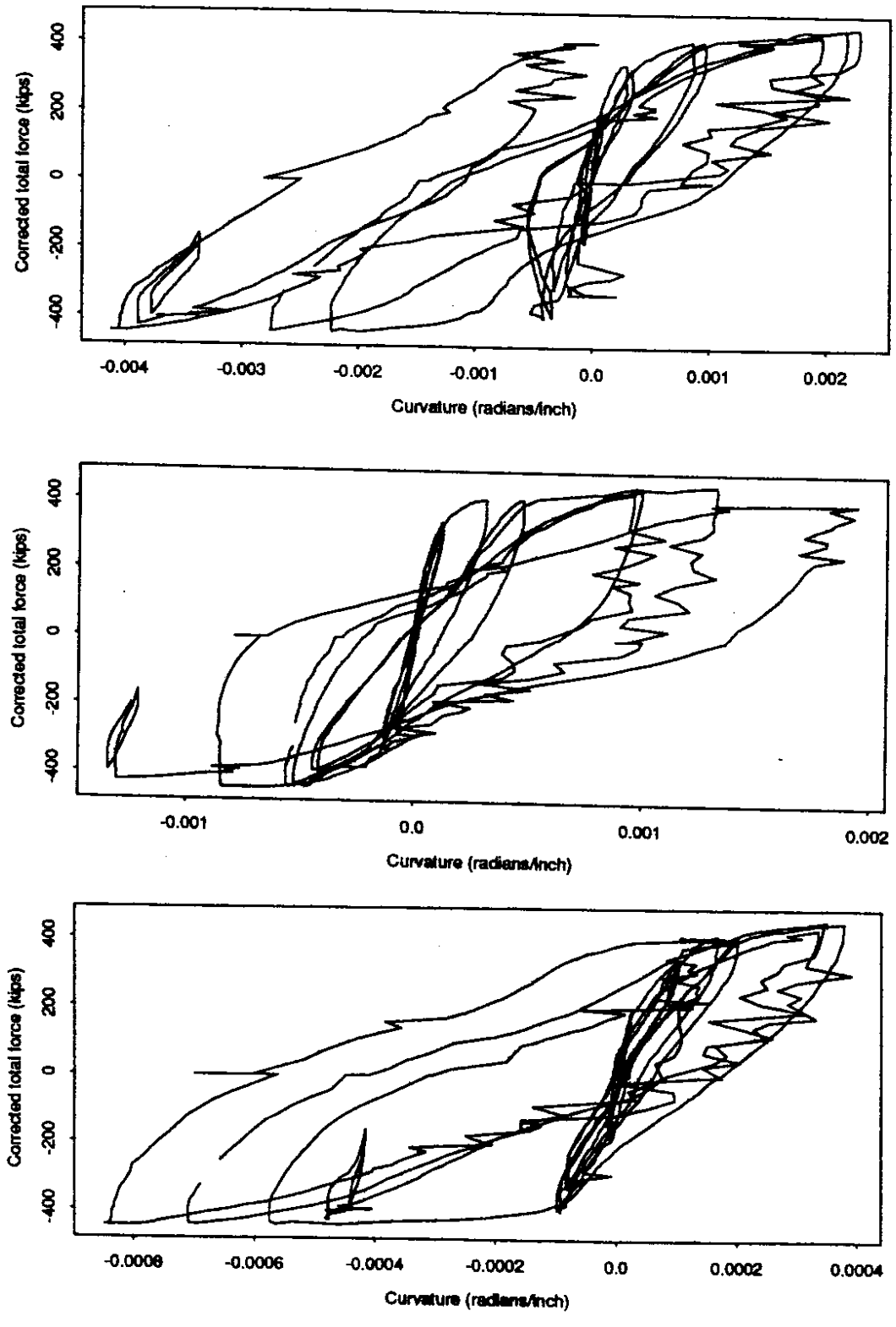

Figure C.7. Curvature Histories for Top of Southwest Column

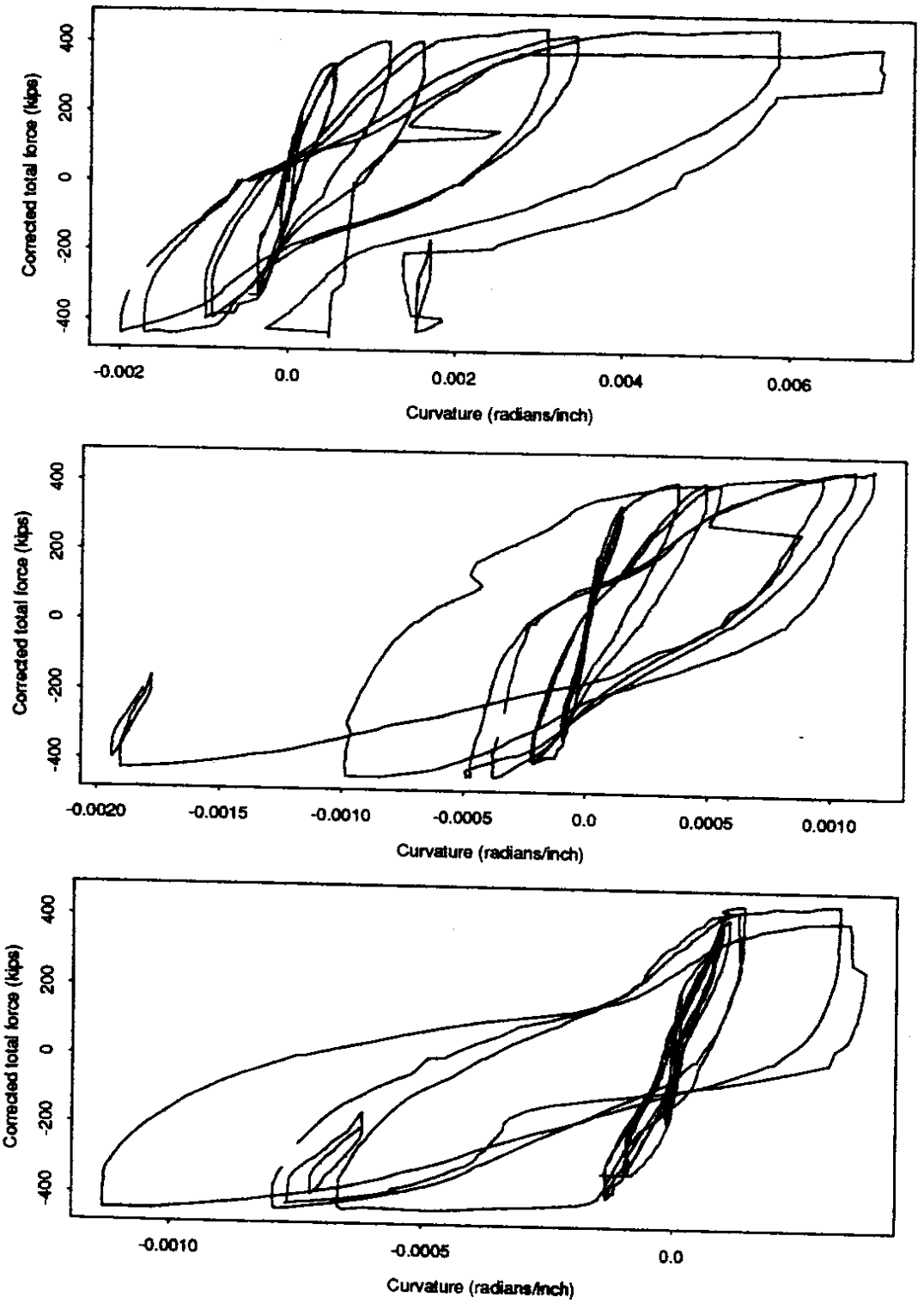

Figure C.8. Curvature Histories for Top of Northwest Column

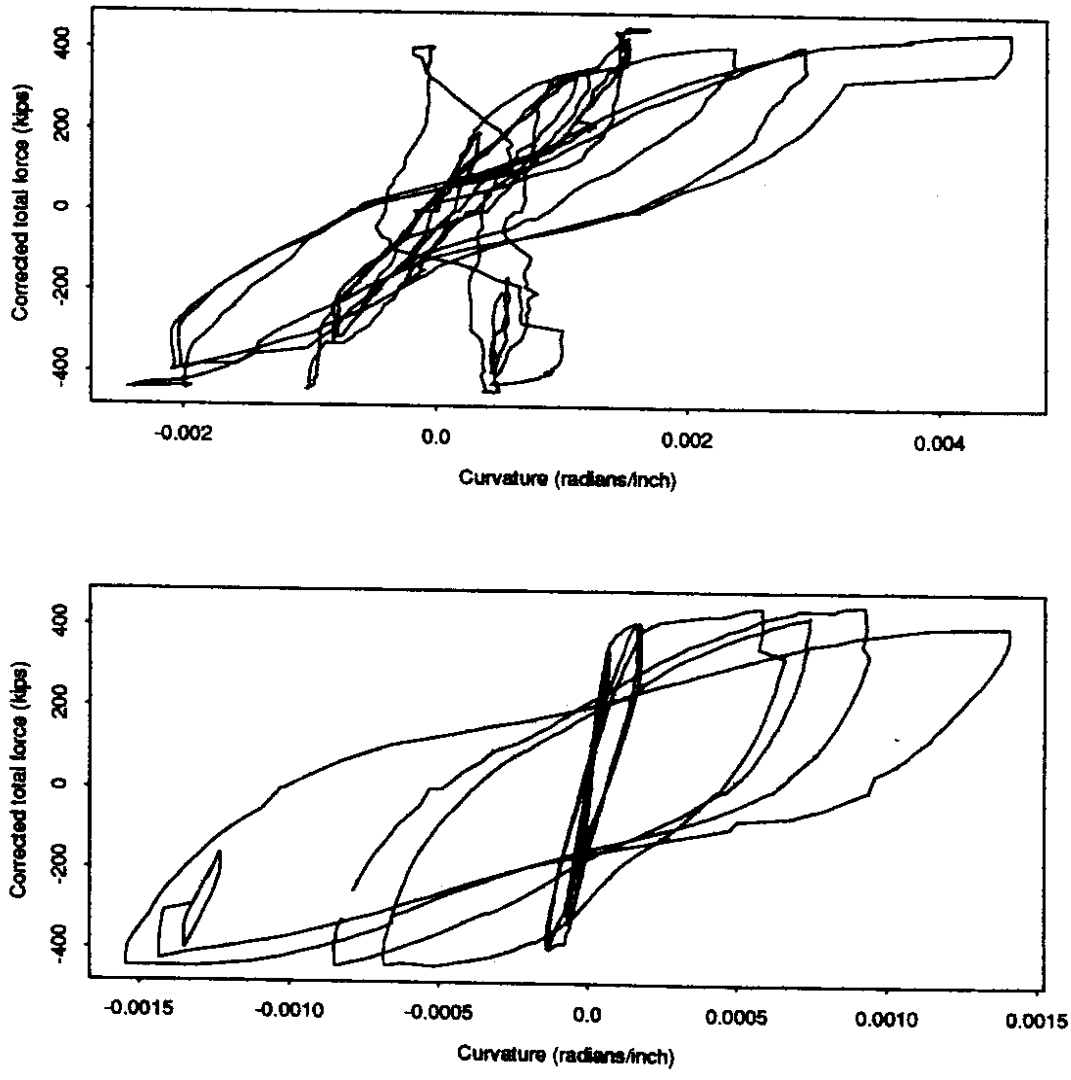

Figure C.9. Curvature Histories for Top of Southeast Column

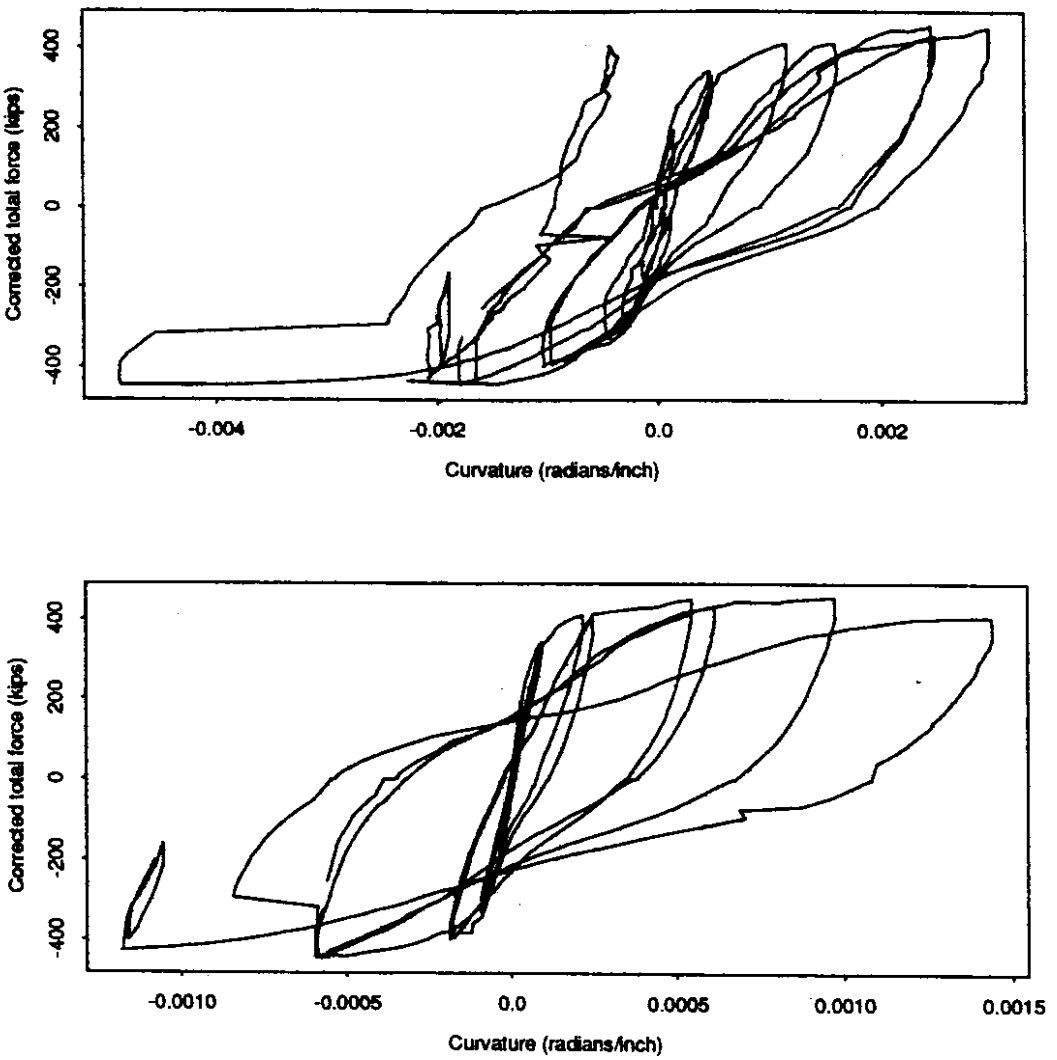

Figure C.10. Curvature Histories for Top of Northeast Column

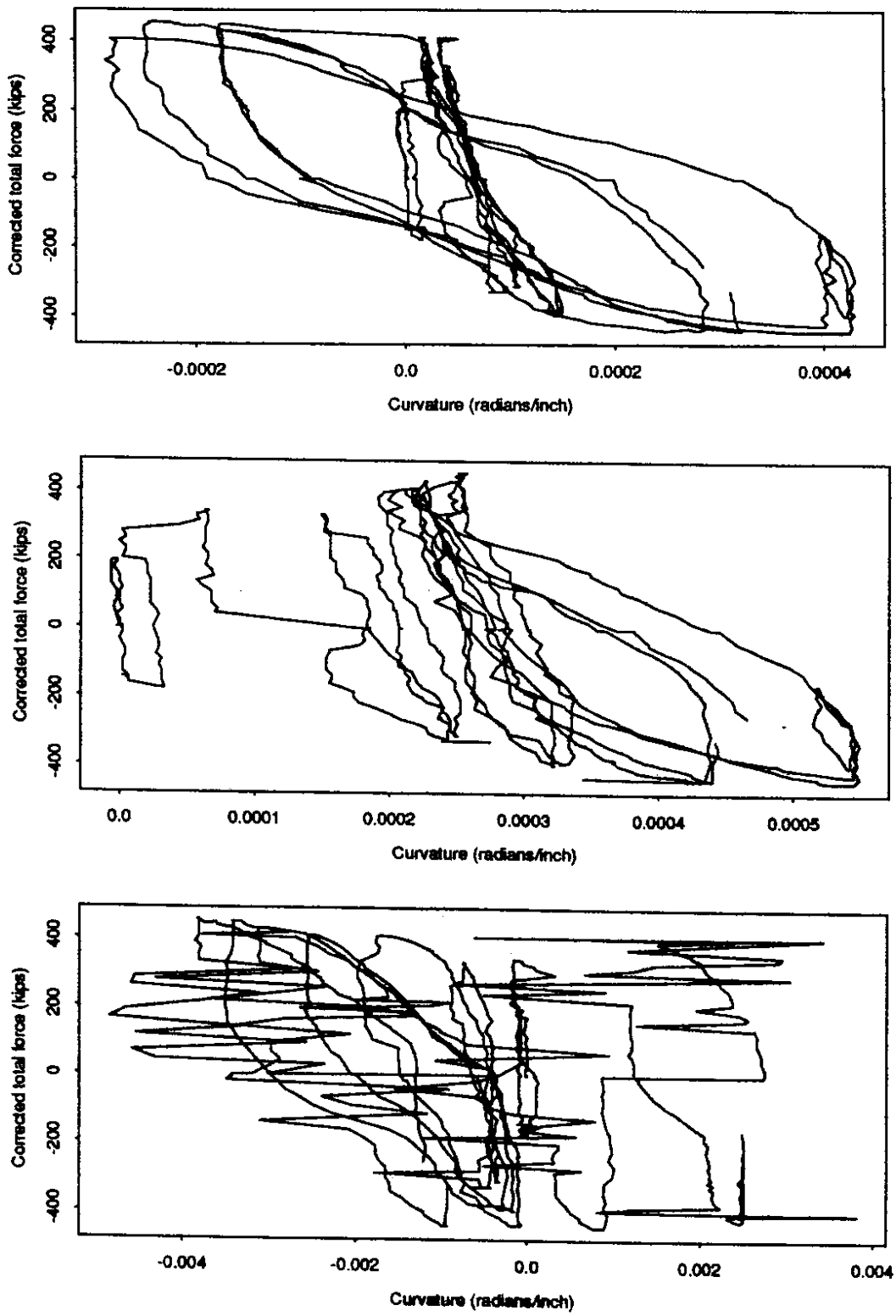

Figure C.11. Curvature Histories for Bottom of Northwest Column

APPENDIX D

TYPICAL SAP90 INPUT FILE FOR UW COLUMN MODEL

APPENDIX D

TYPICAL SAP90 INPUT FILE FOR UW COLUMN MODEL

```
TITLE "phi=38" column model, Moses Lake Bridge Project SAP90 FEM
C
C  This is a finite element model of a column in a reinforced concrete
C  bridge in Moses Lake, WA, that was tested in the summer of 1991.
C  The values of the parameters in this model are derived from concrete
C  tests. The model was written by Jeffrey MacLardy.
C  If you need further information about this model, please contact
C  Marc Eberhard in the Civil Engineering Department at the University
C  of Washington.
C  All units in inches, seconds, kips, and radians.

SYSTEM
L=1

JOINTS
C From bottom to top
1  X=0  Y=0  Z=0
2  X=0  Y=0  Z=12
3  X=0  Y=0  Z=24
4  X=0  Y=0  Z=36
5  X=0  Y=0  Z=48
6  X=0  Y=0  Z=60
7  X=0  Y=0  Z=72
8  X=0  Y=0  Z=84
9  X=0  Y=0  Z=96
10 X=0  Y=0  Z=108
11 X=0  Y=0  Z=120
12 X=0  Y=0  Z=132
13 X=0  Y=0  Z=144
C Soil ends at joint 13 (element 12)
14 X=0  Y=0  Z=156
15 X=0  Y=0  Z=168
16 X=0  Y=0  Z=180
17 X=0  Y=0  Z=192
18 X=0  Y=0  Z=204
19 X=0  Y=0  Z=216
20 X=0  Y=0  Z=228
21 X=0  Y=0  Z=240
22 X=0  Y=0  Z=252
23 X=0  Y=0  Z=264
24 X=0  Y=0  Z=276
25 X=0  Y=0  Z=288
26 X=0  Y=0  Z=300
C Top of column
```

```
RESTRAINTS
C  Bottom and top of column
1   R= 1,1,1,1,1,1
26  R= 0,1,0,1,1,1

SPRINGS
C  Soil springs around first 12' of column, from bottom to top
C  Soil springs are divided among 12 joints; top 3/4' of soil is not
C  modelled to account for unconfined soil behavior
2  K= 269,0
3  K= 221,0
4  K= 168,0
5  K= 119,0
6  K= 81,0
7  K= 53,0
8  K= 34,0
9  K= 21,0
10 K= 12,0
11 K= 6,0
12 K= 2,0
13 K= 0,0

FRAME
NM=25
C  From bottom to top
C  Column (AS= .9 Pi r^2 from SAP90 manual)
1  A= 1017.9 J= 164900 I= 90000,90000 AS= 916,916 E= 4600 G= 1E+12 W= .09
2  A= 1017.9 J= 164900 I= 90000,90000 AS= 916,916 E= 4600 G= 1E+12 W= .09
3  A= 1017.9 J= 164900 I= 90000,90000 AS= 916,916 E= 4600 G= 1E+12 W= .09
4  A= 1017.9 J= 164900 I= 90000,90000 AS= 916,916 E= 4600 G= 1E+12 W= .09
5  A= 1017.9 J= 164900 I= 90000,90000 AS= 916,916 E= 4600 G= 1E+12 W= .09
6  A= 1017.9 J= 164900 I= 90000,90000 AS= 916,916 E= 4600 G= 1E+12 W= .09
7  A= 1017.9 J= 164900 I= 90000,90000 AS= 916,916 E= 4600 G= 1E+12 W= .09
8  A= 1017.9 J= 164900 I= 90000,90000 AS= 916,916 E= 4600 G= 1E+12 W= .09
9  A= 1017.9 J= 164900 I= 90000,90000 AS= 916,916 E= 4600 G= 1E+12 W= .09
10 A= 1017.9 J= 164900 I= 90000,90000 AS= 916,916 E= 4600 G= 1E+12 W= .09
11 A= 1017.9 J= 164900 I= 90000,90000 AS= 916,916 E= 4600 G= 1E+12 W= .09
12 A= 1017.9 J= 164900 I= 90000,90000 AS= 916,916 E= 4600 G= 1E+12 W= .09
13 A= 1017.9 J= 164900 I= 90000,90000 AS= 916,916 E= 4600 G= 1E+12 W= .09
14 A= 1017.9 J= 164900 I= 90000,90000 AS= 916,916 E= 4600 G= 1E+12 W= .09
15 A= 1017.9 J= 164900 I= 90000,90000 AS= 916,916 E= 4600 G= 1E+12 W= .09
16 A= 1017.9 J= 164900 I= 90000,90000 AS= 916,916 E= 4600 G= 1E+12 W= .09
17 A= 1017.9 J= 164900 I= 90000,90000 AS= 916,916 E= 4600 G= 1E+12 W= .09
18 A= 1017.9 J= 164900 I= 90000,90000 AS= 916,916 E= 4600 G= 1E+12 W= .09
19 A= 1017.9 J= 164900 I= 90000,90000 AS= 916,916 E= 4600 G= 1E+12 W= .09
20 A= 1017.9 J= 164900 I= 90000,90000 AS= 916,916 E= 4600 G= 1E+12 W= .09
21 A= 1017.9 J= 164900 I= 90000,90000 AS= 916,916 E= 4600 G= 1E+12 W= .09
22 A= 1017.9 J= 164900 I= 90000,90000 AS= 916,916 E= 4600 G= 1E+12 W= .09
23 A= 1017.9 J= 164900 I= 29436,29436 AS= 916,916 E= 4600 G= 1E+12 W= .09
24 A= 1017.9 J= 164900 I= 29436,29436 AS= 916,916 E= 4600 G= 1E+12 W= .09
25 A= 1017.9 J= 164900 I= 29436,29436 AS= 916,916 E= 4600 G= 1E+12 W= .09
```

```
1  1  2  M= 1,1   LP= 2,0
2  2  3  M= 2,2   LP= 2,0
3  3  4  M= 3,3   LP= 2,0
4  4  5  M= 4,4   LP= 2,0
5  5  6  M= 5,5   LP= 2,0
6  6  7  M= 6,6   LP= 2,0
7  7  8  M= 7,7   LP= 2,0
8  8  9  M= 8,8   LP= 2,0
9  9  10 M= 9,9   LP= 2,0
10 10 11 M= 10,10 LP= 2,0
11 11 12 M= 11,11 LP= 2,0
12 12 13 M= 12,12 LP= 2,0
13 13 14 M= 13,13 LP= 2,0
14 14 15 M= 14,14 LP= 2,0
15 15 16 M= 15,15 LP= 2,0
16 16 17 M= 16,16 LP= 2,0
17 17 18 M= 17,17 LP= 2,0
18 18 19 M= 18,18 LP= 2,0
19 19 20 M= 19,19 LP= 2,0
20 20 21 M= 20,20 LP= 2,0
21 21 22 M= 21,21 LP= 2,0
22 22 23 M= 22,22 LP= 2,0
23 23 24 M= 23,23 LP= 2,0
24 24 25 M= 24,24 LP= 2,0
25 25 26 M= 25,25 LP= 2,0
LOADS
C  Shear and axial load applied at top of column (axial load=210 psi)
26 L= 1   F= 10,0,-214,0,0,0 : Fx,Fy,Fz,Mx,My,Mz
C EOF
```